Detection of oxygen profiles through a spheroid tumour model

Ioanni Veras

Faculty of Mathematics and Natural Sciences

Department of Physics

Biophysics and Medical Physics

UNIVERSITETET I OSLO

June 2015

Year 2015

Detection of oxygen profiles through a spheroid tumour model

Ioanni Veras

http://www.duo.uio.no/

Trykk: Reprosentralen, Universitetet i Oslo

Contents

Abstract

The traditional liquid overlay method and the spinner flask technique have proven successful in spheroids formation over the past decades. A new spheroid formation and maintenance method that combines the basic principles of those two techniques, was proposed and tested on HT29, T-47D, MCF-7 and T98G.

Moreover, HT29-cell spheroids, formed by the newly-established spheroid generating method proposed in the present thesis, were immobilized in agarose matrix and oxygen profiles were acquired by the use of manipulator-controlled oxygen microsensor.

In addition, histological section for Pimonidazole binding, were obtained for HT29 spheroids cultured with the same newly-established method as the HT29 spheroids used in the oxygen concentration profiles acquisition.

The following were observed in the experiments performed in the current thesis:

1. For the experiments performed in agarose-coated 25 cm^2 cell culture flasks

- HT29-cell spheroids were formed with mean diameter of 800 μm.
- T-47D-cell spheroids with diameters up to 300 μm diameters were successfully formed.
- MCF-7-cell spheroids with diameters up to about 250 μm were successfully generated.
- T98G-cell small spheroids (150-200 μm diameter) were successfully formed.

2. For the experiments performed in non-agarose-coated 25 cm^2 cell culture flasks

- Only HT29-cell spheroids were successfully generated, while T-47D, MCF-7, and T98G did not formed any spheroid in the experiments involved non-agarose coated flasks.

3.For the oxygen profiles acquisition of HT29-cell spheroids:

- Successful oxygen profile acquisitions were performed for 2 HT29-cell spheroids with diameters above 1000 µm. The measured thickness of viable rim was about 186 to 216.2 µm.

Overall, the results of this thesis lead to the conclusion that the HT29 cells formed the largest spheroids and thus seems best suited for this technique without further optimization. For the next 3 cell lines (T-47D, MCF-7, and T98G) tested in the present thesis, optimization process must be performed. For all the cell lines used, more successful spheroid formation results were obtained from experiments that were performed in agarose-coated flask than from experiments performed in flasks without agarose coating.

Moreover, the immobilization of spheroids in agarose matrix and its use for experiments that involve acquisition of oxygen profiles through penetration of a computer-controlled oxygen microsensor was successfully performed. The oxygen profiles, acquired for HT29-cell spheroids, revealed viable rim thickness values which are comparable to values that Sutherland et al. (1986) obtained for HT29-cell spheroids of comparable diameters (~1 mm).

Preface

The whole work on the present thesis was performed at the Biophysics and Medical Physics group, Institute of Physics, University of Oslo. This thesis was submitted for the degree of Master of Science at the Biophysics and Medical Physics section.

My supervisor has been professor dr.philos Erik Olai Pettersen and my co-supervisor has been senior engineer Joe Alexander Sandvik. This thesis would have never been complicated without their knowledge and encouragement. Thank you both very much for helping me in all phases of the work with this thesis.

Also thanks to the scientist dr.scient Nina F. J. Edin for her invaluable help, her contribution to the completion of the present thesis was very important.

In addition, I would like to thank you, my co-students and employees at the biophysics and medical physics group for your help and valuable suggestions.

Last but not least I want to thank my family and lovely girlfriend for being so helpful and supportive during the last year.

Oslo, June 2015

Ioanni Veras

1. Introduction

Cancer is the second most frequent cause of death per year in Norway, U.S.A and many other countries with numerous victims, and also one of the greater medical challenges of our times. In spite of the large amount of money and time invested in cancer research, the new knowledge obtained cannot compensate the increasing mortality rate of the disease. In addition, as the life expectancy of the population in the western world increases, the probability of developing cancer also increases.

We can define cancer as a common name for a wide range of diseases which are characterized by uncontrolled cell proliferation with a potential to spread to other parts of the human body. There are two categories of tumors, malignant (which are denoted cancer) and benign (which are denoted non-cancer). There are many differences between benign and malignant tumors, but important differences are that benign tumors do not infiltrate surrounding tissues and do not spread to other parts of the body while malignant tumor cells have a tendency both to infiltrate surrounding normal tissues and to use the lymph and/or the blood system to spread to other body parts.

The main modalities for radical cancer treatment aiming to cure cancer patients by local control include radiotherapy and surgery. Radiotherapy can be used in combination with other treatment modalities to achieve the desirable result. It involves delivery of a certain amount of dose to as high a percentage of the cancer tumor as possible, by making use of ionizing radiation. Ionizing radiation has the ability to control the cell growth by inducing DNA damage which can halt cell proliferation, cause cell death during cell division (mitotic death) or lead the cell to commit suicide.

The biggest challenge radiation therapists have to face when they make the treatment plan is to deliver the desirable dose to the cancer tumor while minimizing the level of radiation-induced damage to the normal, healthy surrounding tissue. The radiosensitivity of a cancer tumor is determined by many micro-environmental factors, one of which is oxygen. The oxygen concentration present can critically influence the radiosensitivity of a population of cells exposed to radiation of low LET. Low oxygen concentration, present at the time of irradiation, can cause decreased radiosensitivity of cancer cells; the effect is quantitatively measured by the Oxygen Enhancement Ratio OER (which is usually calculated as the dose needed to induce a certain effect in the absence of oxygen divided by the dose necessary to induce the same effect in the presence of oxygen, see figure 2.5).

The reason for the importance of oxygen for radiotherapy has to do with the special vascularization of cancer tissues. As a tumor grows, it rapidly outgrows its blood supply, leaving portions of the tumor with regions where the oxygen concentration is significantly lower than in healthy tissue. The metabolism of oxygen by the respiring cancer cells, near the oxygen supply, limits the distance that the oxygen can diffuse in the cancer tissue, resulting in the development of cell regions that will be characterized by low oxygen concentration (hypoxia).

Most human solid cancer tumors develop regions that are characterized by some type or degree of hypoxia. The presence of hypoxic cells limits the success of radiotherapy because it causes specifically reduced radiosensitivity of cancer cells. It is furthermore known to increase the ability of the tumor to form distant metastasis during tumor progression.

Measurement of tumor oxygenation is therefore important in relation to radiation therapy and different methods are in use. Perhaps the most important technique used for exact detection of the oxygen concentration is oxygen microsensors which can pierce the tumor in situ or in vitro and acquire the exact values of oxygen concentration at different depths in the tumor tissue.

As cancer research was evolving, the need of reproducing different tumor micro-environmental characteristics in vitro became critical. Different techniques for cancer tumor modeling in vitro have been developed over the years. The most utilized way to imitate the different tumor functions and characteristics in vitro is by 3D multicellular aggregates which are also known as spheroids. The spheroids are 3-dimensional cellular structures which ideally are spherically symmetric. This 3D cell culture has been extensively employed as a model for tumor micro-environmental characteristics such as oxygen and nutrients metabolism and diffusion, tumor growth rate and many others.

In vitro- formed spheroids can mimic the oxygen diffusion process and the development of hypoxic and necrotic regions makes spheroids important as biological models in cancer research. The measurement of oxygen profiles, from in vitro formed spheroids, can provide valuable information about the oxygen diffusion as well as the respiration rate in different types of cancer cells organized as a tissue-like structure. There is always a question concerning the size of the hypoxic areas and which is the critical distance from the oxygen supply where hypoxia is induced.

Spheroids can be formed by many different methods and techniques. In this thesis the liquid overlay technique associated with continuous orbital movement of the spheroid culture was proposed. There are many established spheroid formation methods in the literature and in this thesis we describe a new and standardized setup for reproducible, easy-handling multicellular spheroid culture.

The purpose of this thesis has been to test and establish a routine for the creation and culturing of spheroids of 4 different cell lines and to characterize the spheroids regarding extent and degree of hypoxia. Oxygen profiles through the spheroids were recorded by use of microsensors penetrating the spheroid stepwise and performing individual oxygen recordings at short distances both outside and inside of the spheroid structure. Also the investigation of any possible correlation between the oxygen profile and the histology of tumor spheroid is an important objective of this thesis. The aim is for the present study to provide useful information for further studies of radiation effects under controlled oxygenation in a tissue model.

2. THEORETICAL PART

2.1 Cell Biology

A cell is the smallest autonomous unit that may be capable to sustain life on its own. The cells are the main basis of life as we know it, and an understanding of human biology depends on the knowledge of the function of the basic mechanisms of cell biology. Cells of living organisms can be classified on the basis of their structure into two groups: the eukaryotes and the prokaryotes. Eukaryotes keep their DNA in a distinct membrane-enclosed intracellular compartment called the nucleus. Prokaryotes have no distinct nuclear compartment to house their DNA (Alberts et al.2008).

2.2 Cell Cycle

2.2.1 Introduction

The ability of the cells to reproduce in accurate copies of themselves is vital to the sustainment of human life. The cell division is performed through well-studied processes, conserved through the evolution process (Hall E.J., Giaccia A. J., 2012). This controlled process is known as the cell cycle. Two main parts of the cell cycle can be recognized by the use of microscope, the interphase and the mitosis (in the following denoted M-phase).

During interphase, no morphologic difference can be detected through microscope. During M-phase however we can observe the chromosomal condensation by the use of a simple light-microscope with phase contrast optics. The cell cycle contains 5 phases which will be described in the following sections. Interphase constitutes the major duration the cell cycle, in intact tissues lasting for several hours up to in some cases for many days and even weeks. M-phase usually lasts for less than 1 h.

2.2.2 Interphase

This phase includes the G_0, G_1, S and G_2 phases of the cell cycle. In a typical human cell, established and cultured in vitro, the duplication is about 24 h. The cell cycle phases are illustrated in figure 2.1.

2.2.3 Gap 1 (G_1) phase

This phase is positioned between the end of M-phase and the beginning of the S-phase. The two gap phases (G_1 and G_2) are much more important than simple resting time. They provide time for the cell to watch carefully the internal and external environment and assure that conditions are proper and preparations are accomplished before the cell commits itself to the major change in S-phase and M-phase (Alberts et al.2008).

During the G_1 phase, the cell increases in size, it accumulates proteins and mRNA essential for metabolism and performs also other activities like DNA synthesis. Just after the completion of the required proteins and growth, the cell commits itself to the entry of the next phase of the cell cycle, S-phase. The duration of the G_1 phase can vary largely depending on external conditions and extracellular signals originating from other cells. At the end of the G_1 phase it exists a commitment point which is known as Restriction Point (R). After passing this point, cells are initiating the DNA replication stage (S-phase) (Alberts et al.2008).

In case of lack of nutrients, growth factors or under other generally unfavorable extracellular conditions cells often are halted as they reach the R point. They may then be regulated into the resting phase, called G_0 (known also as G_0) phase. The cell can remain in G_0 for days or weeks before it re-enters the cell-cycle and proliferate, or it can be committed for differentiation and never proliferate again.

The G_1 phase is usually the most long-lasting phase of the cell cycle but there are large differences in the G_1 duration among different mammalian cells. The duration of the other phase's vary comparatively little among different cells in different environments (Hall E.J., Giaccia A. J., 2012).

2.2.4 Synthesis (S) phase

After passing the restriction point (R), in late G_1 phase, the cell advances to the second phase of the cell cycle, the S-phase. With all the proteins required for DNA synthesis available, the replication of the DNA takes place in this phase. This process is controlled with high precision to keep to a minimum the risk of mutations in the next cell generation. It requires about 10 to 12 hours to successfully accomplish the S-phase and may take as much as almost half of the cell cycle in a typical mammalian cell (Alberts et al.2008).

2.2.5 Gap 2 (G_2) phase

G_2, or the pre-mitotic phase, is the next phase of the cell cycle and the last phase of the interphase. This gap phase follows the DNA synthesis and is mainly used by the cell to monitor the internal and external environment to secure that conditions are favorable and preparations are accomplished before the cell commits itself to M-phase. The cell growth and the protein synthesis do not stop at this phase of the cycle. The G_2 phase ends when the cell passes the G_2/M checkpoint and the next phase starts (Alberts et al.2008).

2.2.6 Mitosis (M-phase)

Mitosis (also known as M-phase) is the last phase of the cell cycle. At this phase the cell rounds up and M-phases can be easily identified in the microscope. The M-phase has five main stages. The first stage is called prophase where the cell prepares the division by tightly condensing it' s chromosomes into pairs of rigid rods, called sister chromatids, which remain linked together by sister-chromatid cohesion. At the next stage, which is called prometaphase, the nuclear envelope disassembles, the sister chromatid pairs become attached to the mitotic spindle and two opposite poles appears. The third stage of the M-phase is metaphase where the entire sister chromatids align at the spindle equator (Alberts et al.2008).

The next stage is anaphase. During anaphase, the cohesions that bind sister chromatids are destructed and the sister chromatids are pulled to opposite poles of the spindle. The spindle disassembles and the chromosomes are packaged into separate nuclei at the last stage of mitosis, telophase (Alberts et al.2008). Next comes the separation into two different, identical cells.

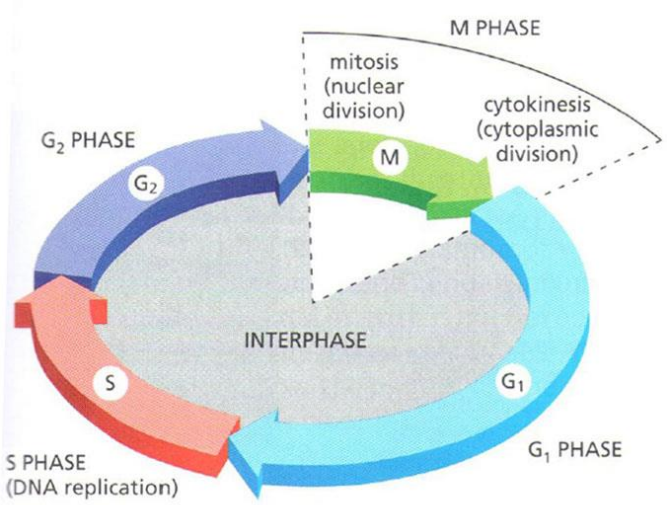

Figure 2.1: The cell cycle with an illustration of the different phases and its main restriction points (Alberts et al.2008). The cell expand progressively in interphase, which is composed of three phases: DNA replication is restricted exclusively to S-phase; G_1 is the gap phase between M-phase and S-phase, while G_2 is the gap phase between S-phase and M-phase. In M-phase, the nucleus and then the cytoplasm divide and two identical cells show up.

.

2.3 Hypoxia

Hypoxia is usually described as the condition of an organism or a tissue which is deprived of adequate oxygen supply. Several chemical and pharmacological agents modify the biological efficiency of ionizing radiation, but none has been found to give such strong radiosensitizing effect as oxygen (Hall E. J., Giaccia A. J.,2012). Regarding radiotherapy of solid tumors, oxygen radiosensitizing has been recognized as a problem since solid tumors are generally characterized by low oxygenation. In solid tumors, hypoxic regions are developed as a result of poor and/or abnormal development of the vascular network as well as intermittent supply and consumption of metabolites (Sutherland, Sordat et al. 1986). Combined with the limited diffusion distance of oxygen and also by characteristic fluctuating blood flow in tumor microvessel, it results in abnormally low levels of oxygen in some areas of the tumor. Cells in such hypoxic areas are relatively radioresistant since they do not experience the oxygen radiosensiting effect.

There are direct and indirect evidence that hypoxia exists in the tumor systems. Hypoxic tumor micro-regions often develop acidosis as well as low levels of vital nutrients such as glucose. These regions usually are associated with neighboring areas of necrosis and toxic products (Sutherland, Sordat et al. 1986). It is demonstrated by several researchers that the extent of tumor hypoxia has a negative impact on the efficiency of radiotherapy most probably related to the resistance of hypoxic cells to killing by radiation. Hypoxic cells have also been found to be resistant to several anticancer drugs. Furthermore, hypoxia in tumors tends to select for a more malignant phenotype, increased mutation rates, and increased expression of genes associated with angiogenesis and tumor invasion (Brown and Wilson 2004).

There are two main mechanisms by which hypoxia can appear in a cancer tumor, one giving rise to long-lasting (chronic) hypoxia and one giving rise to just brief (acute) hypoxia (see figure 2.3). Chronic hypoxia results from the limited diffusion distance of oxygen through the respiring tissue. In contrast to chronic hypoxia, acute hypoxia is the result of the temporary closing of one or more tumor blood vessels containing to the malformed vasculature of the tumor, which lacks smooth muscle and often has an incomplete endothelial lining basement membrane (Hall E. J., Giaccia A. J., 2012).

2.3.1 Chronic Hypoxia

Chronic hypoxia is diffusion-limited and geometrically dependent. The position of a cell in the tumor at a large distance from the nearest oxygen supply may result in permanent lack of oxygen since cells positioned nearer to the oxygen supply use all available oxygen. Total absence of oxygen will eventually drive all cells to death in some hours (Amellem and Pettersen 1991). In most solid tumors such oxygen-inefficiently supplied regions exist and cells within such regions will inevitably necrotize. The necrotic regions indicate the existence of chronic hypoxia. The cells that are positioned between the well oxygenated and the necrotic cells are exposed to a gradient of oxygen supply not necessarily sufficient for normal functioning but also not low enough to kill them.

The existence of necrotic regions in a tumor indicates suboptimal perfusion. The cancer cells are dividing at very fast and uncontrolled rate and the tumor cells thereby accumulate away from the blood vessels and away from positions within the effective diffusion distance of oxygen. Several functional and morphological differences between the normal arterio-venous system and the tumor vasculature have been characterized. One can in reality observe two types of vessels: The normal blood vessels existing in the organ from which the tumor originates; and tumor microvessels arising from angiogenesis initiated by the need of oxygenation of the tumor cells (Brown and Giaccia 1998).

Studies have shown that *'tumor blood vessels are highly irregular, tortuous, have arterio-venous shunts, blink ends, lack smooth muscle or enervation and have incomplete endothelial linings and basement membrane.*'(Brown and Giaccia 1998) As a result, blood flow is often impaired and the vessels are more permeable than the normal ones

The diffusion distance of oxygen is affected by many factors such as the rapid respiration rate of the tumor cells at the proximity of the capillary. It is commonly accepted that the average diffusion distance of oxygen from a microvessel in tumor is about 70 μm. Any cell exceeding this distance from the closest oxygen supplying

vessel is considered necrotic (Hall E. J., Giaccia A. J., 2012). A graphic representation of the situation can be seen in figure 2.2.

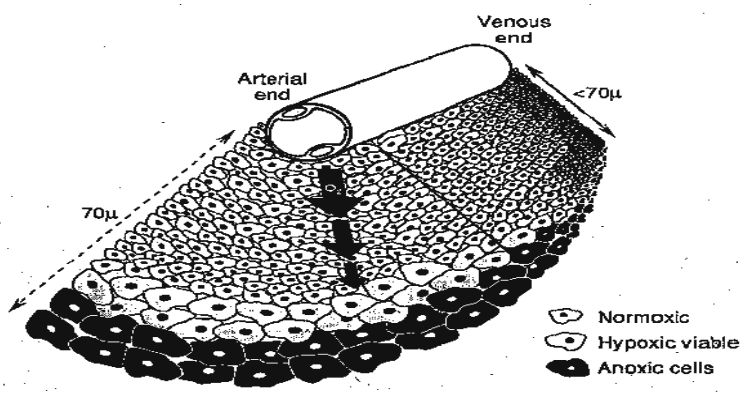

Figure 2.2: The diffusion distance of oxygen from a tumor capillary (Hall E. J., Giaccia A. J., 2012).One should notice that there is an error in this figure related to the size of the cells. Since the cancer cell diameter is usually 10-15 µm, the number of cell layers constituting the 70 µm range of aerobic cells should be drawn as 5-8 (and not 18 as in the drawing in Halls book).

2.3.2 Acute Hypoxia

Acute hypoxia can arise in tumor regions mainly due to unstable blood flow in tumor micro-vessels. Blood vessels supplying tumor cells with oxygen can be blocked, collapsed or temporarily closed in an unpredicted fashion, resulting in inefficient oxygen supply for the surrounding cells. If the blockage of a particular vessel is permanent, the cells downstream will eventually die and be of no further consequence. However, this is usually not the case; at least some of these vessels reopen, thereby reoxygenating the hypoxic cells (Brown 1990).

In the 1980s Martin Brown postulated the existence of acute hypoxia, and it has been confirmed experimentally in transplanted mouse tumors by Chaplin and his colleagues (1986) (Chaplin, Durand et al. 1986, Chaplin, Olive et al. 1987). In 1996 Dewhirst et al. proposed the existence of 2 types of inconstant blood flow; individual short fluctuations in blood flow through single vessels of some seconds duration and periodic fluctuations of blood flow in large vessel groups. The typical duration of such fluctuation can last anywhere in the range of 20-60 minutes (Dewhirst, Kimura et al. 1996). Furthermore, there is evidence that the type of hypoxia depends on the tumor size. In small tumors almost all the hypoxia is chronic, whereas in large tumors considerable hypoxia results from intermittent changes in blood flow (Chaplin,

Durand et al. 1986). Obviously in large tumors the arteriovenous system is not optimal and the blood pressure at some parts of the microvessels cannot compensate with the high pressure of the rapidly proliferating cancer cells leading to collapse of the vessel.

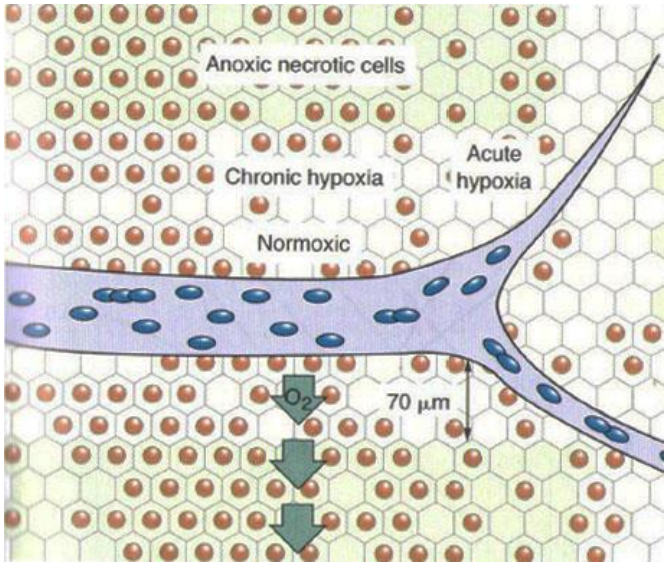

Figure 2.3: Diagram illustrating the differences between acute and chronic hypoxia (Hall E. J., Giaccia A. J., 2012). Chronic hypoxia is developed in cancer tumors as a consequence of the limited diffusion distance of oxygen. Acute hypoxia is the product of provisory blockage of the oxygen supply resulting to oxygen inefficiency in surrounding cells as long as the blockage is active.

2.4 Effects of Hypoxia

2.4.1 Radiotherapy

The Oxygen effect

The increased radiosensitivity of cells during exposure to well oxygenated conditions is widely known in radiobiology as the oxygen effect. For quantification of the oxygen effect a unique quantity is introduced, **the Oxygen Enhancement Ratio (OER)**. This parameter is usually defined as the ratio of the dose delivered under hypoxic condition to the dose delivered under aerated conditions to achieve the same biological effect (thus, an iso-effect parameter). In some cases, especially in older literature, the OER has also been calculated as the difference (meaning the ratio) of the final slopes of the survival curves in presence and absence of oxygen.

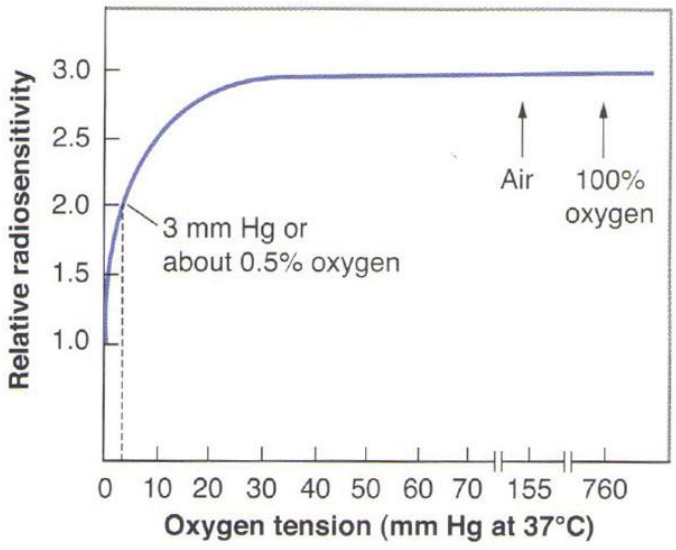

Figure 2.4: Graph illustrating the relation between oxygen tension and relative radiosensitivity (from Hall E. J., Giaccia A. J., 2012). All radiosensitivity values are presented normalized to the radiosensitivity value under anoxic conditions (complete absence of oxygen). The radiosensitivity at pO_2 of 0 mmHg is given the unity value and the presence of as low as 0.5% O_2 can result to radiosensitivity increase by a factor of 2. The presence of pO_2 about 25 mmHg can result in the same radiosensitivity as in the case of dry air and further increase of oxygen concentration will not affect the radiosensitivity values. The authors have in fact used the definition of OER as D_0 (N_2)/D_0 (O_2) in this figure. The authors make clear that this illustration represent an idealized situation and does not represent any experimental results.

By its definition the OER is independent of the amount of oxygen present during irradiation. However the dependence of tumor radiosensitivity on the amount of oxygen is strong. This dependence can be observed in figure 2.4. This figure (2.4) is a representation of how the radiosensitivity is depending on oxygen tension. One should notice that the radiosensitivity is normalized to the radiosensitivity under anoxic conditions (0%). The course of the slope is upward and rises proportional to increasing oxygen concentration. The most spectacular change is at range of 0 to 3 mmHg where the radiosensitivity doubles its initial value. This fact shows that oxygen concentration as small as 0.5% can have dramatic effect to the radiation effectiveness. At increased oxygen concentrations, the rise of radiosensitivity is smoothly reaching a plateau at 3 times more radiosensitive than cells exposed in 0% oxygen, for a range of 5% to 100% oxygen concentration. The plateau shows that there is no gain in radiosensitivity for environments of 5% oxygen or higher.

The oxygen effect is primarily a result of chemical reactions driven by the radical-nature of oxygen, so it can be characterized as a chemical rather than a biological effect. The explanation of the oxygen effect came during the late 1950s/early 1960s as the oxygen fixation hypothesis. The basic principle behind the hypothesis is that DNA lesions are fixed by oxygen binding and thereby prohibited from chemical restoration. With oxygen present, oxygen radicals react with the free radicals in macromolecules produced by ionizations. Without the oxygen presence, such free macromolecular radicals can readily be restituted by sulfhydryl groups on amino acids, but when bound to oxygen the lesions become stable and cannot be restituted. Thus we have increased the lethality by radiation in presence of oxygen. Studies have indicated that the oxygen effect is present even if we induce oxygen to the cell microenvironment within the lifetime of the induced free macromolecular radicals (10^{-5} s)(Hall E. J., Giaccia A. J., 2012).

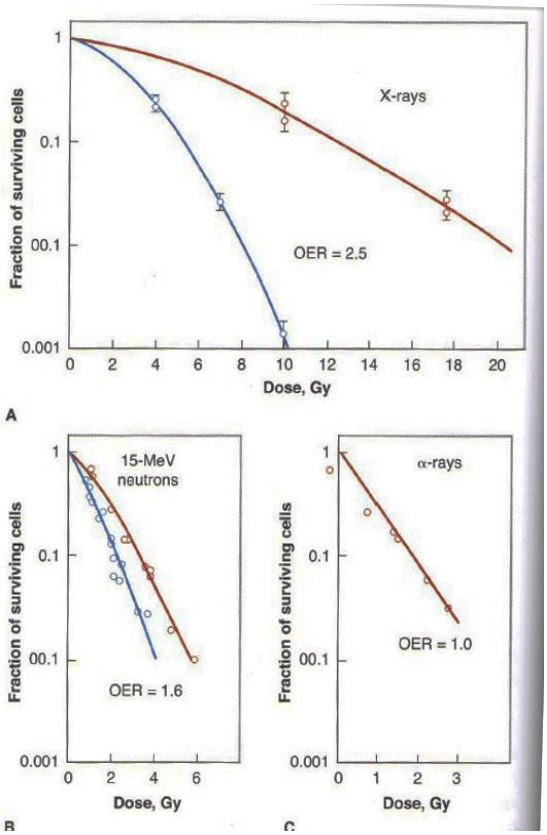

Figure 2.5: Illustration of survival curves of irradiated cells with 3 different radiation types and in hypoxic and normoxic conditions (Hall E. J., Giaccia A. J., 2012). OER representation for different radiation types: (A) X-rays exhibit the largest OER of 2.5 in those graphs (B) OER for 15 MeV neutrons is lower than for X-rays and higher than low-energy α-particles (C) OER has the lowest value (OER=1) for low-energy α-particles.

The effect of oxygen to tumor control depends strongly on two factors. Firstly the OER-value depends on the amount of dose deposited. As we can see from the data in figure 2.5 (Hall E. J., Giaccia A. J., 2012) at low doses (<2-3 Gy) the OER is significantly lower than at higher x-ray doses. Secondly, the OER is strongly dependent on the LET of the radiation. The dependency of OER to the LET is believed to have a direct correlation with the type of damage induced by irradiation to the DNA. Higher LET radiation has more chance to induce Double-Strand Break (DSB) by direct action. With lower LET radiation the damage is dominated by indirect action involving the macromolecular free radicals available. The dependence of OER on radiation type and radiation dose is illustrated in figure 2.5 where it is shown that the oxygen effect is more important for x-rays but is absent for α-rays (Hall E. J., Giaccia A. J., 2012).

2.4.2 Chemotherapy

Hypoxia in solid cancer tumors not only causes crucial complications for the effectiveness of radiotherapy but it is also correlated with resistance to most chemotherapeutic agents. There are plenty of factors associated either directly or indirectly with tumor hypoxia and contribute to anticancer drugs inefficiency. Initially, hypoxia induces delay in cell cycle progression or can even result in cell cycle arrest under severe conditions. The most critical characteristic for the chemotherapy success is that the therapeutic index, for a certain dose level, is increased mainly because the tumor cells are characterized by higher mitotic activity than the normal cells. The decrease of the cycle progression rate will lead to inefficiency of chemotherapy (Brown 1999).

Furthermore, it has been shown that the concentration of chemotherapeutic agents is decreased as the distance from the closest blood vessel increase. Like the case of oxygen, the poor geometry of the vasculature system of tumor is an important factor that is associated with gradient in concentration of the agent. Moreover the anticancer agents are highly reactive and that leads to short diffusion distance for the chemotherapeutic agents (Brown 1999). Additionally, chemotherapeutic agents can be affected by the significantly lower extracellular pH of the hypoxic cells compared to the well-oxygenated cells (Hall E. J., Giaccia A. J., 2012).

2.4.3 Tumor Progression

Hypoxia has been proposed to be correlated with a more metastatic phenotype. It is known that inadequate oxygen supply can inhibit cell proliferation and in severe form can drive the cells to apoptosis and necrosis. In normal human organs the vascular system ensures the optimal oxygen level for all the human cells. On the other hand, in most cases we have regions in cancer tumors that are exposed to hypoxic and severe hypoxic environment. Most of the cancer cells, regions exposed to hypoxic conditions of <1%, will induce apoptosis, but some '*other cells will react to hypoxic stress with adaptive processes*' which in all cases, will induce alteration of gene expression (Vaupel 2008).

Under severe hypoxia <0.01%, genomic alteration and mutagenesis are induced. The malignant progression that results, can be considered as a desperate attempt of cancer cells to adapt to the inefficient oxygenation and inadequate nutrient microenvironment. Such adaptation to hypoxia may result in higher tumor progression rates and further boost of tumor hypoxia (Vaupel 2008). Clinical studies carried out in the United States showed that soft tissue sarcoma patients who received treatment of radiotherapy with measured oxygen tension less than 10 mmHg had double frequency of distant metastasis in comparison to the ones with pO2s greater than 10 mmHg where 35% of the patients developed distant metastasis (Hall E. J., Giaccia A. J., 2012).

2.4.4 Mutation Rate

Genomic instability is a basic feature of cancer cells. As the tumor develops, the mutation rate increases to levels much higher than the spontaneous mutation rates in normal cells. This difference between normal and cancer cells can be explained on basis of the difference in the extracellular microenvironments to which the two different cells are subjected. Low pH values, nutrient inefficiency and regions of fluctuating hypoxia are hallmarks of cancer cell microenvironments and main stress factors that enhance mutation rate (Yuan and Glazer 1998).

Under hypoxic conditions protein synthesis is inhibited (Pettersen, Juul et al. 1986). The increase of mutation rate due to hypoxia can be caused by two mechanisms mainly. First, cells that are exposed to transient hypoxia which is characterized by reoxygenation have shown enhanced levels of several bioactive oxygen radicals which can possibly react with DNA bases. Second, the state of reoxygenation following hypoxia have been proposed to increase the replicating capacity of the cells resulting to over-replication of parts of the genome (Yuan and Glazer 1998).

2.5 Biology of Hypoxia

As early as 1960, scientists started to study the influence of low oxygen on the cell division. Several scientists observed reduced proliferation in microenvironments characterized by low levels of oxygen. Furthermore, it was also observed that long-lasting hypoxia had some specific effects on cell-cycle distribution of cells.

An important article that was published by Koch et al. in 1973b, revealed that cells that were kept for 4 days under severe hypoxia (<25 ppm O_2 in the medium), were arrested almost completely in G_1 phase even if those cells had a very short G_1 phase under air oxygenation (Koch, Kruuv et al. 1973). This publication gave the first important clue for the main effect of hypoxia on the cell cycle. In the same publication Koch et al.(1973) reported that the radiosensitivity of cells arrested in G_1 under severe hypoxic conditions was different from the radiosensitivity of synchronized cells that are in an undisturbed G_1 phase.

This was a clear indication of the existence of a hypoxia induced check-point in the G_1 phase which could not be seen at normoxic conditions. The observation of such a check-point was one year later confirmed by Bedford and Mitchell (Bedford and Mitchell 1974). Pettersen and Lindmo 9 years later demonstrated that the so called G_1-arrest occur only for oxygen concentrations below 0,1% (or 1000 ppm), Additionally, it was shown that total cell arrest occur in G_1-phase only if the oxygen concentration dropped below 100 ppm or 0,01, thus providing us with actual concentrations of oxygen (Pettersen and Lindmo 1983).

Another obvious question was what happens to the cells that are in other phases of the cell cycle than the G_1 under hypoxia. Several researchers using different cell-types published articles reaching to the same main conclusion; that cells under conditions of moderate to severe hypoxia proceed normally from G_2 to mitosis and into G_1 where they had gotten arrested (Bedford and Mitchell 1974).The main damaging effects of hypoxic conditions affect cells that are in the synthesis (S) phase of the cell cycle because the cells in S-phase cannot tolerate the damaging effects under extreme hypoxia (Pettersen and Lindmo 1983, Amellem and Pettersen 1991).

That is the main reason why the hypoxia-sensitive G_1 checkpoint is of special importance for the cancer cells. In addition to the radioprotection by hypoxia due to the oxygen effect itself, the G_1-checkpoint prohibits the entrance into the S-phase under extremely hypoxic conditions because this would be lethal for the cells. The cells in S-phase can tolerate no more than a few hours under extreme hypoxia before they get lethally damaged.

Cell growth by means of accumulation of protein is also inhibited by hypoxia. Kraggerud et al (1995) showed that almost immediately after onset of extremely hypoxic conditions it was observed reduced protein synthesis/accumulation (Kraggerud, Sandvik et al. 1995). Taking into consideration the information that cell proliferation can occur under extreme hypoxia, it can be concluded that protein accumulation is not absolutely needed for the cell to complete G_2- and M-phase of the cell cycle.

Hypoxia by itself does not induce DNA damage and it does not take place activation of ATM or ATR by the mechanism of DNA damage response. However, Bakkenist et al (2003) have shown that under hypoxic conditions cells activate ATM genes even in the absence of DNA damage (Bakkenist and Kastan 2003). Moreover, with cycling hypoxia involving repeated reoxygenation ROS, reactive oxygen species, are created and ROS has been proven able to induce DNA damage (Hammond, Dorie et al. 2003).

The p53 protein is considered a critical tumor suppressor. p53 is a known transcription factor that preserves genomic integrity and is involved in DNA damage repair process, cell cycle arrest and programmed cell death induced by extracellular stress stimuli like hypoxia and DNA damage (Obacz, Pastorekova et al. 2013). Under normal micro-conditions, the level of p53 expression is low and characterized by short half-life. In the case of DNA damage p53 is activated and induces cell-cycle arrest at the G1/S checkpoint which may provide the cell with the necessary time to repair the damage. If the damage cannot be repaired, the cell is driven to programmed death and no more harm occurs to the organism.

2.6 Hypoxia-inducible factor

Hypoxia-inducible factors (HIFs) are transcription factors regulating gene expression under oxygen deficient environment. In well oxygenated cells, the HIF level is low but as the cells experience oxygen alterations in their microenvironment, they respond by homeostatic changes at both systemic and cellular level (Smith, Robbins et al. 2008). HIFs play an important role in those such changes as HIFs are associated with regulation of genes that are involved in angiogenesis, glucose uptake and metabolism, p53 expression, cell proliferation, metastasis and apoptosis (Hall E. J., Giaccia A. J., 2012). Up to date, three members of the HIF family (HIF-1, -2, -3) have been associated with the regulation of transcriptional pathways in response to instable oxygen level.

There are clear indications that hypoxic conditions can result in p53 activation in cells. An et al. (1998) proposed the mechanism for hypoxia induced p53 activation which is widely accepted today. An et al. (1998) showed that p53 activation is triggered by directly interacting with the HIF-1a (An, Kanekal et al. 1998). Recent studies have shown that HIF-1 is very important in the determination of tumor response and radiotherapy. After radiotherapy, reoxygenation of tumor follows, process which results in both HIF-1 stabilization and increased expression of HIF targets by generation the of oxygen reactive species (Hall E. J., Giaccia A. J., 2012).

.

2.7 Cell Culture

2.7.1 3D cell culture

The most efficient method in cancer research and anti-tumor agents testing as the trials performed clinically, but ethical and patient security limitations prevent this method from being extensively employed. To overwhelm these barriers, preclinical tumor models are often utilized to imitate tumor microenvironment physiology tumorgenesis study and anti-cancer agent screening (Zhao, Yao et al. 2014)

The well-established monolayer cell culture has been utilized in cancer studies for many decades, mainly due to its simple function protocols and its reproducibility. The highly regulated cell environment present at two-dimensional cell cultures does not however correspond to microenvironment characteristics of tissues present in vivo. Many studies have shown notable differences to the way two-dimensional and three-dimensional cultures mimic the in vivo tumor microenvironment as far as oxygen and nutrient gradients, cell-cell interactions, cell-matrix interactions and cellular heterogeneity are concerned (Vinci, Gowan et al. 2012).

These limitations and hurdles, led to the need of more sophisticated, 3D tissue structures to be induced in the cancer research. In vitro 3D tumor models based on human cancer cells have been progressively utilized in order to precisely mimic the cancer tumor microcharacteristics. In vitro modeling of cancer tumor is highly developed in the present days, with many different methods and techniques for 3D cancer mimic culture already established: scaffold-based cell cultures, human tissue explants, isolated perfused organs, gel/matrix-based cell cultures and organotypic cultures (multicellular spheroids) (Vinci, Gowan et al. 2012).

Tumor spheroids represent heterogeneous cell aggregates that, when greater than 500 μm diameter, often develop hypoxic regions (Vinci, Gowan et al. 2012). The spheroids represent one of the most utilized in vitro tumor models and they are in-between standard 2-Dimentional cell culture systems and animal tumors as far as the complexity is concerned. Sutherland et al. (1971) first established multicellular spheroids (MCS) as an in vitro model for the systematic study of tumor response to therapy. MCS are spherically symmetric aggregates of cells analogous to tissues, with

no artificial substrate for cell attachment (Sutherland, McCredie et al. 1971) Three-dimensional spheroids are considered highly accurate models to mimic features of tumor microregions, intravascular domains or micrometastases (Vinci, Gowan et al. 2012). Since then, several techniques and methods have been employed in tumor spheroid culture with hanging drops, liquid overlay on agar, spinner flasks, representing the mostly utilized ones in cancer research. A brief description of these different methods is presented in the following paragraphs.

Liquid overlay culture on agar is a commonly used technique for generating multicellular spheroids. Its basic principle contains cells which are seeded on non-adhere surface and the cell-cell interactions are promoted. The flask/dish used for the culture have been pre-covered by agar, agarose or other substrates so as to form a basement membrane/layer where cells are not allowed to adhere but cells can grow on. The cells migrate and meet other cells were they form cell aggregates and potentially spherically symmetric aggregates depending on the cell type (Friedrich, Seidel et al. 2009).

Hanging drop technique is often used in 3D cell culture due to its simplicity, low cost and reproducibility. The principle behind this method is that multicellular aggregates are formed inside drops of cell suspension which is hanging from a supporting surface. Gravity forces are used so as to promote cell aggregation and the growth medium presence provides the cells with all the nutrients, vitamins and salts

Spinner flask technique is based in the rotation movement of the flask that contains the cell suspension. The gentle movement of the flask prevents the cell from sinking to the flasks bottom and aids the cells to stick on each other and form aggregates. The continuous rotation is essential for the final formation of spherically shape multicellular aggregates. Moreover, the rotation is essential for the nutrient and waste exchange rate (Wartenberg, Donmez et al. 2001). Each method has advantages and limitations but simple, standardized and rapid protocols appropriate for routine preclinical drug development studies within academic or pharmaceutical labs are lacking (Vinci, Gowan et al. 2012).

2.7.2 Spheroid Formation Biological Model

The spheroid formation is a complex process. Plenty factors that do contribute are complex cell adhesion, differentiation and morphogenesis. The process of spheroid formation is dominated by the importance of cadherins and integrins while the formation consists of 3 major stages.

On the beginning, the cells rapidly form loose aggregates as cell-cell interactions are favored. The ECM long fibers give the possibility of rapid aggregation and long range of the suspended cells. The ECM fibers contain plenty binding sites for cell-surface integrins (Lin, Chou et al. 2006). After the initial stage of rapid aggregation, the second stage follows. E-cadherin plays an important role in increasing the cell bindings through homophilic cadherin-cadherin bindings between neighboring cells. At the last stage of the spheroid formation, the multicellular spheroids become more compact by strong binding to ECM fibers induced by β-integrins which exist on the cellular surface and interact with the receptors on the ECM fibers (Lin, Chou et al. 2006).

2.8 Techniques to measure tumor oxygenation

2.8.1 Oxygen Probe Measurements

The first device that could provide a reading of the oxygen concentration was developed by Leland Clark in 1953 (CLARK, WOLF et al. 1953). This invention is widely believed to be the initial step at the current bio-sensors development. The Clark-type electrodes consist of two electrodes, one electrode that functions as anode and a second functioning as cathode. The anode electrode is used as reference electrode and the cathode one is considered the working one. The cathode is kept in negative external potential relatively to the anode. Noble metals are used in the cathode so as the surface of the electrode not to take part in the chemical reactions. The noble metals that are most commonly used are Platinum (Pt) or Gold (Au) (CLARK, WOLF et al. 1953).

The oxygen probe measurements are based in the direct injection of the oxygen sensor into the tumor microregion. This technique became popular mainly after the development of Eppendolf probe. The main characteristics of this oxygen probe were the fast response time and the quick, computer-controlled movement through the tumor. This gave the ability for acquisition of oxygen concentrations along multiple tracks in the tumors microregion (Hall E. J., Giaccia A. J.,2012).

The probe measurements can be held both in situ and in vitro. However, this method is applied to clinically approachable tumors suitable for electrode injection. The data from different studies indicate that oxygen measurements acquired in situ by oxygen probes can be used to predict treatment outcomes for various tumor sites (Hall E. J., Giaccia A. J., 2012).

2.8.2 Hypoxia Markers

The concept of utilizing hypoxia markers in the measurement of tumor oxygenation was introduced after the development of 2-nitroimidazoles, hypoxic radiosensitizers that bind permanently to macromolecules in hypoxic cells. The hypoxia markers are administered systematically, but their metabolism by the cells is oxygen dependent. Only in hypoxic environments, cells can metabolize those compounds (Hall E. J., Giaccia A. J.,2012). Pimonidazole is increasingly activated in a hypoxia-dependent way and is covalently bound to thiol-containing proteins in hypoxic cells. Pimonidazole-protein adducts in hypoxic tumor cells can be identified through tumor biopsy, immunohistochemistry, enzyme-linked immunosorbent assay, or flow cytometry (Varia, 1998).

Immunohistochemical hypoxia markers have both some advantages and a disadvantage compared to oxygen probes. The main disadvantage is simply that they cannot give an exact estimate of the degree of hypoxia, i.e. the oxygen concentration. The main advantage is that they can give a detailed estimate of variations in oxygenation between individual cells. Furthermore, they can be used to separate the viable from the necrotic region, and even to separate acute from chronic hypoxia (Hall E. J., Giaccia A. J.,2012). In addition, the formalin-fixed sections permit the study of the spatial distribution of hypoxic and normoxic cells as well as several tumor microenvironmental factors like cell proliferation, blood vessels and angiogenesis (Varia, 1998).

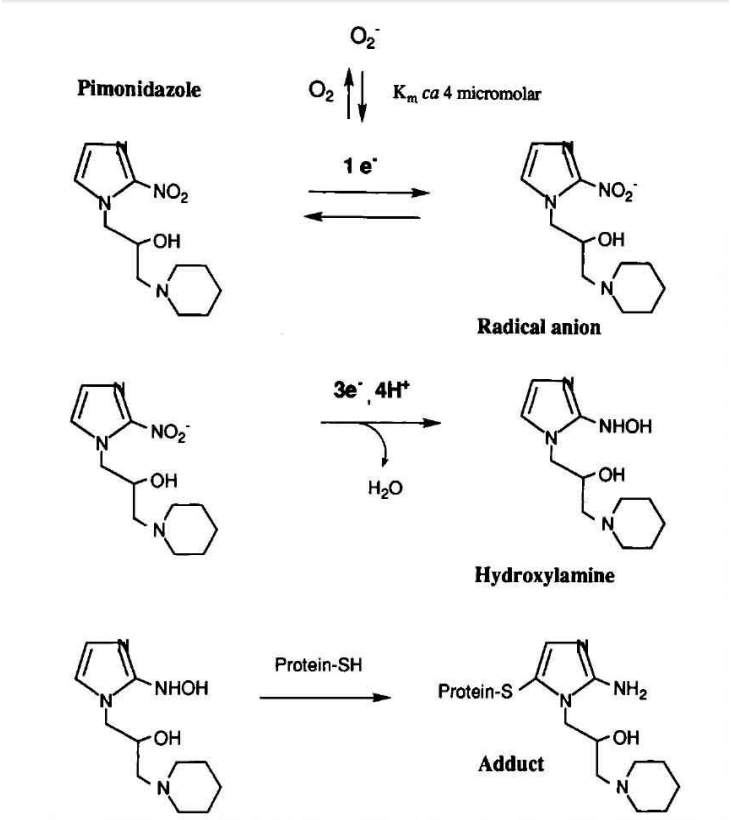

Figure 2.6: Illustration of the in vivo reductive pimonidazole's chemical activation under hypoxic conditions. The activation begins by an electron addition derived from the cellular transport system. After the electron addition takes place, a nitro radical anion is formed. This step is highly oxygen-dependent with oxygen concentrations ≥ 14 μM being able to completely prevent the process. The activated intermediate that binds to hypoxic cells is believed to be a hydroxylamine derivative resulting from the sequential addition of four electrons to pimonidazole. The hydroxylamine intermediate reacts with thiol-containing peptides and proteins to create highly stable adducts which can be uncovered by immunochemical assays (Varia, 1998).

In figure 2.6 is presented a short description of the reductive activation of pimonidazole under hypoxic environment. The presence of oxygen in concentrations higher than 14 μM can inhibit completely the process of the metabolism of pimonidazole by cells. In figure 2.7 an illustration of immunostaining section for pimonidazole binding is presented. Necrotic, hypoxic and fully oxygenated regions are presented in the image as well as blood vessels.

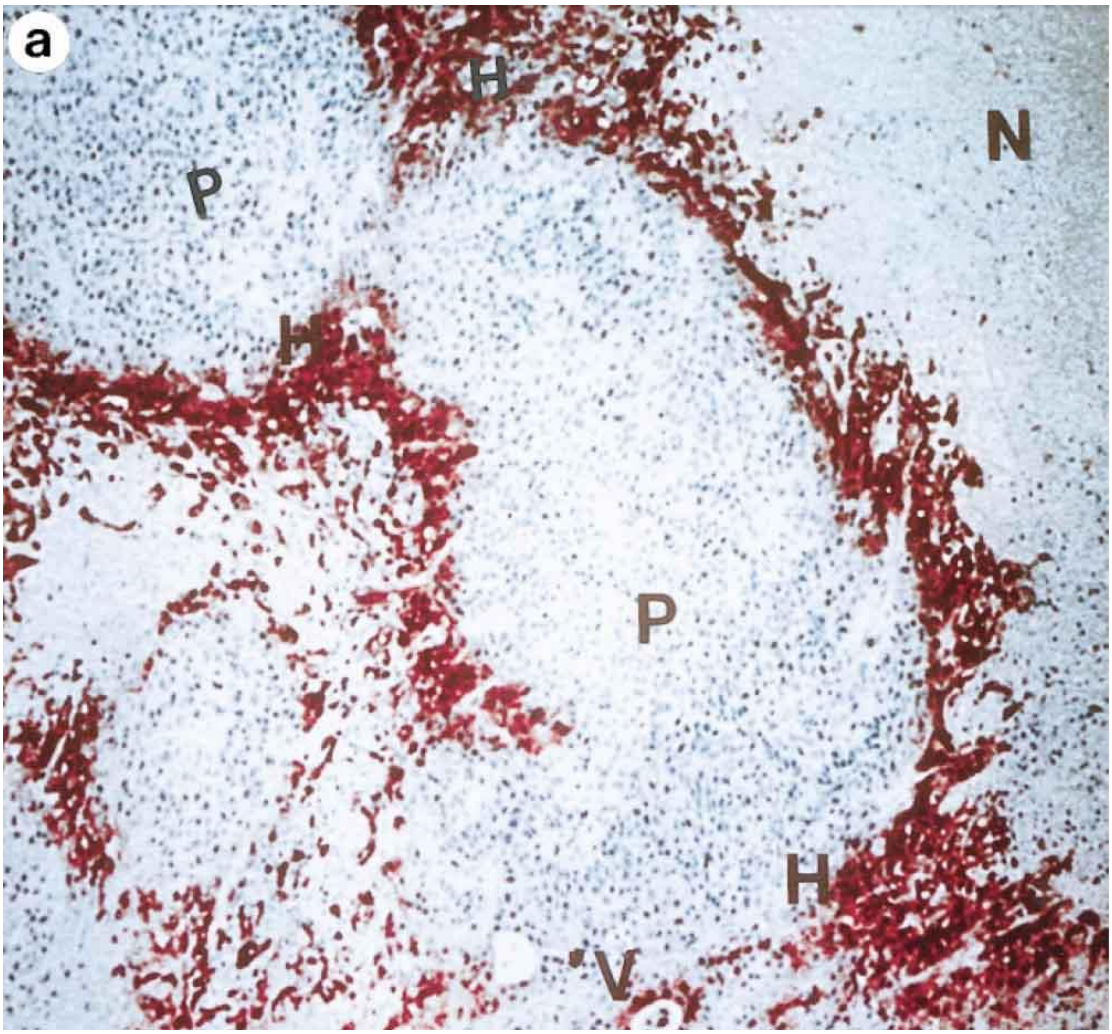

Figure 2.7: This image is from an immunostaining for pimonidazole binding with the red color of the AEC chromogen. Letters H show the hypoxic areas; letter N indicates the region with necrotic cells; Ps represent the proliferating cells; V indicates a blood vessel (Illustration obtained from Varia, 1998).

3. MATERIALS AND METHODS

3.1 Cell cultivation

3.1.1 The cell lines

The established cell lines used in this project are all of human origin, viz colorectal adenocarcinoma HT29, human breast adenocarcinoma MCF-7, human breast tumor T-47D and human glioblastoma T98G.

The MCF-7 cell line originates from tissue sample isolated in 1970 from pleural effusion taken from a 69-year-old Caucasian woman with metastatic breast cancer (Soule, 1973). The acronym MCF-7 stands for Michigan Cancer Foundation-7 referring to the institute the cell line was established. The HT29 cell line originates from tissue sample isolated in 1964 from the primary tumor of a 44-year-old Caucasian female patient with colorectal adenocarcinoma. The cells have epithelial morphology (Fogh, 1977). The T-47D cell line was derived from pleural effusion in metastatic site of a 54-years-old female patient (Keydar, 1979). The T98G cell line was established from tissue isolated from a 61-year-old Caucasian male patient with glioblastoma multiforme (Stein, 1979).

3.1.2 Laboratory equipment

All -laboratory tasks involving cell treatment were performed in a laminar air flow (LAF) bench, on a surface sterilized with 70% ethanol (Kemetyl Norge AS, Norway) before and after any cell tasks were performed so as to ensure an infection-free environment for the cells. In all tasks, disposable sterile plastic pipettes (Sarstedt, Germany) were used along with electric handles (Pipetus-akku, HirschmannLaborgeräte).

3.1.3 Growth medium

For routine cell cultivation in 25 cm^2 cell flasks (Nunc, Denmark) $NaHCO_3$ buffered RPMI 1640 medium, supplied with 10% fetal calf serum, 1% penicillin, 1%streptomycin, 1% L-glutamin and 0,2% insulin[1] was used for all cell cultures, including all experiments regarding generation of spheroids. The growth medium provided all nutrients, vitamins and salts essential for the cells to survive, and calf serum and insulin supplied the cells with the necessary growth factors for proliferation. Penicillin and streptomycin are functioning as bacterial growth inhibitors providing extra protection from bacterial contamination in the medium.

The growth medium is buffered with bicarbonate balanced with 5% CO_2 in the gas phase so that the pH of the cell culture is maintained within the range 7.2 to 7.5. The visual pH monitoring is eased by the addition of the pH- indicator phenol red (Merck, Germany) to the medium. When the color of the growth medium changed from red towards yellowish it was taken as an indication for need of medium change.

3.1.4 Trypsin

Trypsin is a proteolytic enzyme, and it's basic function is to cleave the protein bonds between neighboring cells as well as cells and the substrate on the bottom of the flask. In the present thesis was mainly utilized to detach the cells from the flask floor for cell recultivation. Floating single cells became spherical due to the cell membrane tension. The trypsin used (PAA Laboratories, Austria) was enriched with EDTA (Fluka, Switzerland), binding Ca^{2+} ions necessary for the intracellular protein bonds.

3.1.5 The cell recultivation process

The procedure for cell recultivation was performed as follows. First, the old RPMI medium was removed. Then, the flask was washed with trypsin (PAA Laboratories, Austria) (1.5 ml to a 25 cm^2 flask), which was removed after a minute. This step was repeated before the flask was left for the cells to detach from the bottom. The new flask was prepared by adding 0.5 ml cell suspension to fresh 37°C RPMI medium (4.5 ml to a 25 cm^2 flask).

[1] See appendix H for manufacturers of the chemicals.

The cell culture split ratio is the fraction of the cells from the old flask that is transferred to the new flask by recultivation. The ratio depends on the doubling time of the cells and varies for different cell lines and laboratories. If a ratio of 1:5 was necessary, 2.5 ml RPMI was initially added to the old flask. Then, 0.5 ml cell solution was added to 4.5 ml new RPMI in the new flask to achieve a total of 5 ml medium in the new flask.

3.1.6 Medium change

2-3 days following recultivation, a complete medium change was performed. The fresh medium ensured a fresh and new cellular environment by providing new nutrients and correct pH. Afterwards the flask was placed back in the CO_2- incubator so as to ensure optimal growth temperature and air composition.

3.2 Spheroid culture

3.2.1 Cell lines

The cell lines used in the spheroid culture were HT29, T-47D, MCF-7, and T98G. For all the cell lines RPMI was used as growth medium. All the cell lines were cultivated and sustained as monolayer cultures with the process that have been described in chapter 3.1.

3.2.2 Laboratory equipment used

All the laboratory equipment used for the monolayer cell culture was used also for the spheroid culture. Additional equipment exclusively used in the spheroid culture were: the orbital shaker (Standard Orbital Shaker, Mode l000, VWR, USA) on which the spheroid flasks were placed during cultivation (figure 3.1); and 15 mL conical based tube (Sarstedt, Germany) used mainly for the medium-exchange stage of the spheroid formation experiments.

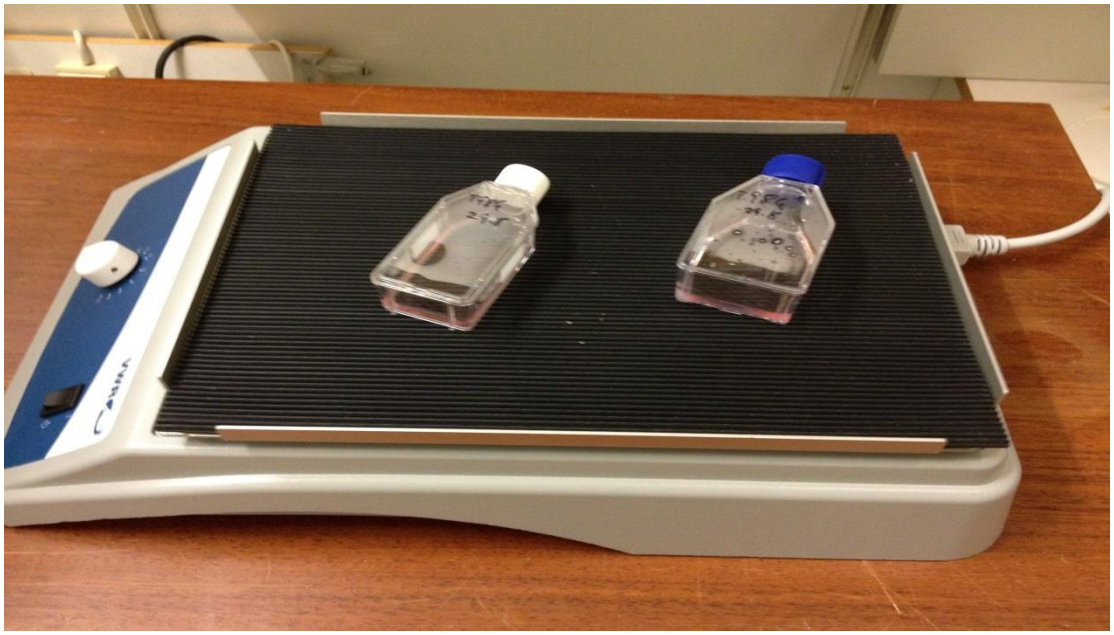

Figure 3.1: Illustration of the stirred liquid-overlay spheroid culture. The shaker provides orbital motion to the spheroid culture. In the first experimental sequence, the 25 cm^2 cell culture flasks were coated with 1.5% agarose layer of 1 mm thickness. In the second experimental sequence, experiments were performed to grow spherically symmetric cell aggregates without the use of agarose coating on the bottom of the used flask. The shaker operated in two different orbital speeds 60 and 75 rpm.

3.2.3 Spheroid culture with agarose coating

3.2.3.1 Flask preparation

For the spheroid culture 25 cm^2 cell culture flasks were utilized. In consideration of the cell adhesion properties, the cell-cell interactions could be enhanced by introducing a 1mm thick layer of agarose on the bottom of the 25 cm^2 culture flask so as to inhibit any cell-substrate interactions. Therefore, the bottom of the flask was coated with 1.5% agarose gel (Agarose Type I Low EEO, Sigma-Aldrich, USA) ahead of the cell addition.

At first, the agarose gel had to take liquid form so as to be transferred in the flask. The agarose gel was placed in the microwave oven and remained there until it started to boil. Thereafter, the flask with the liquid agarose was transferred to the LAF bench and 2,5 ml of agarose were transferred to the 25 cm^2 cell culture flask. Then, manual tilting and movement of the flask was performed so as to ensure homogenous spatial distribution of the liquid. The flask was left with the cap closed until the agarose cooled and the separation layer were formed.

Later the flask tip was opened again and 2.5 ml of RPMI cell growth medium were transferred to the flask. The cap of the flask was then closed and the coated flask was left overnight in a shelf of the laboratory. The next day the flask was opened again, the old medium was removed and 2.5 ml of fresh RPMI were transferred. The flask was then securely closed and moved to its previous location in the shelf. After 4 hours, the old RPMI medium was disposed and the flask was ready for use.

By the RPMI addition processes, the water and medium content of the gel was given time to complete mixing. Thus, after the first 2.5 ml of RPMI the medium content of the gel would be 50%. After the second change, the RPMI content of the gel increased, reaching value of 75%. The main purpose of this process was to prevent a vast drop of nutrient content and mainly the osmolarity drop after addition of cell suspension.

3.2.3.2 Spheroid formation

In brief, spheroid formation was initiated by gentle orbital shaking of 25 cm^2 flasks having gel coating as described above and with cell numbers seeded as described in table 1. The whole procedure took place in a walk-in incubator room at 37^o C. For all the cell lines used, the process was the same with only the starting cell density to differ. When the confluence of the monolayer culture had reached 90%, cells were trypsinized and a predetermined number of cells were transferred to the agarose-coated flask. In table 1 the number of cells transferred and the utilized orbital stirring speed are reported. The cells in the spheroid culture flask were supplied with 8ml of RPMI growth medium. So that the final volumes of the flask was 8 ml of RPMI and 2.5 ml of agarose gel. The cell seeding day was mentioned as day 0 in all the experiments performed and reported in the present thesis.

Table 1: Overview of the parameters utilized in the experiments performed and reported in the present thesis which involve the use of agarose-coated 25 cm^2 cell culture flask. With the notion "--" is presented a parameter combination that was not utilized in the experiments performed in present thesis.

Shaker speed	T-47D ($x10^6$)		HT29 ($x10^6$)		MCF-7 ($x10^6$)		T98G ($x10^6$)	
60 rpm	1.6	--	1.4	2.7	2.4	4.5	0.9	--
75 rpm	1.6	4.1	1.4	2.7	2.4	4.5	0.9	1.3

All the pre-agarose-coated 25 cm^2 flasks were immediately placed in the CO_2-incubator after cell seeding and remained there for two hours with the cap of the flask open. The main purpose of this step was equalization of the CO_2 content in the flask with the CO_2 incubator so as to ensure the 5% necessary for the cell cultivation.

When the CO_2 equalization process came to an end, the spheroid culture flasks were removed from the incubator. It was essential to close the cap of the flask just when we removed the flasks from the incubator so as to maintain the CO_2 level at 5%. The flasks were transferred to the walk-in incubator of the cell laboratory and placed on the platform of the orbital shaker (Standard Orbital Shaker, Mode l000, VWR, USA). The shaker was able to deliver an orbital motion with a speed ranging from 30 to 300 rounds per minute (rpm). The 2 main stirring speeds applied in the experiments were 60 rpm and 75 rpm. The shaker was placed in the incubator room at 37,0 ^oC, temperature which is optimal for the cell growth and division. We used an inverted microscope (Diaphot, Nikon, Japan) connected to an microscope camera (PaxCam, USA) to measure and photograph the spheroid diameters at different days of the experiments. An illustration of the spheroid culture can be seen in figure 3.1.

3.2.3.3 Medium and Flask change

After 2 days following recultivation, the medium of the spheroids had to be exchanged with fresh medium, as indicated by the color of the pH-indicator phenol red. The fresh medium ensured a fresh and new cellular environment by providing new nutrients and correct pH. When the transfer of the cell aggregates and spheroids was performed, the basic process of spheroid transfer to new flasks was to place all the medium and the cell aggregates into a 15 ml conical based tube (Sarstedt, Germany) and just leave the cell aggregates to sink, to the tube bottom, for 15 minutes.

Afterwards, the old medium was removed from the tube until only the aggregates and a very small portion of the old medium remained inside. Then 8 ml fresh medium were added. The tube content was then transferred to a new agarose-coated 25 cm^2 flask. Immediately after the transfer was performed, the flask containing the cell aggregates, was placed in the CO_2-incubator with the cap open for two hours so as to obtain 5% CO_2 in the flask. At the end, the flask was removed from the incubator, the cap was closed and the flask was brought back to the shakers platform at the same speed as at the start of the culture.

After the first medium change, the medium changes were given every 2 days. When spheroids had grown to form large inhomogeneous aggregates, they were removed from the culture so as not to interrupt the homogeneous growth of the other spheroids in the culture.

3.2.4 Spheroid culture without agarose coating

3.2.4.1 Flask preparation

No special preparation was needed in this case as there was no agarose-coating in these experiments. The same type of 25 cm^2 cell culture flasks was used as in the monolayer culture.

3.2.4.2 Spheroid formation

As described for spheroid formation with agarose coating, the shaking method without agarose coating was also utilized for the culture of the spheroids. For all the cell lines used, the process was the same with only the starting cell density to differ. At the day that the confluence of the monolayer culture had reached 90%, the cells were trypsinized. At this stage, the initial cell density of the spheroid culture had been decided in advance and the desired cell number were transferred to the 25 cm^2 flask after the trypsinization of the monolayer 25 cm^2 cell culture flask. The cells in the spheroid culture flask were suspended in 8ml of RPMI growth medium. The different starting cell numbers and stirring speed combinations used in the second set of the cell culturing experiments is illustrated in the table 2.

Table 2: Overview of the parameters utilized in the experiments performed and reported in the present thesis in 25 cm^2 cell culture flask without any agarose coating. With the notion "--" is presented a parameter combination that was not utilized in the experiments performed in present thesis.

Shaker speed	T-47D ($x10^6$)		HT29 ($x10^6$)		MCF-7 ($x10^6$)		T98G ($x10^6$)	
60 rpm	1.6	4.1	1.4	2.7	--	--	--	1.3
75 rpm	1.6	4.1	1.4	2.7	2.4	4.5	0.9	1.3

The process afterwards was the same as in the previous experiments and the reader is referred to the chapter 3.2.3.2 and for additional information.

3.2.4.3 Medium Change

As was described for spheroid formation with agarose coating, the first medium change was held after 2 days on the shaker. The exchange of the medium with fresh RPMI was routinely done every second day. The aggregates were not transferred to a new flask in all experiment remaining in the same flask for the whole duraation of the experiment. For the medium change, a 15 ml conical based tube (Sarstedt, Germany) was utilized as previously described. The cell aggregates were left to sink in the medium and later the old medium were disposed. Fresh growth medium was added to the tube until the volume reached 8 ml. Then the cell aggregates suspension were

transferred back to the 25 cm^2 flask and transferred to the CO_2-incubator for two hours with the cap of the flask being open.

Afterwards, the flask's cap was closed and the flask was transferred to the orbital shaker in the walk-in incubator room of the cell laboratory. An illustration of the spheroid culture is shown in figure 3.1.

3.3 Oxygen profile measurements

The microsensor used for the oxygen concentration profiles acquisition was provided by Unisense A/S, Aarhus, Denmark. It involved an oxygen microsensor (figure 3.2) attached to a computer-controlled micromanipulator. The micromanipulator was mounted on the stage part of a microscope inside the InVivo hypoxia cabinet (Ruskinn, Great Britain). The oxygen microsensor had a tip diameter of 10 μm and a guard-cathode (not illustrated in figure 3.2) to stop any oxygen diffusion from the electrolyte reservoir affecting the oxygen-sensing cathode (Pettersen, 2005).

Electrolyte was used in the sensor to shield signals from interacting with electrochemical fields, thus making unnecessary the use of a noise-shielding Faraday cage. The main working function of the probe follows the process described in the following lines. The oxygen diffuses through the sensors silicone tip membrane to an oxygen-decreasing cathode, which is polarized against an internal Ag/AgCl anode. The oxygen partial pressure at the area surrounding the sensor is indicated by the electron flow from the anode to the oxygen-reducing cathode (Pettersen, 2005).

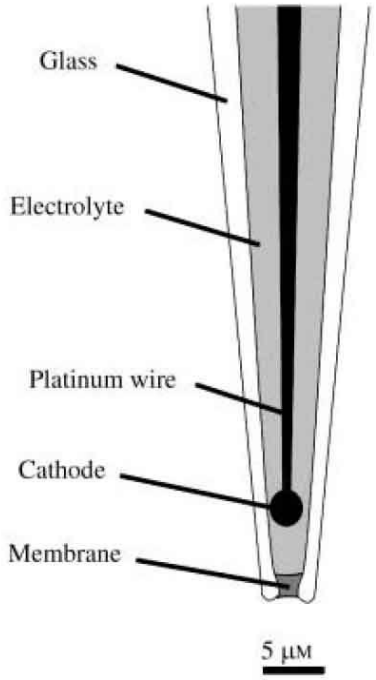

Figure 3.2: Demonstration of the sensor tip of the OX-10 oxygen probe used to obtain oxygen concentration profiles (Illustration from (Pettersen, 2005)).

The weak electrical current (10^{-12} -10^{-10} A) produced was acquired by the Unisense picoammeter PA2000. The picoammeter contains two main channels and has a built-in polarization source. The oxygen microsensor was fixed at the motorized micromanipulator mounted on a metal frame of the microscope stage. The motorized micromanipulator was controlled with a motor controller (MC-232) connected to a laptop computer running the dedicated computer software SensorTrace Profiler 1.1 (Unisense A/S, Aarhus, Denmark) (Pettersen, 2005).

3.4 Experimental Set-up

3.4.1 Dish preparation

Lower agarose layer

The dish used in the oxygen profile measurements was a 35 mm diameter Petri dish (EASY GRIP^{TM}, Falcon, USA)(area 961.63 mm^2). In order to produce the lower layer of agarose to define the distance of separation between spheroids and dish bottom, the bottom was coated with 2 ml of 1.5% agarose gel (Agarose Type I Low EEO, Sigma-

Aldrich, USA) before the spheroids were added (parallel to the bottom coating described for the flasks). Volume of 1 ml of gel corresponds to layer with thickness of 0.96 mm. Thus, the 2 ml agarose gel constitutes a 1.92 mm agarose layer over the bottom. The recipe for the agarose gels can be found at Appendix E. As the temperature fell, the agarose began to gel and covered the bottom of the dish. After the end of the gelling process, 2 ml of RPMI medium were added on the top of the lower agarose layer and the dish was placed in the incubator and remained there overnight so as to obtain free diffusion into the gel of nutrients, salts and vitamins vital for the cell survival.

By this process the agarose content of the gel was not reduced but only the medium in water content would change. After the first equilibration step the medium to water content of the gel reached to 50%. The next day, the medium was removed and a new portion of 2 ml of fresh medium was added in the dish. Immediately the dish was returned to the CO_2-incubator were it stayed for at least 4 hours so as to ensure complete equilibrium of concentrations and steady-state after mixing.

The dish was then removed from the CO_2-incubator and the growth medium was again completely removed. After the second equilibration step the medium to water content reached 75%. Those steps were very essential so as to prevent the vast drop of nutrient content, and most importantly the osmolality drop after the upper agarose layer with the spheroids was added.

After this procedure, the lower agarose gel was considered ready to serve as a supporting layer for the upcoming agarose and spheroid mixture (figure 3.3). The main function and necessity of this lower agarose layer at the bottom of the dish was to prevent the spheroids from falling down to the plastic surface and attach to the substrate. It furthermore served as a protective means against possible damage to the sensor tip which could be caused from the interaction with the bottom of the dish.

3.4.2 Spheroid immobilization

Initially the selected spheroids were manually removed from the 25 cm^2 flask and placed in a 15 ml conical based tube (Sarstedt, Germany) with 0.5 ml of medium coming from the same flask. To ensure immobilization of the spheroids, a new upper agarose layer was added on the top of the lower agarose layer, having the spheroids suspended. In order to keep temperatures for the spheroids within a physiologically acceptable range a different agarose type than in the previous step was in this case preferred for use. The upper 1.5% agarose gel (SeaKem® LE, Lonza, USA) was chosen mainly because the SeaKem agarose has its gelling temperature at a range of 34.5 ^{o}-37.5 ^{o} and thus maintains its liquid phase at temperatures which are not dangerous for the normal function and survival of the cells.

The agarose content of the SeaKem agarose gel was 1.5% and the formation recipe is presented in Appendix E. The SeaKem 1.5% agarose was first heated until it boiled. Then left to cool until its temperature was sufficient for use (37 ^{o}C). Afterwards 1.5 ml of the liquid SeaKem 1.5% agarose were placed in the same 15 ml tube as the 0.5 ml spheroids suspension. The total mix was then immediately placed in the Petri dish and left there until the agarose had completed gelling. During the period before gelling the spheroids sank down to the lower agarose gel layer and thus were positioned directly on the top of that layer during the experiment (figure 3.3). The final agarose content of the upper layer was 1.125%. As the final volume of the upper layer was 2 ml the thickness of the layer was the same as the lower one (1.92 mm).Then 3 ml of medium (RPMI) were placed on the top of the upper spheroid-containing agarose layer so as to ensure the normal supply to the spheroids of necessary nutrients and growth factors. The nutrient consumption of the spheroids was almost homogenous as both the lower layer and the upper layer contained nutrients and vitamins. At the end, the dish was safely transferred to the InVivo hypoxia cabinet so as the oxygen profiles acquisition experiment to be performed.

3.4.3 Calibration of the microsensor

Based on the fact that the microsensor reading was proportional to the existing oxygen concentration (i.e. a linear calibration curve) at the sensor tip, it was found acceptable to calibrate the software at two known oxygen concentrations (Stenersen Espe, 2009). This was done by first setting the O_2 concentration at 19% in the cabinet's gas phase and using it as reference point and second, to read the signal in an anoxic solution made from 0.2 g sodium sulfate (Sigma-Aldrich, USA) in 10 ml Milli-Q water (Millipore, France) and defining that to be 0% O_2. For the precise measurement of the sodium sulfite a highly sensitive weight (AG245 Mettler Toledo, Switzerland) was used. The process of determining and reading the calibration points followed strictly the dedicated calibration section of the Unisense software.

3.4.4 Experimental Set up and procedure for measuring oxygen profiles

All the oxygen measurements were performed in an InVivo hypoxia cabinet in a gas mixture controlled by a dedicated gas mixer (Ruskinn, Great Britain). The oxygen concentration in the gas phase of the cabinet was kept at a fine controlled level of 19% for the complete duration of the experiment. The dish containing the spheroids was placed on the associated dish holder of the manually operated XY microscope stage. A rough layout of the experimental set-up is illustrated in figure 3.3 and 3.4. The next step was the determination of the appropriate spheroid for oxygen profile measurement. The spheroids picked for measurement were those which were isolated in such a way that they did not have any close neighboring spheroid. This choice was done to avoid a situation where the oxygen consumption rate should be affected by the respiration of other proximate spheroids.

Before measurements started, the center of the spheroid was identified. Initially we focused the microscope on the selected spheroid until we found the plane passing from spheroid's center. The procedure could not be guided through direct observation through oculars on the microscope since the microscope was positioned within the cabinet. Instead all the micro-movements of the mechanical stage and the oxygen sensor were recorded online and visualized on the TV-screen by the use of a digital

microscope camera (OptixCam,USA). Photographs were acquired and stored directly by the software program ToupView (ToupTek, China). Once the focus point of the center of the spheroid was found, the spheroid was withdrawn from its initial position by the help of the mechanical stage knobs (cross-table) on the microscope. Then the sensor slowly was driven deeper in the dish until the sensor tip reached the focus point of the microscope objective.

For all the movements of the sensor the computer-controlled micromanipulator mounted on the microscope was used. The exact position of the sensor tip at the focus plane of the spheroid's center was marked on the TV-screen. Then the sensor was withdrawn back and the spheroid center placed at the marked point so as to ensure that the oxygen sensor would pass through the center of the spheroid. All the manipulations of the spheroid position were guided by the help of the TV-screen and the mechanical stage knobs of the microscope. For the TV visualization of the microscope camera the ToupView (ToupTek, China) software was used.

Finally, the sensor was positioned outside the spheroid, but at a reasonable distance from the spheroid surface and within the upper agarose layer, and the measurement process was initiated by the computer-program moving the sensor stepwise towards and through the spheroid while performing measurements. For the oxygen profile, the sensor was inserted with an inclination of 45 ^{o} and was advanced by single steps of 19.45 μm. Before each measurement the sensor stopped for about 20 s to obtain steady state O_2values.

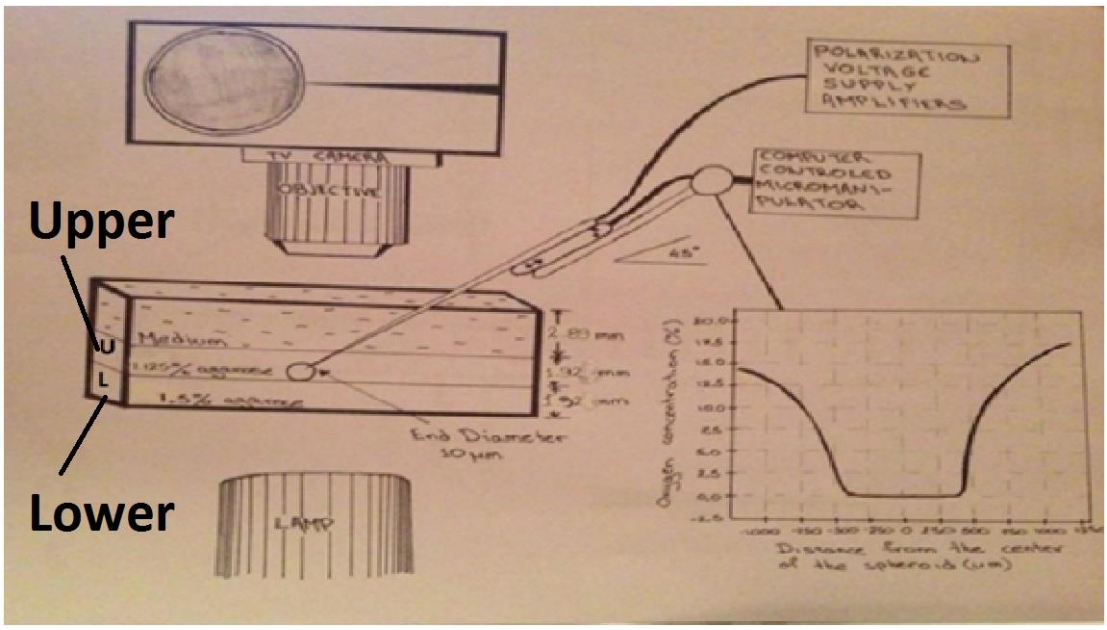

Figure 3.3: Measurements of local oxygen concentration in spheroids with 10 µm oxygen probe. The sensor was inserted with an inclination of 45 º and the micromanipulator was programmed for a step-length of 19.45 µm. **For the lower dish coating, 1.5% agarose layer of 1.92 mm was used, indicated with the notion L**. Immobilization of the spheroids in space was accomplished by the use of 1.125% agarose matrix of thickness 1.92 mm. **The upper agarose layer is indicated with the letter U**. To ensure the nutrients and vitamins supply, 3 ml of medium were added on the top of the upper agarose layer. The fine movement of the electrode was done by a computer-controlled micromanipulator. All the movements were visualized on the TV-screen by the use of a digital microscope camera.

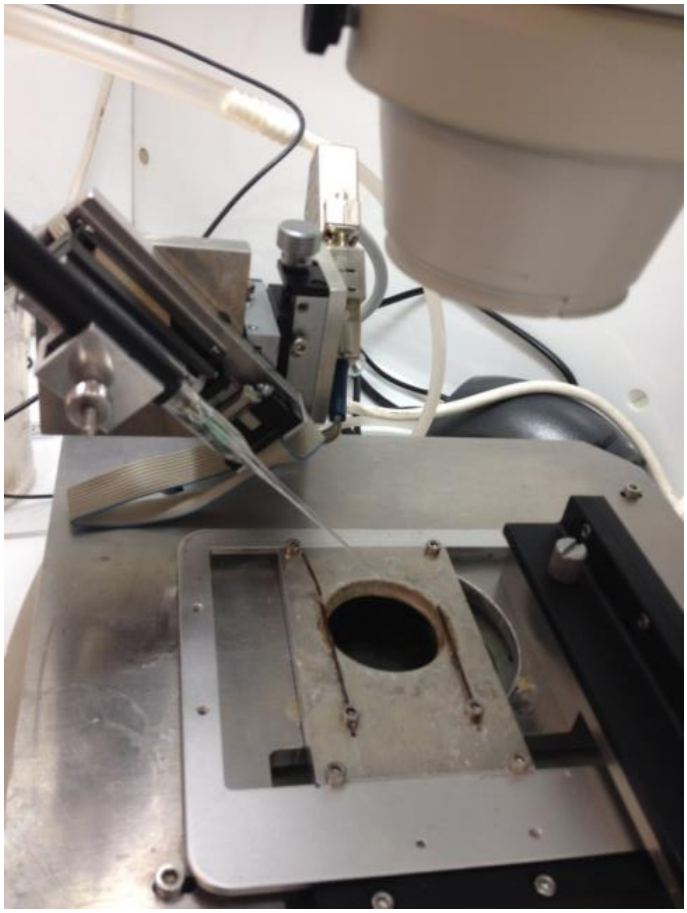

Figure 3.4: Picture illustrating the manipulator-controlled microsensor, mounted on incline of 45 °. The dish containing the spheroids was placed on the associated dish holder of the manually operated XY microscope stage.

3.5 Measurement of the oxygen diffusion gradient in agarose gel

3.5.1 Cell lines

This experiment was performed in order to test the oxygen diffusion rate in agarose gel compared to in medium. For this purpose we needed an oxygen-consuming entity within the agar and we chose to use a suspension of single-celled T-47D-cells.

3.5.2 Glass tube preparation

In this experiment a 10 cm long glass tube (Pyrex, Great Britain) was used as a container of the agarose, cells and medium mix. Two cell culture flasks with T-47D breast cancer cells were specially prepared for that experiment. When the cells reached 100% confluence in the monolayer culture (the 25 cm^2 cell culture flasks were used), the cells were all harvested and placed in the glass tube suspended in 1 ml of RPMI. Then, 1 ml of prewarmed 1.5% agarose in liquid form was added to the glass tube and left there until the temperature fell sufficiently for agarose gelling. From this process the agarose content of the cell-containing agarose layer, fell to 0.75%.

Afterwards, a solution containing 0.5 ml of RPMI and 0.5 ml of 1.5% agarose was added on top of the cell-containing agarose layer. The achieved agarose content of the cell-free agarose layer was the same as the cell-containing one (0.75%). When the cell-free agarose layer had completed gelling, 2 ml of fresh RPMI were added to the glass tube. Immediately the glass tube was covered with aluminium foil and placed in the CO_2-incubator where it remained for 30 minutes. After this time interval, the used medium was removed and 2 ml of fresh RPMI was added in the glass tube which was again covered with aluminium foil and transferred to the CO_2-incubator were it remained for 30 minutes more.

The glass preparation ended with the dispose of the old medium and the addition of 2 ml of fresh RPMI. Then the glass tube was transferred to the InVivo hypoxia cabinet (Ruskinn Technology Ltd., Bridgend, Great Britain) where optimal environment of 19% oxygen and 5% CO_2 were provided. The oxygen gradient was built up only in the vertical direction as no oxygen could penetrate through the glass tube walls. The probe measured in a range of 1 cm with a step size of 100 μm. The initial position of the microsensor was in the upper layer filled with growth medium.

The thickness of the 2 agarose layers were measured by the use of a ruler. The cell-containing agarose layer was 1.5 cm, the cell-free agarose layer was 0.65 cm and the final medium layer on top had a thickness of 1.35 cm.

3.5.3 Experimental set up

Oxygen concentrations recorded in this experiment were given as %. During O_2-measurements, the set-up (Figure 3.5) was kept within the hypoxia work-station operated at 19.0% O_2 and 5% CO_2 with relative humidity of ~80-100%. The Clarke-type, 10 µm end diameter, oxygen microsensor used in the previous experiments was used also here. It was connected to a picoammeter and mounted on a computer-controlled micromanipulator, both connected to a desktop computer with integrated software. Measurement logging and motor control (all manufactures by UniSense, Aarhus, Denmark) was employed to acquire oxygen concentration as a function of the position of the microsensor in the system.

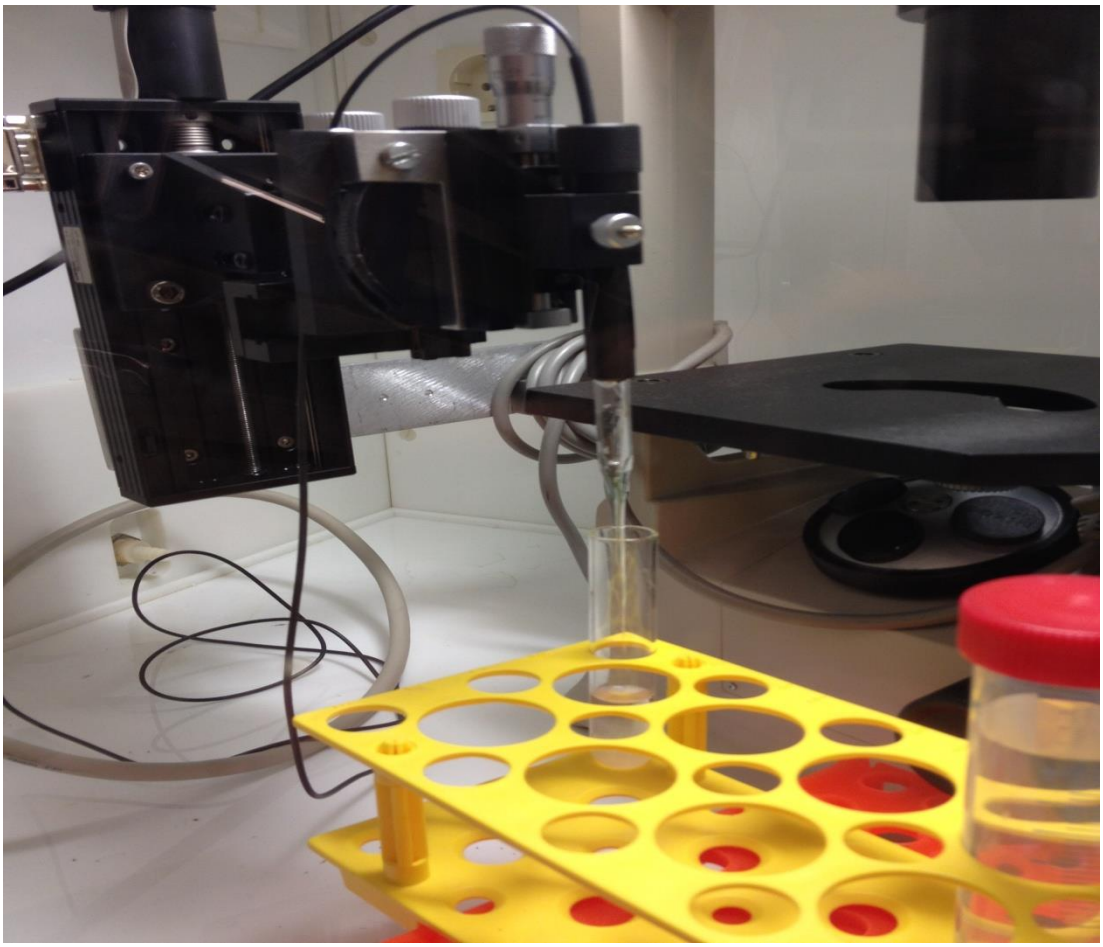

Figure 3.5: The set-up for measuring oxygen concentration is shown as positioned inside the InVivo hypoxia cabinet. The oxygen microsensor was mounted on a motorized micromanipulator and measurements were performed with a step-length 100 µm over a range of 1 cm covering partially the medium and the agarose layer regions.

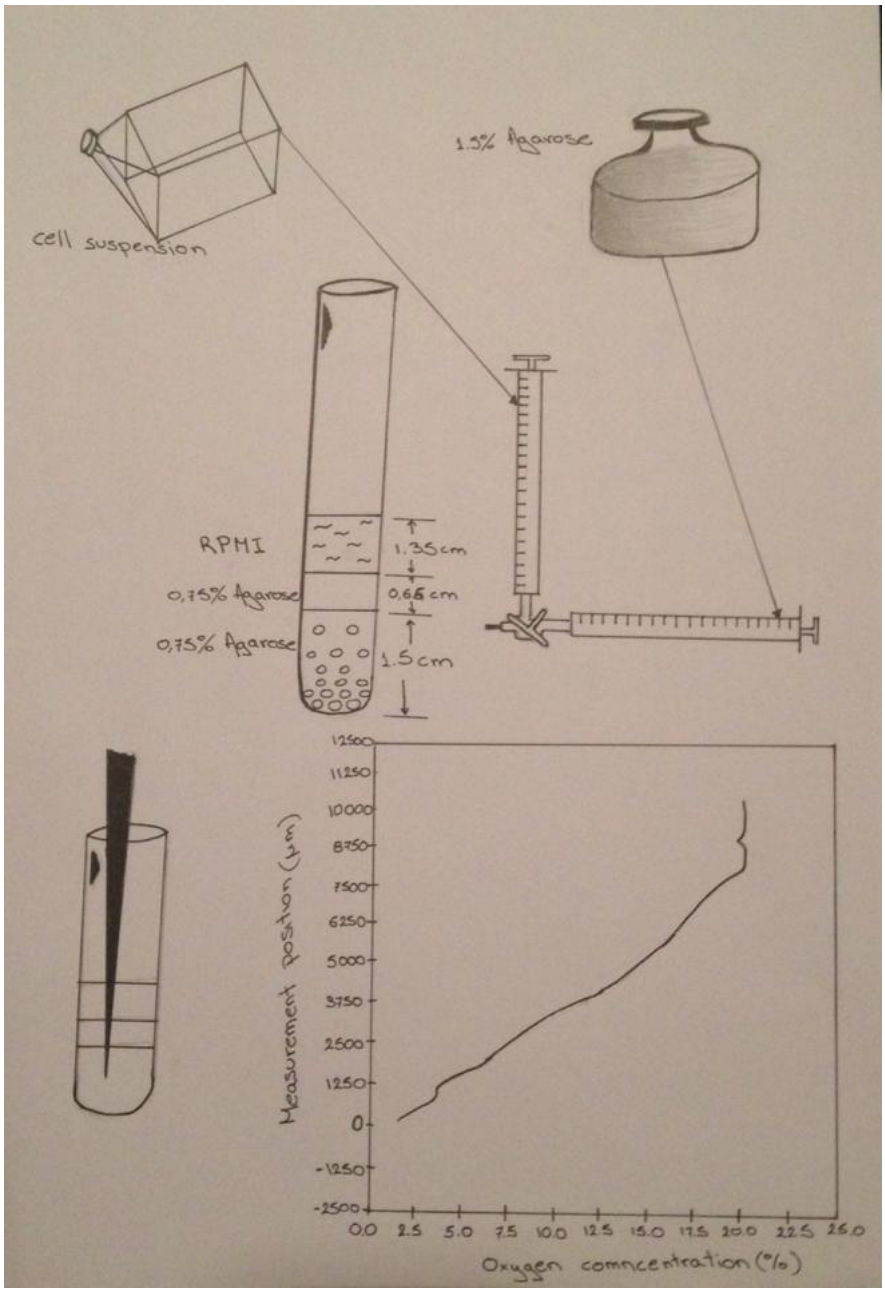

Figure 3.6: Illustration of the sample development, system dimensions, methods and characteristic data. Measurements of oxygen concentration in the agarose gel filled with T-47D cells by 10µm oxygen probe. The sensor was inserted vertically and operated with a step-length of 100 µm. The cells were immobilized in the 0.75% agarose gel of thickness 1.5 cm. The upper cell-free 0.75% agarose layer had thickness of 0.66 cm. To ensure the nutrients and vitamins supply two equilibration steps with 2 ml of medium and a final addition of 2 ml of RPMI were performed prior to the initiation of the measurements. The fine movement of the electrode was done by a computer-controlled micromanipulator.

For the calibration of the sensor we followed the same procedure as was described in chapter 3.4.3. In this experiment, acquisition sequences were programmed. For the presentation of the data, Origin 8.5 (OriginLab, Northampton, MA, USA) was used. A flow-chart illustrating the sample development, system dimensions, methods and characteristic data are shown in figure 3.6.

3.6 Mathematical model of oxygen diffusion to growing spheroids

The spheroid culture was based on cultivation in stirring suspension. In this case the spheroids were covered with medium and cultured in stirring agarose-coated flasks as described in chapter 3.2. This experimental set up requires the available oxygen to diffuse from the air contained in the spheroid culture flask, through the growth medium to the spheroids in the culture. The medium and the air in the culture flask were renewed every 2 days after the first spheroids were formatted in the culture. This analysis has been concentrated on the case that the spheroid is stable and is growing in stationary medium. Any movement of the spheroid, as in the case of our experiments, will disrupt the external concentration gradient, resulting in change of the oxygen gradient within the spheroid. Unfortunately the continuous orbital movement of the spheroid in the experiments of this thesis, is inducing high complexity in the development of a mathematical model and may be a challenge for future work and development.

This analytical model was derived to investigate the oxygen consumption rate for individual spheroids as well as the prediction of the extent of hypoxic, necrotic and proliferating regions. Because the oxygen diffusion distance in the spheroid is highly dependent on the oxygen concentration at a region surrounding the spheroid, a solution may be necessary for assessing the concentration of oxygen in the medium surrounding the spheroid. The model developed is suitable in the case that the boundaries are known but it does not possess a predictive character as far as how and where these boundaries occur. The present analysis is a reproduction of the past work of Grimes et al. (2014) and is based on their assumptions resulting to the same relation for the Concentration in the spheroid interior.

Model analysis and derivation

The concentration of oxygen within the spheroid is named C_{in} and the concentration of the oxygen within the medium surrounding the spheroid is presented as. Consider the diffusion equation, which relates the change in oxygen concentration in the spheroid with time to the spatial distribution

$$\frac{\partial C_{in}(x,y,z,t)}{\partial t} = D_{in}\nabla^2 C_{in}(x,y,z,t) + p(x,y,z) \qquad (1)$$

Where D_{in} is the oxygen diffusion constant within the spheroid and p(x,y,z) is the consumption rate of the cell type in question, which in general case varies with the position in the spheroid.

For the development of this mathematical model some assumptions had to be made. Those assumptions are listed below and are all very critical for the resulting relationship (Grimes et al., 2014).

(A) The cancer cells in question had formed spheroids which are spherically symmetric at all stages of the culture such that the concentrations of the oxygen and different nutrients depend only on the radial distance, r, from the center of the sphere.

(B) Since the time-scale for growth is large compared with a typical diffusion time, the tumor is in a state of diffusive equilibrium at all spheroid culture points.

(C) The oxygen and nutrient are consumed by living cells only and the tumor cells die when the concentration of oxygen falls below the critical value C_d which is usually very close to the 0% but not always accurately 0.

(D) The supply of the oxygen and other nutrients in the spheroid is regulated by diffusion processes.

(E) All the voxels at the volume of the spheroid contribute the same to the oxygen consumption rate of the spheroid

(F) The tissue consumption rate of oxygen is assumed constant in the whole spheroid.

According to the assumptions (A), (F) spherical symmetry governs the whole spheroid growth process. Taking this assumption into consideration the differential equation is transformed into the spherical coordinates:

$$\frac{\partial C_{in}(r,t)}{\partial t} = D_{in}\left(\frac{\partial^2 C_{in}(r,t)}{\partial r^2} + \frac{2}{r}\frac{\partial C_{in}(r,t)}{\partial r}\right) + p(r) \quad (2)$$

In this analysis the oxygen consumption rate in tissue is assumed relatively independent from the position in the spheroid (F). The oxygen supply of the spheroid is assumed to change slowly compared to the spheroid expansion rate so that the concentration at a certain position within the spheroid does not change in the time scale of the oxygen diffusion process (B). In that case the equation (2) is driven to

$$D_{in}\left(\frac{\partial^2 C_{in}(r)}{\partial r^2} + \frac{2}{r}\frac{\partial C_{in}(r)}{\partial r}\right) + p=0 \quad (3)$$

The differential equation (3) can take the final form (4)

$$\frac{\partial^2 C_{in}(r)}{\partial r^2} + \frac{2}{r}\frac{\partial C_{in}(r)}{\partial r} = \frac{-p}{D_{in}} \quad (4)$$

The equation (4) has general solution which have the form of (5).

$$C_{in}(r) = \frac{A}{r} + B - \frac{p}{6D_{in}}r^2 \quad (5)$$

For the constant's determination, the boundary conditions existing in this case play a vital role in this mathematical development. In our case, the spheroid in question is assumed to have a radius of r_{sph} and a necrotic region within the spheroid region is assumed to exist with a radius of r_{nec} . An illustration of the structure it is shown in the figure 3.7.The oxygen concentration in this region is assumed to have a very low

value which is assumed to not change in the whole region of the necrotic area, which is translated to the condition (i). Also is assumed that the concentration at the very edge of the spheroid is equal to C_b (ii)

$$\text{(i)} \qquad \mathrm{C_{in}}(r_{nec}) = \mathrm{C_{nec}},\ \frac{\partial C_{in}(r_{nec})}{\partial r} = 0$$

$$\text{(ii)} \qquad \mathrm{C_{in}}\left(\mathrm{r_{sph}}\right) = \mathrm{C_b}$$

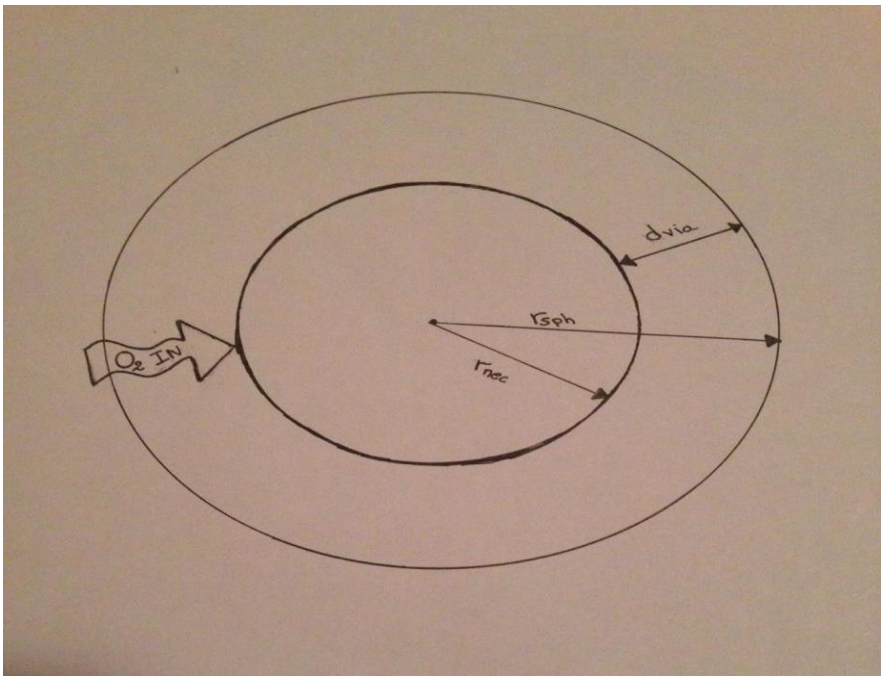

Figure 3.7: Cross section of a tumor spheroid of radius r_{sph} for which diffusion is analyzed. r_{nec} is the radius of the necrotic region which is beyond the diffusion distance of oxygen concentration is non-zero in the region of the illustration between r_{sph} and r_{nec}. This region consists of all viable cells both hypoxic and well oxygenated. Growth medium exists out of the boundary of the spheroid in distances from the spheroid center larger than r_{sph}. Illustration taken from (Grimes et al, 2014) and transformed..

Based on those two boundary conditions we end up with the values below for the four constants.

$$A = -\frac{p}{3 \cdot D_{in}} r_{nec}^3$$

$$B = \frac{p}{6 \cdot D_{in}} \left(2\frac{r_{nec}^3}{r_{sph}} + r_{sph}^2 \right) + C_b$$

Based on the values of the two constants the final expression takes the form (6) that describes the oxygen concentration with in a spherical spheroid of radius r_{sph}, which has a necrotic region of radius r_{nec} and is covered by growth medium. By following the assumptions that Grimes et al. (2014) did and the diffusion differential equation that they used, all the mathematical formulations that are reported in this section led to the same expression for the concentration of oxygen at the inner region of the spheroid (Grimes, 2014).

$$C_{in}(r) = C_{nec} + \frac{p}{6 \cdot D_{in}} (r^2 - r_{sph}^2 + 2r_{nec}^3 (\frac{1}{r} - \frac{1}{r_0})) \quad (6)$$

4. Results and Analysis

4.1 Spheroid culture

4.1.1 Attempts of formation T47D-cell spheroids

The main goal of the experiments, presented in this sub-chapter of the thesis, was the formation and establishment of a reproducible routine for spheroid formation of T-47D cells using orbital stirring motion of the flasks containing the cellular aggregates. The experiments are grouped in 2 sections with the experiment reported in section 1 and Appendix A.1 being performed without the use of agarose-coating in the 25 cm^2 cell culture flasks, while the experiment reported in the section 2 and Appendix A.2 were performed in agarose-coated flasks.

When the stirring technique is utilized for spheroid formation, the critical factors that influence the successful completion of the spheroid culture are:

- the presence of no-adhere coating to the culture flask
- the starting cell number
- the orbital speed induced in the culture.

In the following sections and in Appendix A, they are described various combinations (successful and not) of the different critical factors utilized in the experiments and the final results of each experiment performed in the present thesis. It is essential to be mentioned that the same magnification was utilized for all the photographs acquired in all experiments. In the Appendix A can be found photographs and brief description of all the experiments performed with T-47D cells. In all the experiments utilizing T-47D cells for spheroid formation, the growth medium exchange was performed every second day with first exchange performed on day 2 in all the experiments. More information about the experimental process can be found in chapter 3.2.

Section 1

In section 1, one out of the four individually performed experiments with the purpose of developing a system for formation of spherical cell aggregates and spheroids of T47D cells utilizing agarose-free flasks, is reported. The rest of the experiments of this section are presented in Appendix A.1. All the combinations of stirring speed and starting cell number utilized in these experiments are presented in the table A.1 in Appendix A.

In the present experiment, 4.1 x 10^6 T-47D single cells were seeded in a 25 cm^2 cell culture flask without pre-coating with agarose. The cells were maintained under stirring motion at 60 rpm. Photographs were taken at different days of the experiment and they are illustrated in figure 4.1 and in Appendix A.1.2. As day 0 is noted the seeding day of the single cells into the spheroid formation flask. The suspension was maintained under air environment and optimal temperature (37^{o}C) in the walk-in incubator. As it was observed, most cells attached to the bottom of the culture flask and very few cells contributed to the cell aggregates formation. Some aggregates were formed in the culture but they were of irregular shape and far from being characterized as spheroids (figure 4.2). The cells were not transferred to a new flask during the whole duration of the experiment. After day 5 the experiment stopped, as spherical aggregates were not successfully formed. Additional photographs from different stages of the experiment can be found in Appendix A.1.2. The spheroids were constantly kept in an atmosphere with 19% O_2 and 4% CO_2 in N_2.

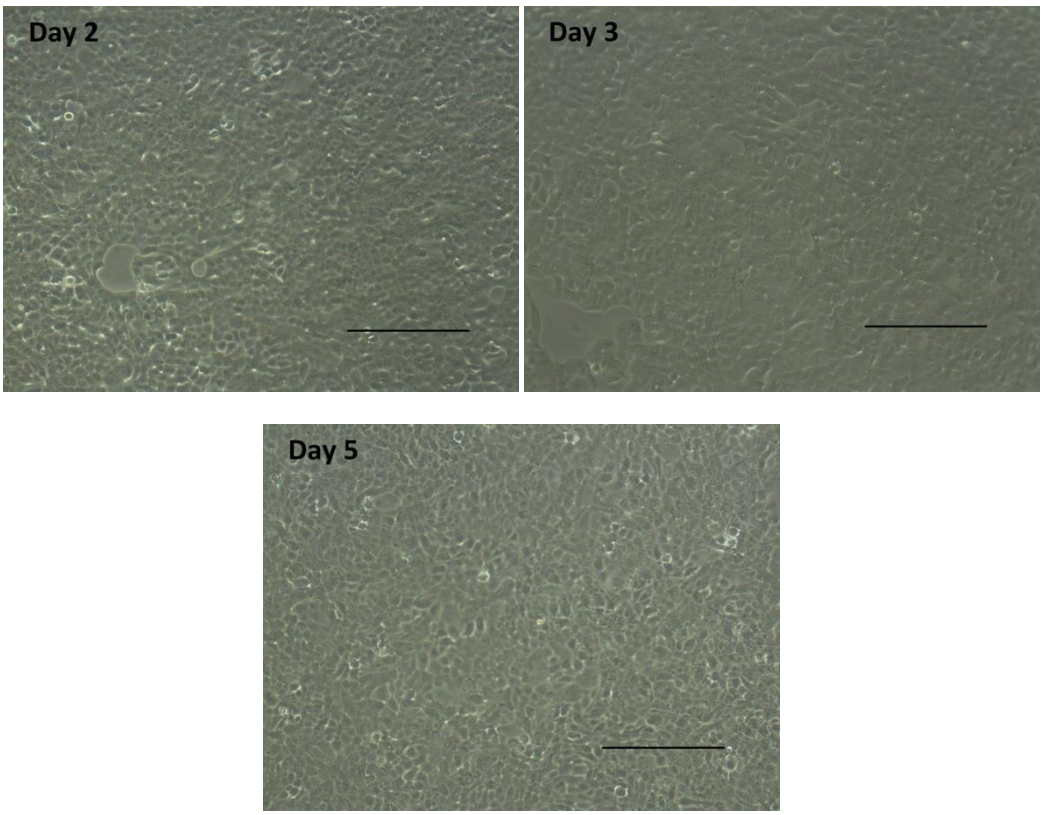

Figure 4.1: Photographs taken at different stages of this spheroid formation experiment. The absence of agarose coating in the culture flask drove the T-47D cells to attach to the substrate of the 25 cm^2 cell culture flask at the first days of the culture. The 4.1 x 10^6 cells present at the beginning of the experiment were maintained under continuous orbital motion at 60 rpm. It can be seen that some rather small aggregates of containing about 3 to 4 cells showed up on day 2 but they did not grow and evolve to form spheroids. The culture flask did not change at all in that duration as no indication of successful formation of any spheroid had shown. The scale bar stands for distance of 333.33 μm.

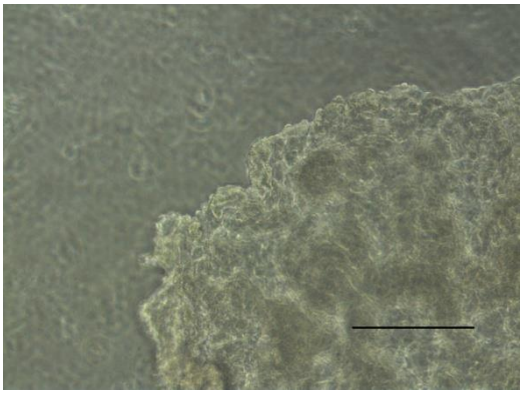

Figure 4.2: Illustration of a big, irregularly-shaped cell aggregate. The presence of such aggregates was noticed during the experiment. They cannot be characterized as spheroids as there is complete absence of spherical or any kind of symmetry in their shape. They were removed manually during the experiment as its presence has been observed to affect the spheroid formation and growth of spherically symmetrical cell aggregates. The scale bar stands for distance of 333.33 μm.

Section 2

In the second group of experiments with T-47D cells, agarose-coated 25 cm^2 flasks hosted the three individual spheroid cultivation experiments. All parameters used in the spheroid culture experiments with T-47D are given in Appendix A.2 table A.2. The presence of agarose layer in the bottom of the flask, prevented any cell attachment and, in combination with the continuous stirring motion, boosted the cell-cell interactions. In section 2 is presented only one of the three spheroid formation experiments with the rest being presented in Appendix A.2.

In the first experiment, 1.6 x 10^6 cells were seeded, on day 0, in the spheroid culture flask containing agarose-coating which was then given continuous orbital movement at speed of 60 rpm in the walk-in incubator. Photographs taken at specific days of the culture are shown in figure 4.3 and Appendix A.2.1. Successful multicellular spheroid formation was observed during the whole duration of the culture. During the first four days of the culture, some spheroids were formed which later grew into spherical aggregates of diameters in the range 250-350 μm at the day 7 and day 11. The spheroids were transferred to a new culture flask culture flask once per week with the first transfer taking place at day 3. Additional photographs illustrating the various stages of the culture are presented in the chapter A.2.1 of the Appendix A. As described in chapter 3.2, the growth medium exchange was performed every second day with the first exchange performed on day 2. The spheroids were constantly kept in an atmosphere with 19% O_2 and 4% CO_2 in N_2.

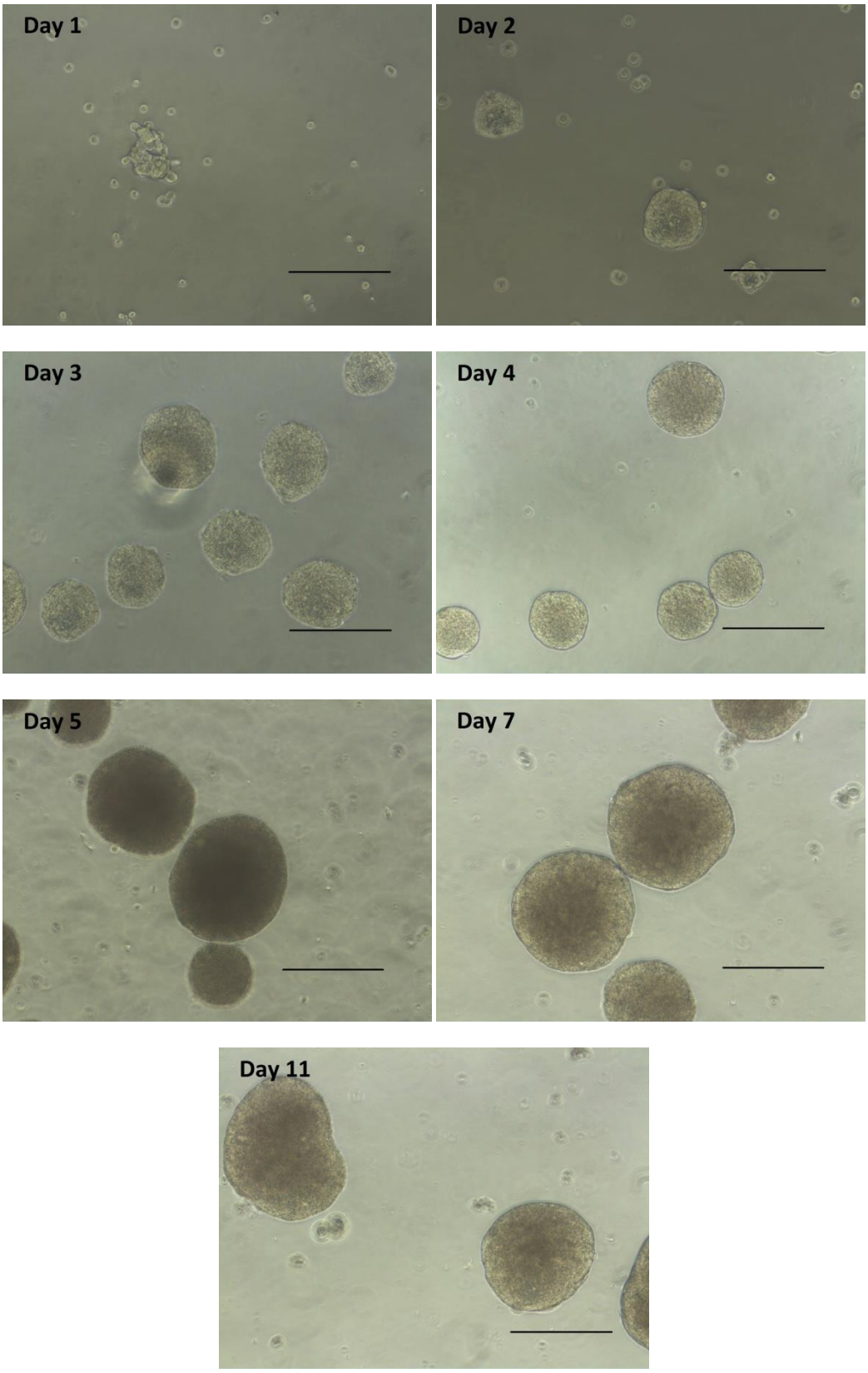

Figure 4.3: Photographic demonstration of the first attempt for spheroid formation with T-47D cells using agarose-coated 25 cm^2 cell culture flasks. 1.6 x 10^6 T-47D cells were seeded in an agarose-coated

25 cm^2 culture flask given orbital motion of 60 rpm speed by the shaker. The spheroids were maintained under optimal environment (19% O_2 and 4% CO_2) and medium exchange was performed every second day. The successful spheroid formation was shown when spheroids were formed as fast as at day 3. At days 7 and 11 some spheroids had reached to diameters about 300 μm. The scale bar stands for distance of 333.33 μm.

In figure 4.4 the different forms observed in the present series of experiments using T-47D cells are summarized. In photograph A is illustrated a cellular aggregate from an agarose-coated 25 cm^2 flask. As can be noticed, the background is clear indicating that cells did not attach to the agarose layer except very few single cells that seam blurred as they were not in the focus plane of the aggregate. In photograph B a big cellular aggregate is visualized. The lack of any spherical symmetry is the main reason this aggregate cannot be characterized as a spheroid. In photograph C spherical aggregates are observed, exactly the shapes we are seeking. There is a clear difference between the two photographs B and C. Moreover, the background appearance in the first three pictures indicates that the photographs were taken from flasks that were coated with agarose. In the last photograph (D) the cell attachment to the bottom surface of the culture flask is illustrated.

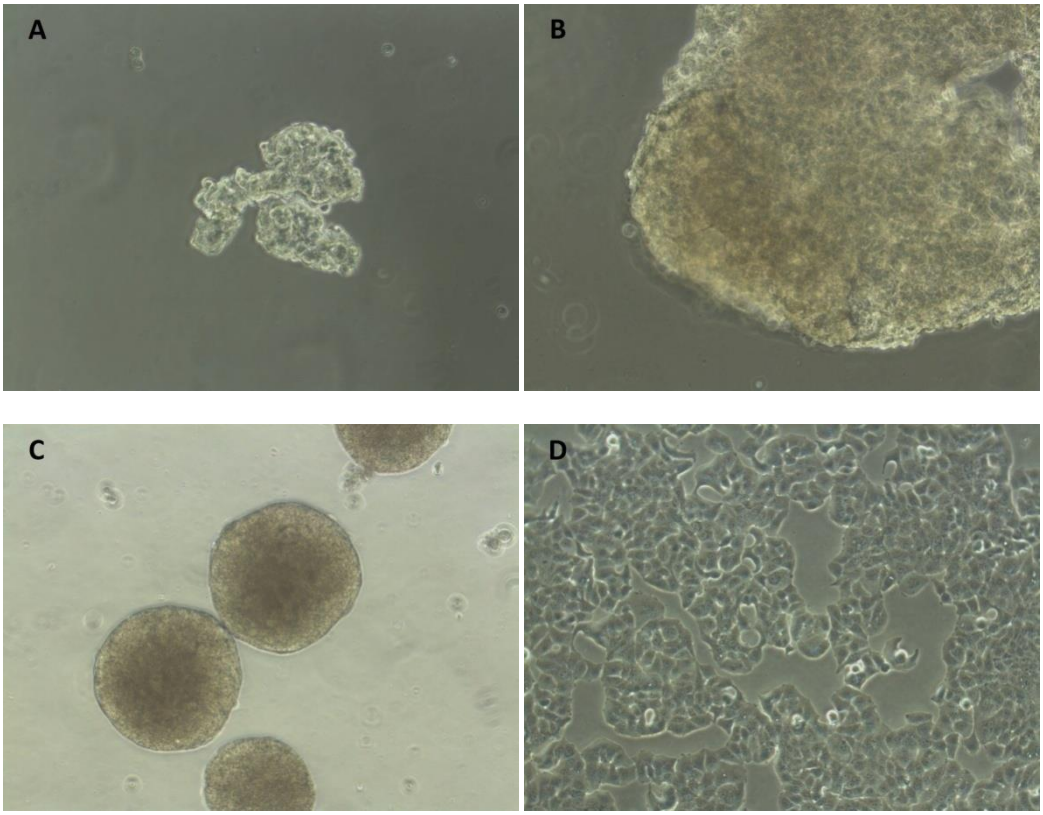

Figure 4.4: Characteristic shapes summarized from different experiments utilizing T47-D cells. (A) Photographic representation of an irregularly-shaped aggregate in a culture flask coated with agarose layer. The background clearness is indicating a low level of cell attachment to the agarose layer in that specific experiment. (B) Photograph representing a large cellular aggregate. The difference with the third picture (C), visualizing T47-D spheroids, can be observed. Such aggregates as shown in B were formed in most attempts and it was observed that their presence in the culture often had negative influence on the final result of the culture as they attracted many cellular aggregates and single cells which then could be lost as potential spheroids. The aggregates were therefore manually removed as soon as they were observed in the culture. (C) Illustration of successful T47-D spheroid formation. There is spherical symmetry in these aggregates which can apply in the category of spheroids. Most spheroids had the tendency to bind to each other when they were close as can be seen also in this picture. (D) Visualization of the attempt without using agarose coating in the culture flask. The cells have attached to the bottom and have covered a big part of the flask bottom surface.

4.1.2 Attempts of formation HT29-cell spheroids

Several experiments were performed in order to optimize spheroids formation of HT29 cells. The total extend of the undergone experiments is described in the following two sections and in Appendix B. In the first section and Appendix B.1, the results from spheroid cultures in non-coated flasks are shown and in the second section and Appendix B.2, the results from all the experiments using 25 cm^2 agarose-coated culture cell culture flasks are reported. In chapter 3.2 the cultivating method is described. The number of cells seeded and the stirring speed utilized, are described in two tables B.1 and B.2 (Appendix B). All the photographs that are presented in the following sections and in Appendix B were acquired under the same microscope magnification. During all the experiments there was a tendency of large irregularly-shaped aggregates formation. It had been observed that the presence of such aggregates in the culture had a negative effect on the successful spheroid formation as many single cells and cellular aggregates were attached to them, making those aggregates progressively even larger. It was preferred to be manually removed from the culture as long as they were observed.

Section 1

The first group of experiments involved the use of 25 cm^2 flasks without any agarose-coating, which were maintained under orbital movement for the whole duration of the experiment. The attachment of the cells to the substrate of the culture flask was not prevented as flasks did not contain agarose coating in the first group of experiments so the aggregates formation was only promoted by the continuous stirring motion which was induced by the shaker. In the first section and Appendix B.1, results and photographs from four individual experiments are presented. In all experiments reported in the first section and Appendix B.1, the exchange of medium performed every second day, with the first change taking part on day 2. In all experiments air environment was provided for the single cells and cellular aggregates.

1.4 x 10^6 HT29 cells were seeded, on day 0, in 25 cm^2 cell culture flask without agarose coating. The flask was put on the shakers platform and was kept under continuous stirring movement at the speed of 60 rpm. Photographic illustration of the culture is presented in figure 4.5 and in Appendix B.1.1. The experiment was successful for spheroid formation as spherical aggregates were present in various stages of the culture. On day 2, cellular aggregates were already formed even if the flask was not coated with agarose. In figure 4.5 can be observed cellular aggregates, spheroids and cells attached to the bottom surface of the flask. Some cells contributed in the aggregates formation but some other cells attached to the substrate of the flask and formed monolayer culture. In different days of the culture, monolayer cell culture and cellular aggregates coexisted in the same flask as can be observed in figure 4.5. The spheroids were constantly kept in an atmosphere with 19% O_2 and 4% CO_2 in N_2.

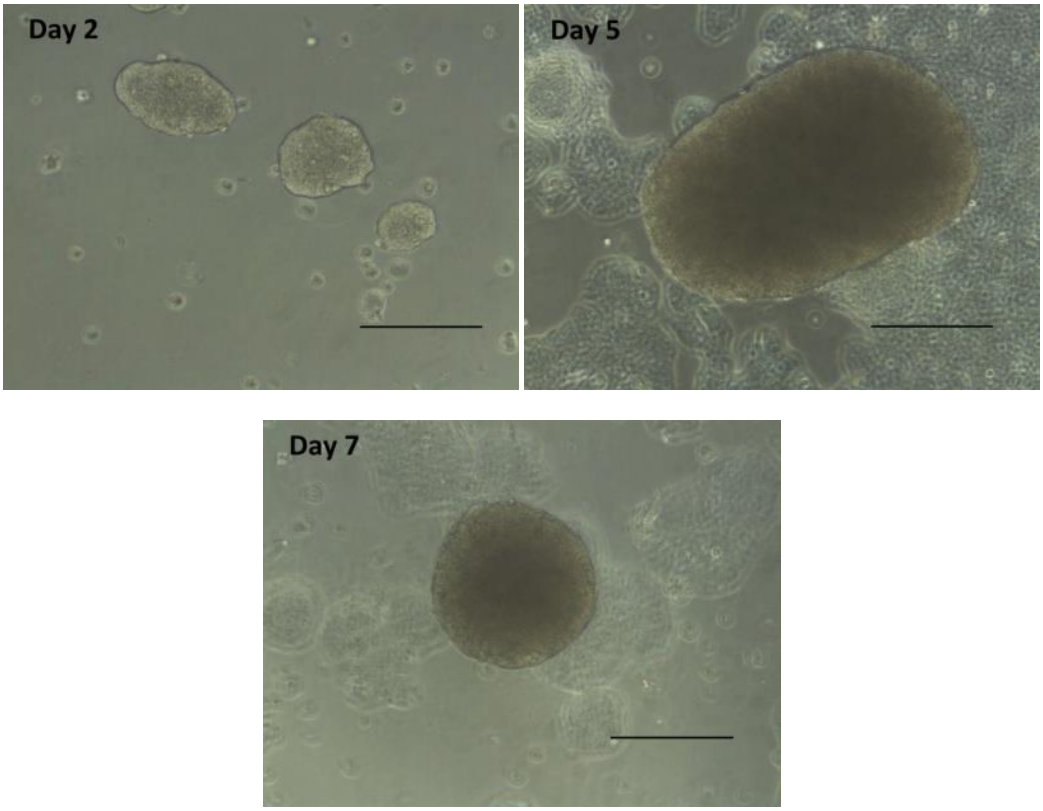

Figure 4.5: Illustration of experiment for HT29 spheroid formation. 1.4 x 10^6 cells were seeded in a 25 cm^2 cell culture flask without agarose-coating and maintained under continuous stirring motion at 60 rpm. Medium exchange took place every second day with the first one being on day 2. Spheroid formation was observed in different stages of the culture. Moreover, extended cell attachment to the bottom surface of the flask was noticed, which is illustrated in the photograph taken from day 5. The scale bar stands for distance of 333.33 μm.

Section 2

The experiments reported in section 2 and Appendix B.2 involve the use of agarose-coated 25 cm^2 flasks which were maintained under stirring motion for the whole duration of the experiment. The thin layer of agarose prevented any cell attachment on the bottom surface of the flask and associated with continuous rotation, which was induced by the shaker, promoted the cellular aggregates formation. In the second section, the results of two out of the total four individual experiments are presented and the rest are presented in chapter B.2 (Appendix B). Photographs were acquired in various experimental stages and are illustrated in the following figure and the Appendix B.2. As in the experiments reported in the first section, the medium exchange took place every second day with the first change performed on day 2.

In this experiment, the initial cell number seeded was 1.4 x 10^6 HT29 cells with stirring speed of the flask at 75 rpm. Photographs are shown in figure 4.6 and appendix B (B.2.3). Successful spheroid formation was indicated under this experiment as was noticed in the previous two experiments described in chapter B.2.1 and chapter B.2.2. Micro-spheroids were observed in the culture flask as early as day 2. Bigger spheroids were observed on day 3 of the culture and they were transferred in a new agarose-coated flask. The experiment was terminated on day 8. As described in chapter 3.2, the growth medium exchange was performed every second day with the first exchange performed on day 2. The spheroids were constantly kept in an atmosphere with 19% O_2 and 4% CO_2 in N_2.

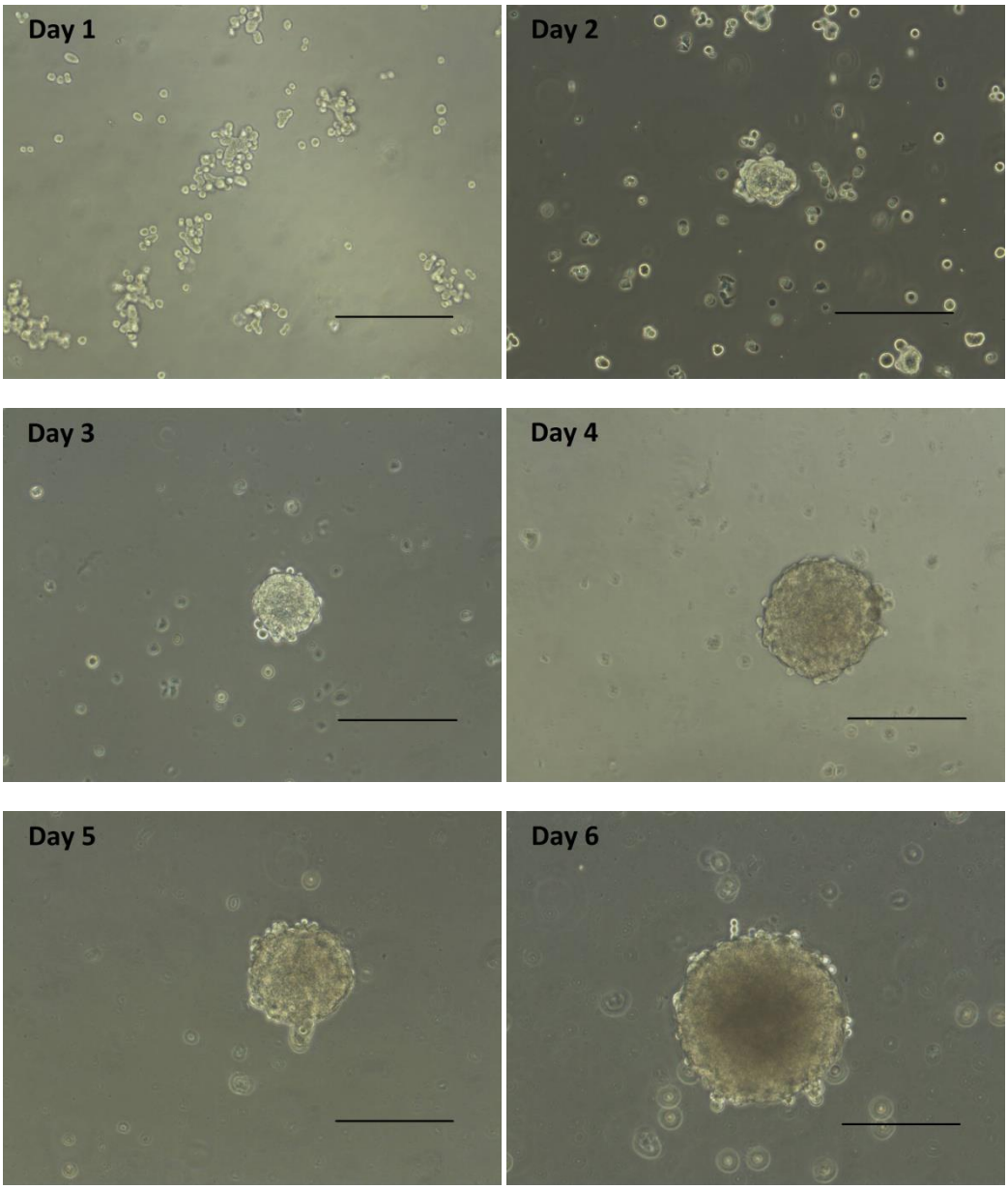

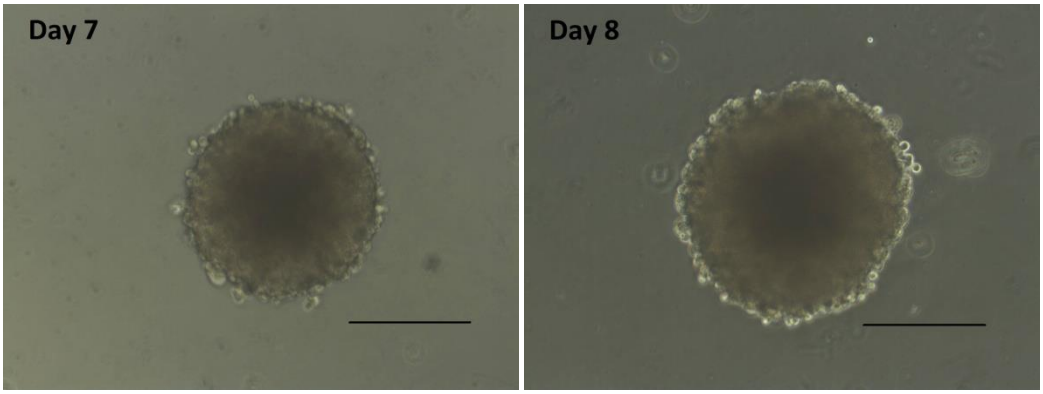

Figure 4.6: Illustration of photographs taken during an experiment for spheroid formation using HT29 cells. 1.7 x 10^6 cells were seeded in a flask containing agarose coating and kept under continuous stirring movement at 75 rpm. Spheroids were successfully formed and grew in this experiment. The increase in the stirring speed did not affect dramatically the final result of the culture as the size of the spheroids presented is not very different from the ones illustrated in the experiment presented in chapter B.2.1(figure B.4). The scale bar stands for distance of 333.33 μm.

In this experiment, the same stirring speed was utilized, as in the experiment presented in the previous page, (75 rpm) while the starting cell number was increased to about 2.7 x 10^6 cells. The 2D photographic representation of different characteristic features of the culture can be observed in figure 4.7 and in appendix B (chapter B.2.4). In this experiment, HT29 spheroids were successfully formed and grew, with the first micro-spheroids noticed in the culture on day 2. On the next day, the spheroids were transferred to a new agarose-coated flask with continued orbital movement for the next days. The spheroids were constantly kept in an atmosphere with 19% O_2 and 4% CO_2 in N_2.

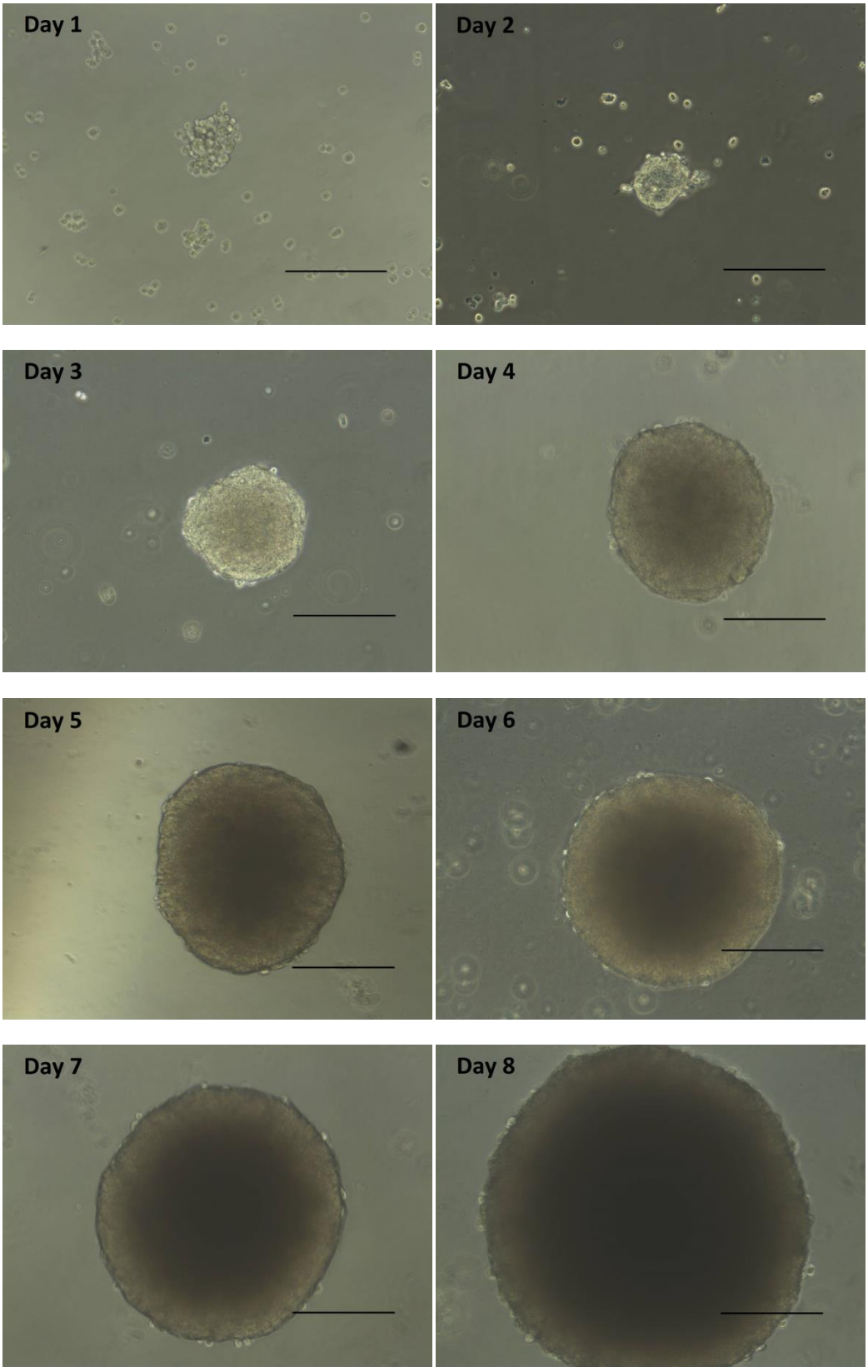

Figure 4.7: Visualization of the forth and last experiment for spheroid formation using HT29 cells. 2.7 x 10^6 cells were seeded in a flask with agarose coating and left with orbital stirring at 75 rpm. All the four experiments utilizing agarose-coated 25 cm^2 cell culture flasks resulted in successful spheroid formation with the last experiment producing the spheroids with the largest diameter from all the

experiments in day 7 and day 8. On day 3 the spheroids were transferred to a new flask. Exchange of the medium was performed every 2 days during the whole duration of the experiment. The scale bar stands for distance of 333.33 μm.

For the two experiments described in section 2, photographs of all the spheroids present in the culture were taken from day 3 to day 8, with day 0 being the day when the HT29 cells were seeded and orbital shaking was started. The spheroids were measured at the two experiments were not the same individual spheroids measured every day of the experiments. It was observed spheroid attachment on large cellular aggregates formed in different stages of the experiment and those aggregates, with the attached spheroids, were removed from the culture. Moreover, there was observed formation of new spheroids in the experiment after the initial spheroid formation phase (day 0 to day 2-3). Many single cells were present in the experiment on most days of the experiment meaning that the formation of new spheroids in later days of the experiments was expected.

The diameters of individual spheroids were measured by calculating the average from 2 diameter measurements. For the size measurements of the spheroids, the acquired photographs were utilized. For each culture day, the value for the average spheroid diameter and the standard deviation of the values were then calculated and spheroid diameter growth curves were then obtained for the HT29 cell line and presented in figure 4.8.

As can be noticed from the graph in figure 4.8, spheroids obtained larger diameters with 2.7 x 10^6 as compared to 1.4 x 10^6 HT29 cells seeded at day 0. Exponential regression analysis was performed in both diameter growth rate curves and the results are presented in the table 3. The fitting of the data was based on the relation $lnd = lnd_0 + kt$. The variable d represents diameter of the spheroid on day t after the and d_0 presents the diameter on time t_0 and k represents the growth rate. The growth rate for the smaller cell number had a higher value (k = 0.17) than the one of the 2.7 x 10^6 cells (k = 0.14). By using those values the spheroids diameter doubling time was calculated for both experiments and the data are presented in table 4.

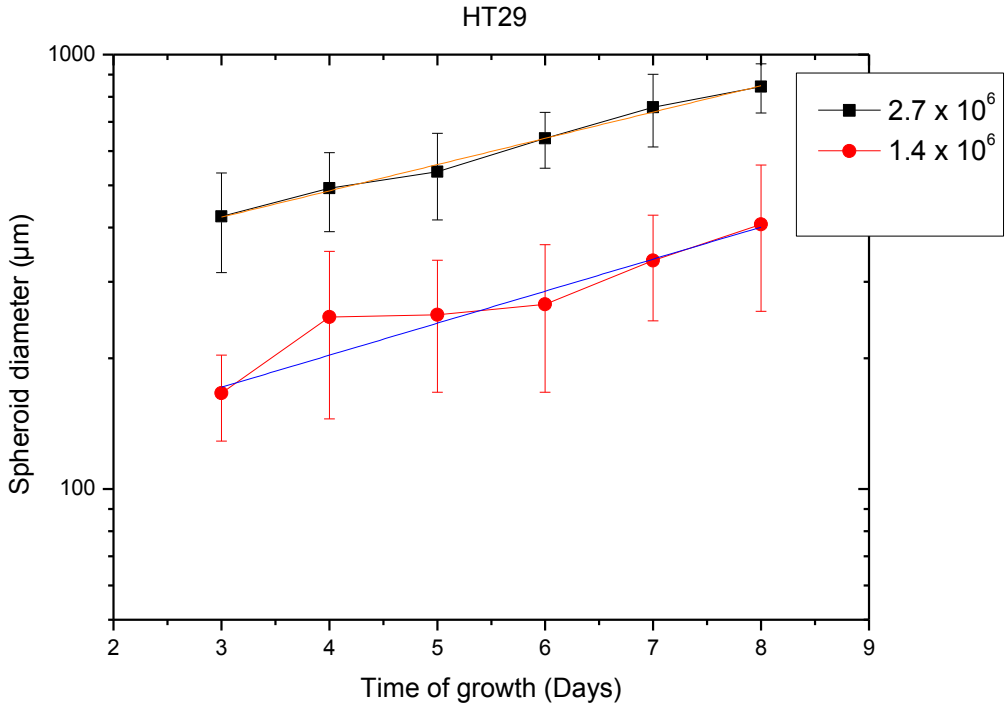

Figure 4.8: Growth rate of HT29 spheroids in agarose-coated 25 cm^2 cell culture flasks under air atmosphere with 4% CO_2 and with change of medium every two days. The red colored curve represents spheroids formed with a starting cell number of 1.4 x 10^6 and the black colored curve represents spheroids formed with a starting cell number of 2.7 x 10^6. Both curves describe experiments were the spheroid flask was kept under constant orbital stirring movement of 75 rpm speed. The first spheroids were observed on day 3 in both experiments. After the transfer of the spheroids into a fresh flask with agarose coating, photographs of all the spheroids present in the culture were taken. Each point in the present graph represents the mean diameter from measurements of at least 25 spheroids present in the flask. These data does not represent the growth rate of specific individual spheroid but present the measurements of all the spheroids were present every day in the flask. New spheroid were formed in later stages of the experiment (after day 3) and some of the existing spheroids were attached on large, irregularly-shaped cellular aggregates and were removed from the culture. Also indications of the standard deviation of the spheroid diameters are presented in the graph.

Table 3: The results from the linear regression analysis from the two growth curves presented in figure 4.8.

Data fitted	$lnd = lnd_0 + kt$
Black curve fitting	$lnd = \ln(248.15) + 0.14t$
Red curve fitting	$lnd = \ln(103.01) + 0.17t$

The factor k derived from the fitting of the curves in figure 4.8 is the one used to calculate the spheroid diameter doubling time for the two experiments. The relation between the growth rate and the diameter doubling time is:

$$k = \frac{ln2}{t_{double}}$$

Table 4: Characteristics of the growth rate of HT29-cell spheroids used in the last 2 experiments of the section 2.

Cell line	Starting cell number	Diameter doubling time (t_{double})	Standard Error
HT29	1.4 x 10^6	4.08 days	± 0.43
HT29	2.7 x 10^6	4.98 days	± 0.19

The diameter measurements of the spheroids formed in the two experiments presented in section 2 were accordingly manipulated so as to calculate the mean spheroid volume values for the 2 experiments. The data calculated, are presented in the figure 4.9 were the mean spheroid volume is plotted against the time of growth for the two individual experiments. Later, exponential regression analysis was performed for both curves and the results are presented in the tables 5 and 6. The mean volume doubling time was lower for smaller spheroids than for larger ones with a difference of 8 hours for the two cultures as presented in table 6.

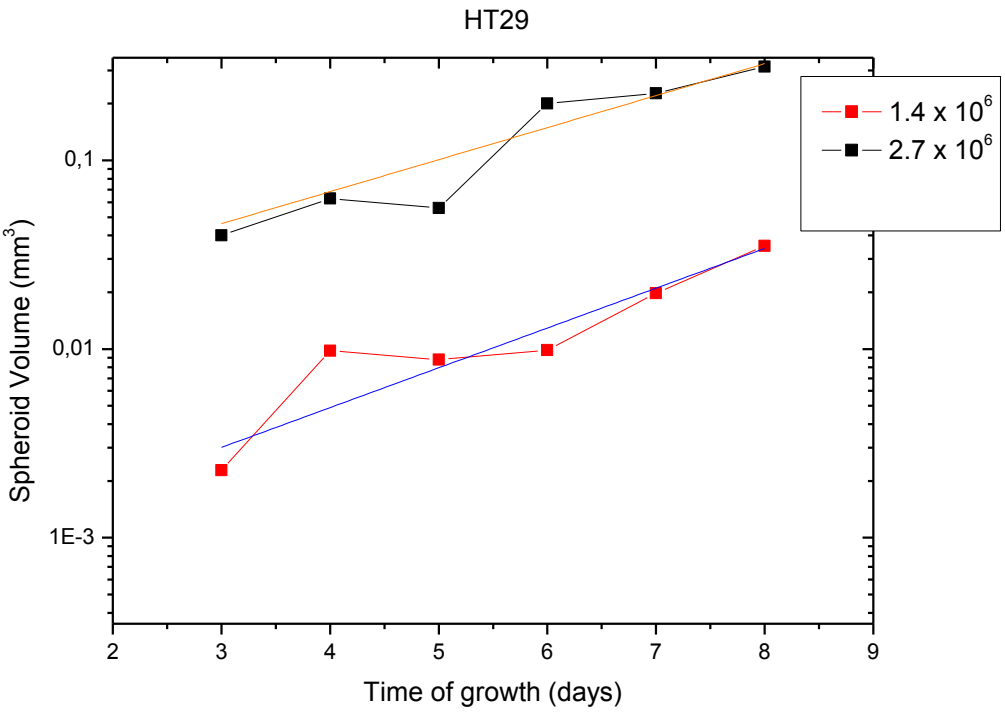

Figure 4.9: Growth rate of HT29 spheroids illustrating the mean spheroid volume growth during the 2 experiments. As in figure 4.8, the red colored curve represents spheroids formed with a starting cell number of 1.4 x 10^6 and the black colored curve represents spheroids formed with a starting cell number of 2.7 x 10^6. The curves were undergone exponential regression analysis and the results indicated that the cell number doubling times were significantly different for the two experiments.

Table 5: The results from the exponential regression analysis from the two growth curves presented in figure 4.9.

Data fitted	$lnd = lnd_0 + kt$
Black curve fitting	$lnd = \ln(0.014) + 0.390t$
Red curve fitting	$lnd = \ln(0.0007) + 0.485t$

The k factor derived from the exponential regression analysis of the 2 curves in figure 4.9 is utilized for calculation of the mean doubling time of the cell number in the spheroid for the two experiments. The relation between the growth rate and the spheroids cell doubling time is:

$$k = \frac{ln2}{t_{double}}$$

Table 6: Characteristics of the growth rate of HT29-cell spheroids used in the last 2 experiments of the section 2.

Cell line	Starting cell number	Volume Doubling time (t_{double})	Standard Error
HT29	1.4 x 10^6	34.70	± 0.22
HT29	2.7 x 10^6	42.57	± 0.33

4.1.3 Attempts of formation MCF-7-cell spheroids

Experiments took place with main intention the formation of spherical aggregates using MCF-7 cells. The presentation of the experiments is arranged in two sections with the experiments reported in the section 1 and Appendix C.1 being performed without the presence of the agarose layer and the experiments illustrated in section 2 and Appendix C.2 being performed by using agarose-coated 25 cm^2 cell culture flasks. In chapter 3.2 the cultivating method is presented. The number of cells seeded and the stirring speed utilized, are described in the Appendix C table C.1 and table C.2. For the acquisition of all the photographs illustrated in the following 2 sections and Appendix C, the same microscope magnification was utilized.

Section 1

The experiments in this section and Appendix C.1 involved the use of 25 cm^2flasks without any agarose coating, which were kept under stirring motion for the whole duration of the experiment. The cells attachment on the bottom surface of the flask was not prevented as no agarose layer was present in the flask. Then, the formation of the cell aggregates was only promoted by the orbital movement induced by the shaker, and by the presence of an adequate number of single cells on the seeding day (day 0). As in the experiments involved T-47D and HT29 cells, large irregularly-shaped

aggregates were formed in all the experiments and were manually extracted from the culture as soon as they were noticed. Photographs from the two individual experiments are presented in the first section and in Appendix C.1.1, C.1.2.

In the reported experiment, 2.3 x 10^6 MCF-7 cells were seeded in 25 cm^2 cell culture flask. The flask was maintained on the platform of the shaker with a continuous orbital motion at 75 rpm. Illustration of photographs acquired in various stages of the experiment is presented in figure 4.10 and in Appendix C.1.1. The formation of small cellular aggregates was noticed until day 3. Additionally to the aggregates formation, single cells attached on the bottom surface of the flask and formed monolayer cell culture which was covering large part of the flasks surface up to day 5. The exchange of medium was performed every second day with the first medium change taking place on day 2. The cellular aggregates formed in this experiment were irregularly shaped and small in size so the experiment stopped on day 5. During the whole duration of the experiment, the aggregates were maintained in the same 25 cm^2 culture flask. The spheroids were constantly kept in an atmosphere with 19% O_2 and 4% CO_2 in N_2.

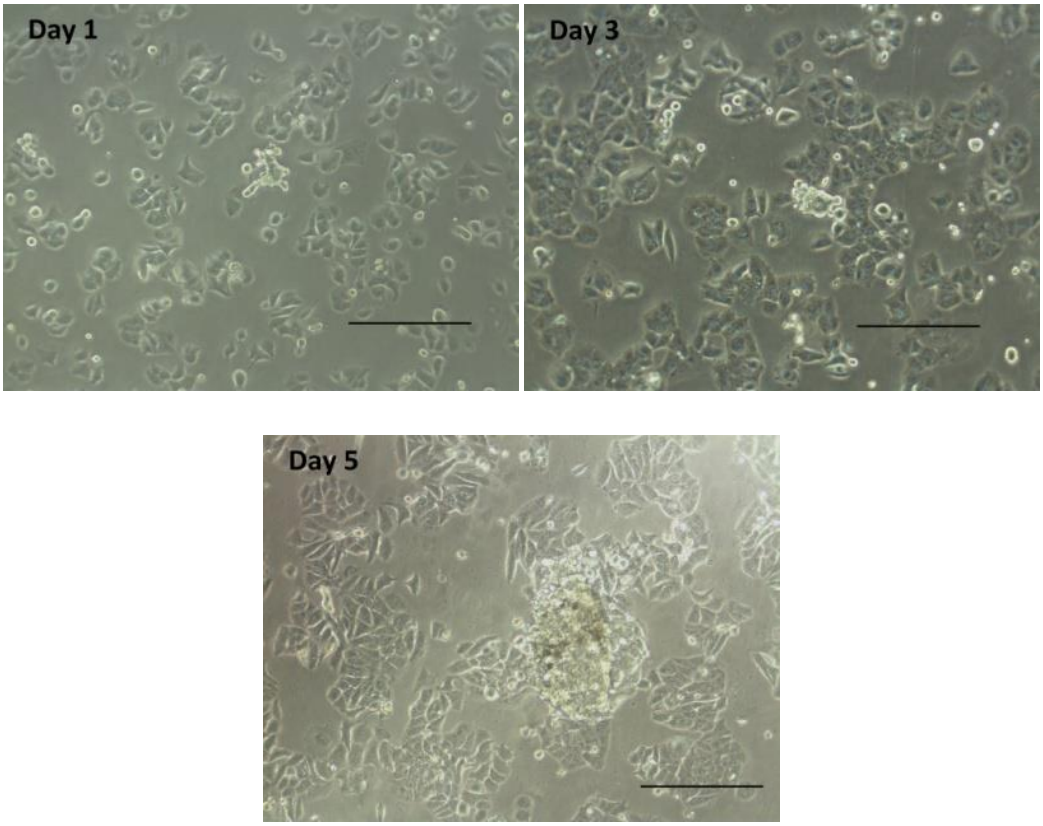

Figure 4.10: Illustration of photographs taken during the first experiment using MCF-7 cells to generate spherical aggregates. 2.3 x 10^6 MCF-7 cells were seeded in a 25 cm^2 cell culture flask and maintained under stirring motion at 75 rpm. The culture were maintained under air conditions and the exchange of growth medium was performed every second day. Small and irregularly-shaped cell aggregates were formed in this experiment, with many single cells attached on the substrate of the flask and formed monolayer cell culture. The scale bar stands for distance of 333.33 μm.

Section 2

In the section 2 and Appendix C.2, the second group of experiments is reported. The results described in this section involve MCF-7 cells seeded in 25 cm^2 flasks which were earlier coated with agarose. As the cell attachment on the bottom surface was prevented by the agarose layer presence, cell aggregates could, in principle, lead to a more successful result. The presence of agarose layer and the continuous orbital motion promoted any aggregates formation in the experiments pre-agarose coated flasks were utilized. Moreover, it was repeatedly noticed the presence of large, irregularly-shaped aggregates in all four experiments reported in the section 2 and Appendix C.2.

In the first experiment, 2.3 x 10^6 MCF-7 cells were seeded in an agarose-coated 25 cm^2 cell culture flask on day 0 and maintained on the main platform of the shaker following stirring motion at 60 rpm. Cell aggregates were generated in the experiment with the first small pre-spheroids formed on day 3. With the term ¨pre-spheroid¨ the early aggregates, which led to spheroid formation, will be described. The exchange of the growth medium was performed every second day with the first medium change taking place on day 2. The pre-aggregates and the single cells were transferred in a new flask containing agarose coating on day 3. Photographs were taken during the experiment and can be observed in figure 4.11 and in Appendix C.2.1. On day 7, spheroids were well observed in the culture, with some spheroids characterized by diameters up to about 250 μm. After day 7 the experiment was ended. The spheroids were constantly kept in an atmosphere with 19% O_2 and 4% CO_2 in N_2.

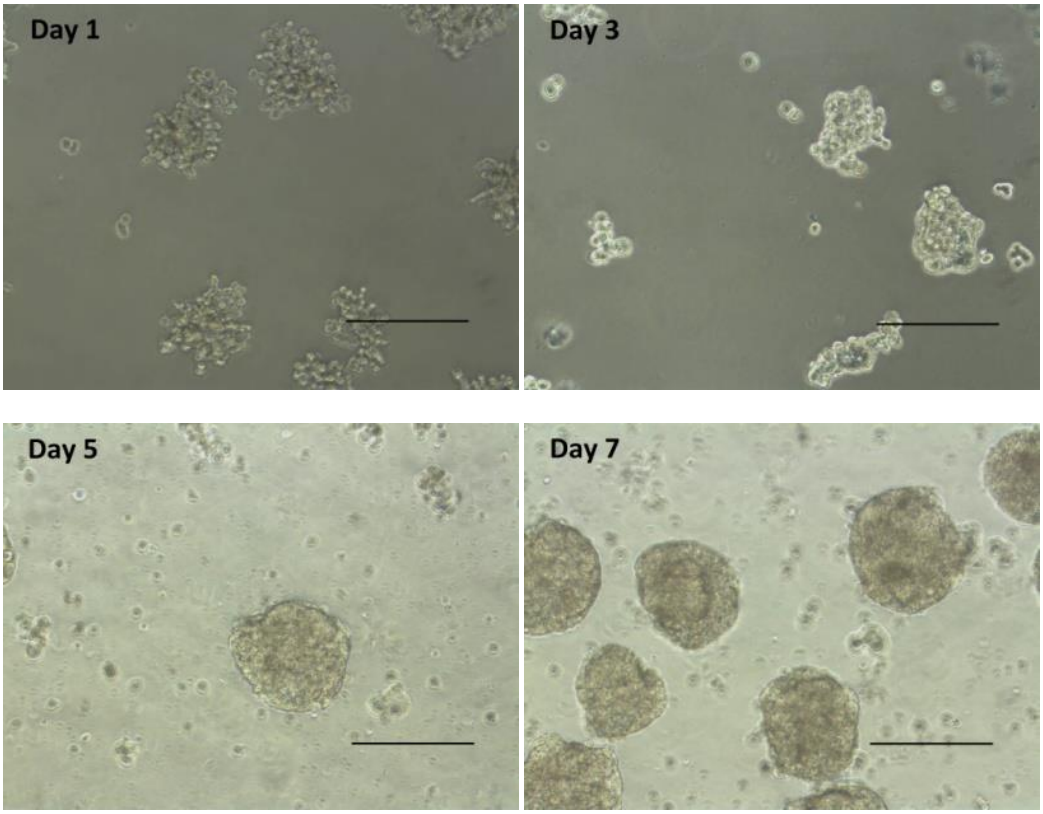

Figure 4.11: Illustration of photographs taken in different days of the experiment. 2.4 x 10^6 MCF-7 cells were utilized for spherical aggregates generation which were maintained in an agarose-coated 25 cm^2 cell culture flask under stirring motion at 60 rpm. The aggregates were kept under air environment and the exchange of medium took place every second day. Successful spheroid formation was observed, with some spherical aggregates growing to diameters of about 250 μm. The scale bar stands for distance of 333.33 μm.

4.1.4 Attempts of formation T98G-cell spheroids

The results from all the experiments performed for spherical aggregates formation using T98G cells are reported in the following 2 sections and Appendix D. In the section 1 and Appendix D.1, the experiments performed in flasks without agarose coating are reported and in the section 2 and Appendix D.2 all the results from the experiments utilizing cell culture flask pre-coated with agarose are presented. In all the experiments, the medium exchange was performed every 2 days. As in the experiments with the other 3 cell lines described until now, large irregularly-shaped aggregates were formed. All the photographs illustrated in the 2 following sections and in Appendix D were acquired under the same microscope magnification. All the

regarging the stirring speed and starting cell number combinations are presented in Appendix D in table D.1 and table D.2.

Section 1

In the section 1 and Appendix D.1, the results from 3 individual experiments are reported. In all the three experiments, cells were seeded in 25 cm^2 cell culture flasks without agarose coating. The cells and cellular aggregates were maintained in the same flask during the whole duration of the experiments in all the three experiments. The spheroids were constantly kept in an atmosphere with 19% O_2 and 4% CO_2 in N_2.

In the presented experiment, 1.3 x 10^6 T98G cells were seeded in the culture flask on day 0 of the experiment. The flask was maintained under continuous stirring movement at 60 rpm. During the whole duration of the experiment, there was not observed any spheroid formation neither extensive aggregates formation. Few aggregates were formed and they always lacked symmetry in their shape. Moreover, they were very small in size being not bigger than 10 cell per aggregate. Most cells attached to the substrate of the flask forming monolayer cell culture. Photographs were taken during the whole duration of this first experiment. Some of those photographs are illustrated in figure 4.12 and in Appendix D.1.1. The culture were ended after day 6. The spheroids were constantly kept in an atmosphere with 19% O_2 and 4% CO_2 in N_2.

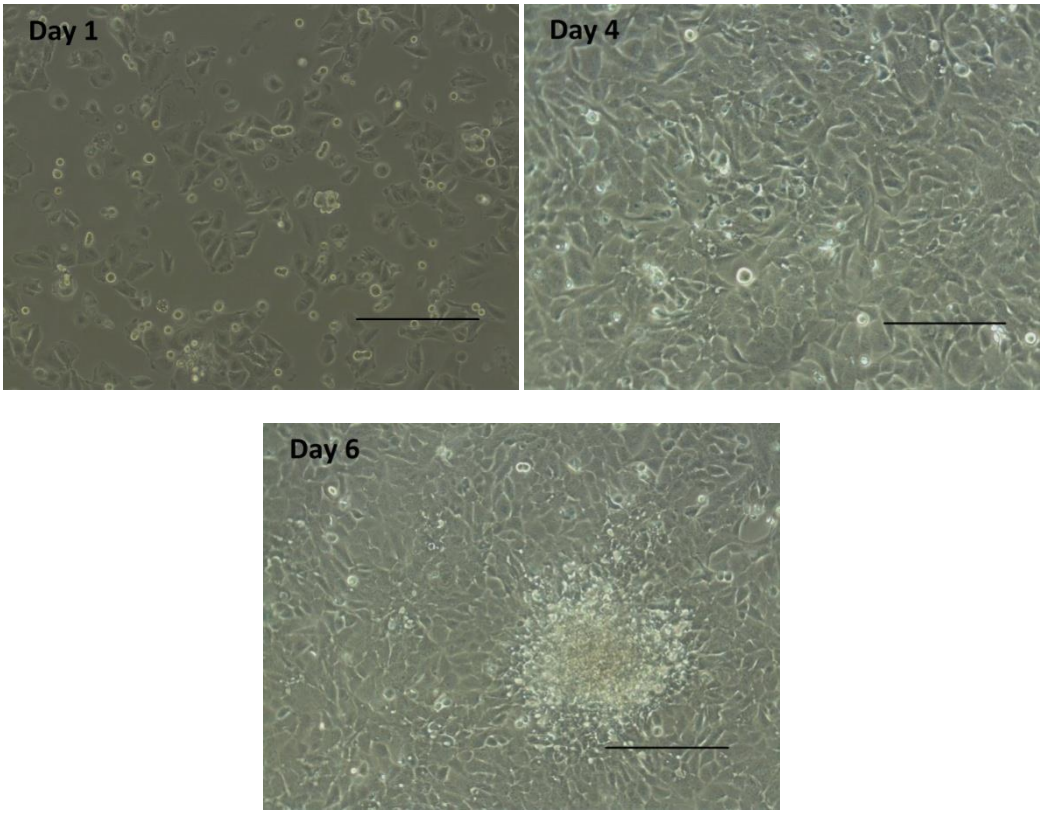

Figure 4.12: Photographic illustration of the presented experiment. 1.3 x 10^6 T98G cells were seeded in a 25 cm^2 cell culture flask without any agarose coating. The flask was kept under gentle shaking at 60 rpm. Spheroids were not generated during this experiment. The vast majority of the cells attached on the bottom surface of the flask and formed a 2D monolayer culture. The scale bar stands for distance of 333.33 μm.

Section 2

In the section 2 and Appendix D.2,the second group of experiments is reported. The results reported in this section and in Appendix D.2, it involve T98G cells seeded in 25 cm^2 flasks which were earlier pre-coated with agarose. The presence of the non-adherent material for coating of the experiments flask, like agarose, could, in principle, lead to a more successful result in the spheroid formation experiments. The presence of agarose layer and the continuous orbital motion promoted the aggregates formation this section. Moreover, it was repeatedly noticed the presence of large, irregularly-shaped aggregates in all three experiments reported in the section 2 and Appendix D.2.

At this experiment, 1.3 x 10^6 T98G cells were seeded in an agarose-coated 25 cm^2 cell culture flask on day 0. The cells were maintained under orbital stirring motion at 75 rpm for the whole duration of the experiment. Photographs were acquired until the experiment end on day 9 and illustrations of those photographs are presented in figures 4.13 and Appendix 2.3.Spheroids were generated at this experiment as shown in the figure 4.13. The spheroids were maintained in the same flask for the whole duration of the experiment. Moreover, extensive cell attachment to the agarose layer was observed in this experiment. The attached cells formed monolayer culture which coexisted with the spheroids in culture flask. The experiment ended on day 9. The spheroids were constantly kept in an atmosphere with 19% O_2 and 4% CO_2 in N_2.

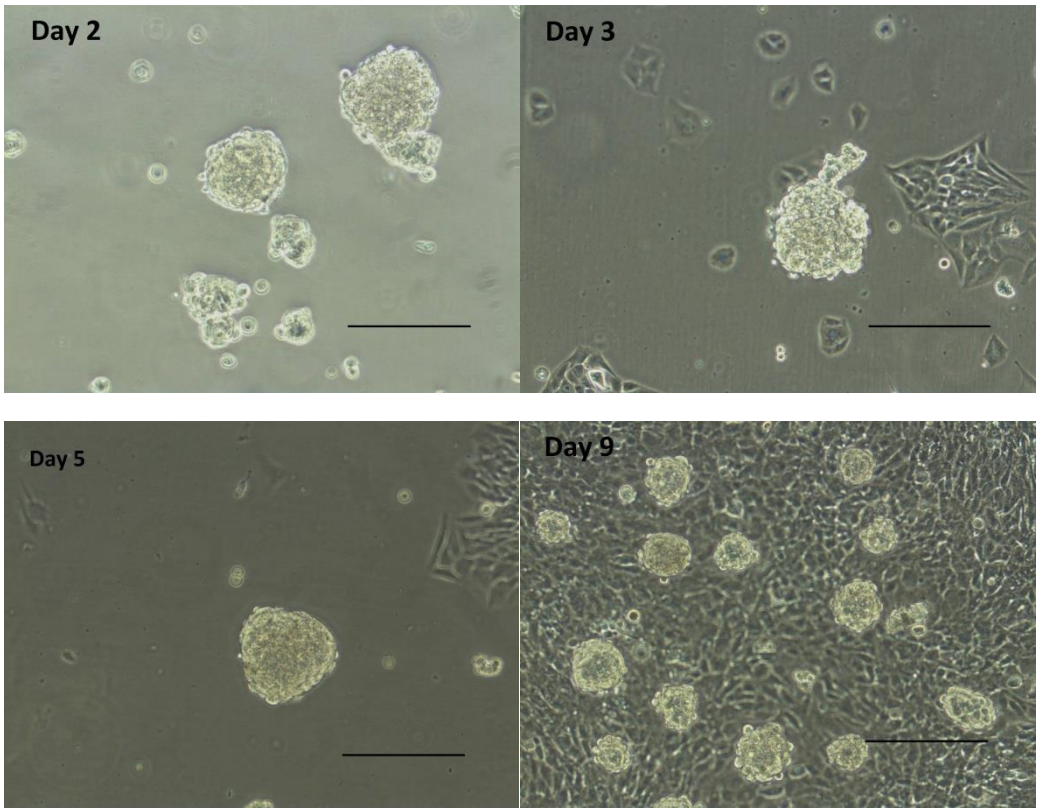

Figure 4.13: Visualization of the experiment where 1.3 x 10^6 T98G cells were seeded in a 25 cm^2 cell culture flask containing agarose coating. The flask was kept under gentle orbital shaking at 75 rpm. Spheroids were formed during this experiment. The many single cells attached on the bottom surface of the flask and formed a 2D monolayer cell culture as illustrated in the photograph of day 9. The scale bar stands for distance of 333.33 μm.

4.2 Oxygen Measurements

4.2.1 First HT29-cell spheroid oxygen profiles

Oxygen profiles through the center of a HT29-cell spheroid have been measured as shown in figure 4.14 and 4.15. The experimental set up utilized is illustrated in the figure 3.3 and figure 3.4. A main characteristic of all measurements is that the oxygen concentration begin to decrease far from the surface of the spheroid. The oxygen concentration in the upper agarose layer, at a sufficient distance from the spheroid, is stable and equalized with the medium. However as the microelectrode approach the surface of the spheroid a rather steep decrease occur and significant difference between the oxygen concentration in the medium and at the spheroid surface can be observed.The diffusion depleted zone that surrounds the HT29 spheroids caused mainly by the high local consumption rate of oxygen at the surface and the viable rim of the spheroid.

The oxygen sensor proceeded in the spheroids viable rim measuring the oxygen concentration at various depths and distance from the center of the spheroid while was kept motionless between measurements for 20 s so as to ensure steady-state measurements. As the sensor comes near the interface between viable and necrotic region, the decrease of oxygen concentration becomes smooth and finally a plateau is reached in the necrotic zone

At the figure 4.14 is illustrated the oxygen profile of a 1072 μm-diameter HT29-cell spheroid. This is the first out of the seven measured oxygen concentration profiles which are all illustrated in the figure 4.15. The sensor direction of movement is from the positive to the negative values of the distance from the spheroid center (<--). The first information that can be observed is the rather low oxygen concentration at the surface of the spheroid. In our case, the 2,3%, that is measured as the oxygen concentration at the spheroid surface, is very low compared to the 19% oxygen concentration of the growth medium. A possible explanation can be that the oxygen diffusion meets transport diffusion limitations induced mainly by the cell-containing agarose layer. A possible reduction in the oxygen diffusion can result in reduction of the oxygen concentration in the surrounding material of spheroid as the already existed oxygen would be rapidly metabolized without the system to be able to provide oxygen in such rate.

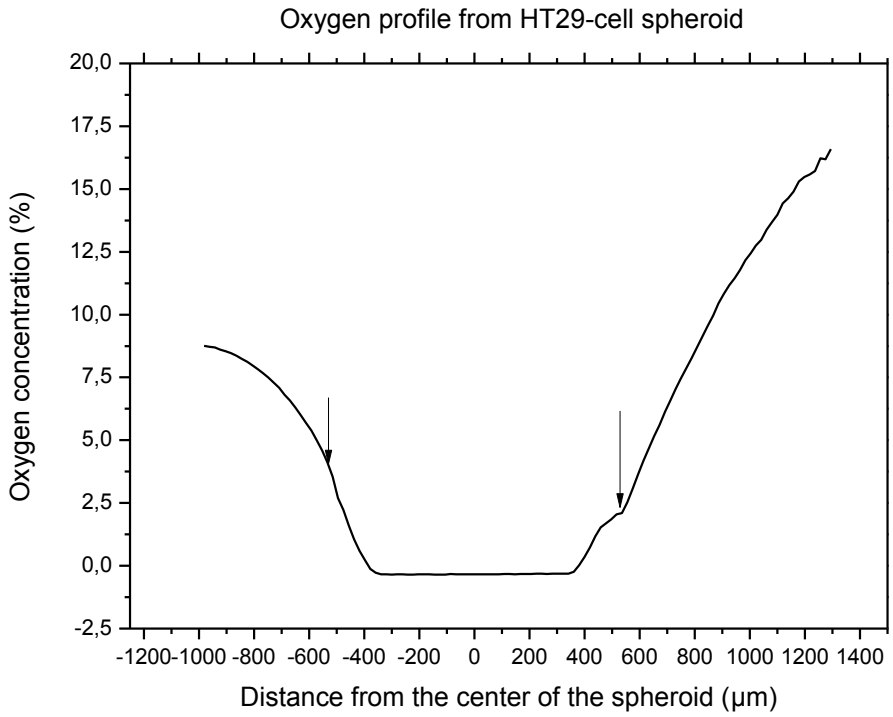

Figure 4.14: 1st Oxygen concentration profile measured for a 1072 μm-diameter HT29 spheroid .↓, spheroid surface. The oxygen sensor propagation direction was from the positive values to the negative values of the distance from the spheroid center (<---).

An oxygen concentration gradient is present in the microenvironment of the spheroid as figures 4.14 and 4.15 indicate. Moreover, a discontinuity of the oxygen gradient can be observed on the spheroid surface. This can be explained by technical difficulties. As the oxygen probe punctures the spheroid, sometimes it does not penetrate smoothly into the spheroid but compresses the spheroid until it can succeed to get in the viable rim. There is also a large necrotic region extending to a 750 μm-diameter sphere. The oxygen concentration in the necrotic region is constant but the negative value indicates a poor 0% point calibration.

The thickness of the viable rim region is 186 μm and the oxygen gradient is much steeper in the spheroid rather than in the spheroid environment. This observation contradicts with the Sutherland et al. (1986) measurement results for HT29 spheroids of the same size. Sutherland et al. (1986) measured oxygen tension at HT29 spheroids surrounded by fully controlled medium at 21% oxygen. His result was that the PO_2

gradient was steeper outside the spheroid and swallower in the viable rim region (Sutherland, Sordat et al. 1986). The difference in the two results can be explained by the use of agarose layer to cover and stabilize the HT29 spheroid instead of fresh medium.

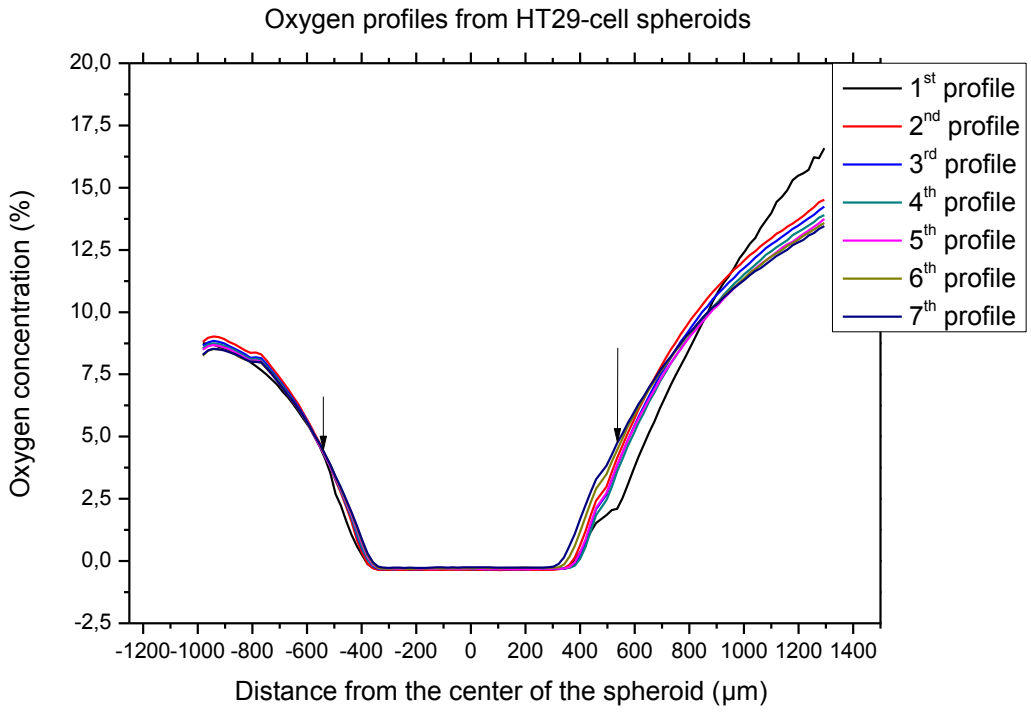

Figure 4.15: All the measured circles from a 1072 µm-diameter HT29 spheroid.↓, spheroid surface. The oxygen sensor propagation direction was from the positive values to the negative values of the distance from the spheroid center (<---).

At the figure 4.15 are illustrated all the 7 oxygen profiles obtained from the same spheroid. The time interval between each measurement is 30 minutes and it takes 20 s to obtain a steady-state situation before each measurement. A massive increase of the surface oxygen concentration can be observed between the first and the second profile. This can be the result of the perturbation of the microenvironment of the spheroid due to the electrode movement. The movement of the sensor can cause some medium to pass through the upper agarose directly to the spheroid. As a consequence the oxygen concentration may increase on the surface and inside the viable rim of the spheroid. Additional to this mechanism, the oxygen diffusion from the medium covering the

upper agarose layer has increased the available oxygen at the environment of the spheroid after each measuring circle.

Moreover, the oxygen concentration at the low end of the spheroid remains constant. At all the profiles the surface oxygen concentration of the entrance and the exit point of the electrode have very close values except the first profile. Furthermore the oxygen gradients from both sides of the HT29 spheroid are very similar indicating a state of homogenous oxygen consumption by the spheroid. The gradient discontinuity that show up in the first profile it not evident in any other profile.

4.2.2 Second HT29-cell spheroid profiles

The oxygen concentration profile measurement was also performed to a second HT29-cell spheroid as illustrated in Figure 4.16. The same experimental set up utilized for all HT29-cell spheroid profiles illustrated in figure 3.3. The measurement is acquired from a 1182.43 μm-diameter HT29 spheroid.

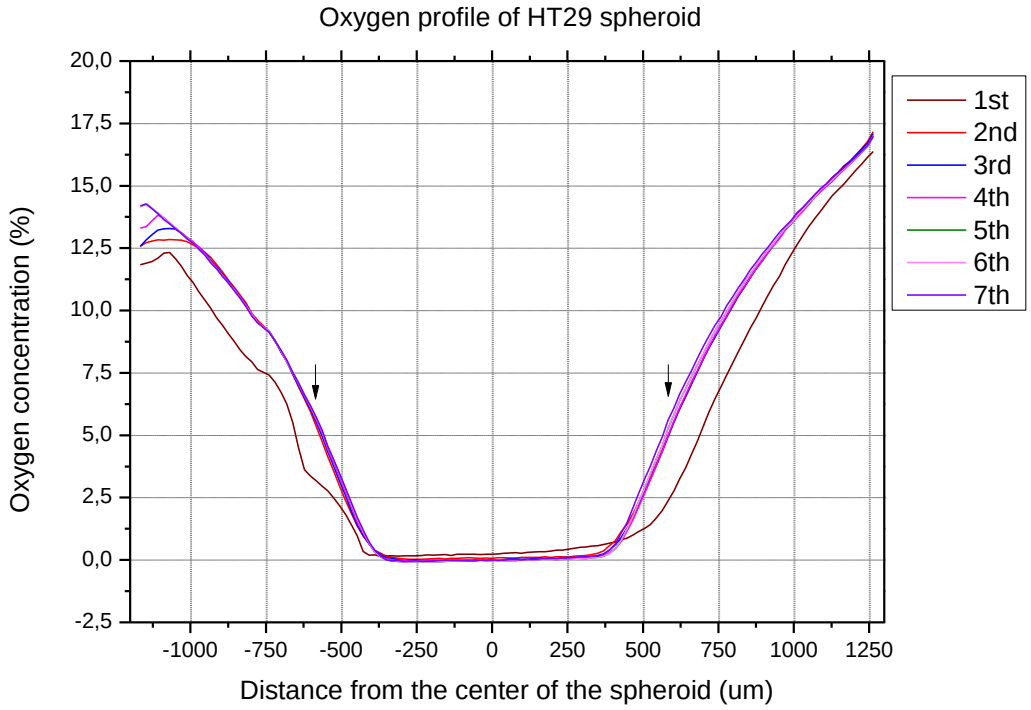

Figure 4.16: All measured profiles from a 1182.43 µm-diameter HT29 spheroid. ↓, spheroid surface. The brown curve represents the first measuring sequence and therefore includes the first penetration of the sensor into the spheroid.The time interval between each acquisition circle was 30 minutes and it took 20 s to obtain a steady-state situation before each measurement. The oxygen sensor propagation direction was from the positive values to the negative values of the distance from the spheroid center (<---).

A main characteristic also observed in acquired oxygen profile of the 1182.43 µm-diameter spheroid, is that the oxygen concentration begin to decrease far from the surface of the spheroid. However as the microelectrode approaches the surface of the spheroid a much steeper decrease occurs and a significant difference between the oxygen concentration in the medium and at the spheroid surface can be noticed. The diffusion-depleted zone that surrounds the HT29 spheroids is caused mainly by the high local consumption rate of oxygen at the surface of the spheroid.

As the oxygen sensor penetrated into the spheroid´s rim of viable oxygen-consuming cells a steep fall in oxygen concentration was recorded until, at a depth of approximately 216,22 µm, the oxygen concentration reached down to the lowest level recorded by the sensor. For the spheroid here studied (1182.43 µm diameter) this was seen at a distance of 375 µm from the spheroid center.

The curves shown in figure 4.16 are all the 7 oxygen concentration profiles measured for this HT29 spheroid. The sensor direction of movement is from the positive to the negative values of the distance from the spheroid center (<--). The first information that can be observed is the rather low oxygen concentration at the surface of the spheroid (2.5%) during the first piercing of the spheroid. Another interesting observation has to do with the increase of the oxygen concentration on the spheroid surface between the first and all the other acquisition circles. The oxygen concentration on the surface of the spheroid is 6.25% at the second measured oxygen profile and it does not vary a lot between the other measuring profiles.

Moreover the oxygen concentration at the sensor-exit-side of the spheroid remains constant. Additionally the oxygen gradients from both sides of the HT29 spheroid are very similar indicating a state of homogenous oxygen consumption by the spheroid. Further information regarding the anatomy of the spheroid were obtained by the use of histology sections for Pimonidazole binding presented the hypoxic cells with a brown color while the necrotic are presented with a different color as presented in figure 4.17. The HT29 spheroid used for the histology analysis were not cultured in the same flask as the HT29-cell spheroids utilized for the measurement of the oxygen concentration profiles.

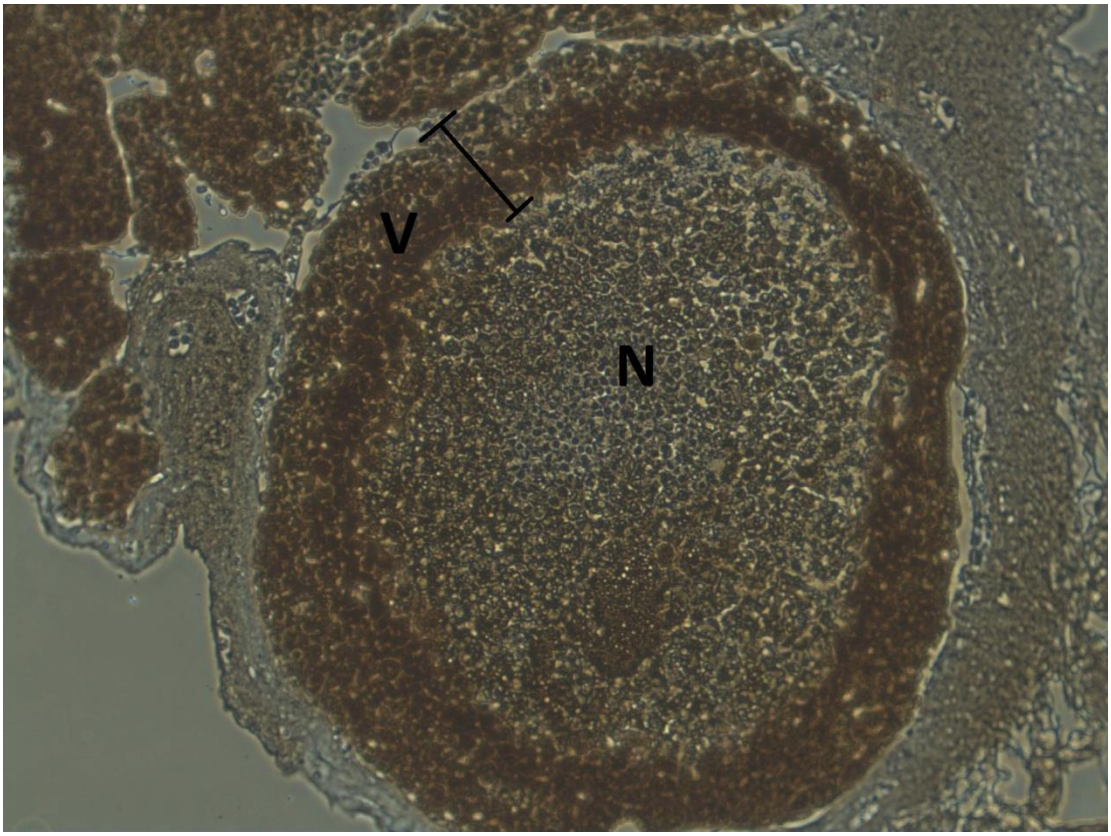

Figure 4.17: Histology section for Pimonidazole binding of HT29-cell spheroid. The cell ring illustrated with brown color indicates the hypoxic cells region containing hypoxic cells which are still alive (H). The development of necrotic core at the inner part of the spheroid can be observed in the photograph where the letter N stands for the necrotic region. The scale bar stands for distance of 333.33 µm.

4.3 Oxygen profiles through a cell-free agarose layer

System characterization

Using the system described in figures 3.6 and 3.5 the sensor tip was first placed 1.12 cm below the RPMI medium surface, by the use of the software and the computer-controlled-micromanipulator. The sensor initiated the oxygen measurements from this uppermost position and performed separate measurements at 100 μm steps down to the upper level of the cell-free agarose layer, through the 0.66 cm layer and ending 0.11 cm below the surface of the T47D-cell-containing agarose column (see figure 3.5). The sensor was not programmed to proceed further down so as to avoid placing the very fragile glass microsensor at risk. The final position of the sensor thus was 1.39 cm from the bottom of the glass tube. From the starting point, which in figures 4.18 and 4.19 is marked as position 10000 μm, measurements were recorded at 100 μm downwards steps until the ending point was reached, each step with a 20 s equilibration period prior a 5 s acquisition period.

There was a resting period of 30 min between the subsequent acquisition sequences. Aquisition of the first oxygen profile was started 90 min after the seeding of the cells. This first profile indicates that the oxygen concentration through the cell-free agarose layer falls linearly with depth from about 21% at the agarose-medium border at the top of the agaroselayer down to about 4% at teh border between the cell-free and the cell-containing agarose layers at the bottom of the cell-free agarose layer. This means that at the time when this first profile was measured no oxygen had yet started to diffuse from the medium and down into the cell-free agarose layer. However, for the 4^{th} and 5^{th} profile, whichwere run 1.5 to 2 h after the first profile acquisition, it is clearly seen that the oxygen content in the medium is reduced below 20% at the medium-agarose boarder. Oxygen originally present , in the 0.75% agarose column accommodating almost 8×10^6 viable cells and in the upper 0.75% cell-free agarose column, was consumed within 24 h and measurements were recorded (figure 4.18, 4.19). As the measurement sequences continued the oxygen gradient appearing in the growth medium became gradually more pronounced, as can be observed in figure 4.19.

At the first acquisition, a discontinuity in the oxygen gradient can be observed at the interface of the two agarose layers. This can well be a technical artefact caused by

possible small resistance of the gel surface to the microsensor piercing. This explanation is supported by the fact that the oxygen gradient discontinuity did not show up again on the following acquisitions as seen in figure 4.19. Moreover, difference in the oxygen gradient in the two agarose layers can be recognized in both figures 4.18 and 4.19. The oxygen drop is more dramatic in the cell-containing agarose layer than the cell-free layer of agarose.

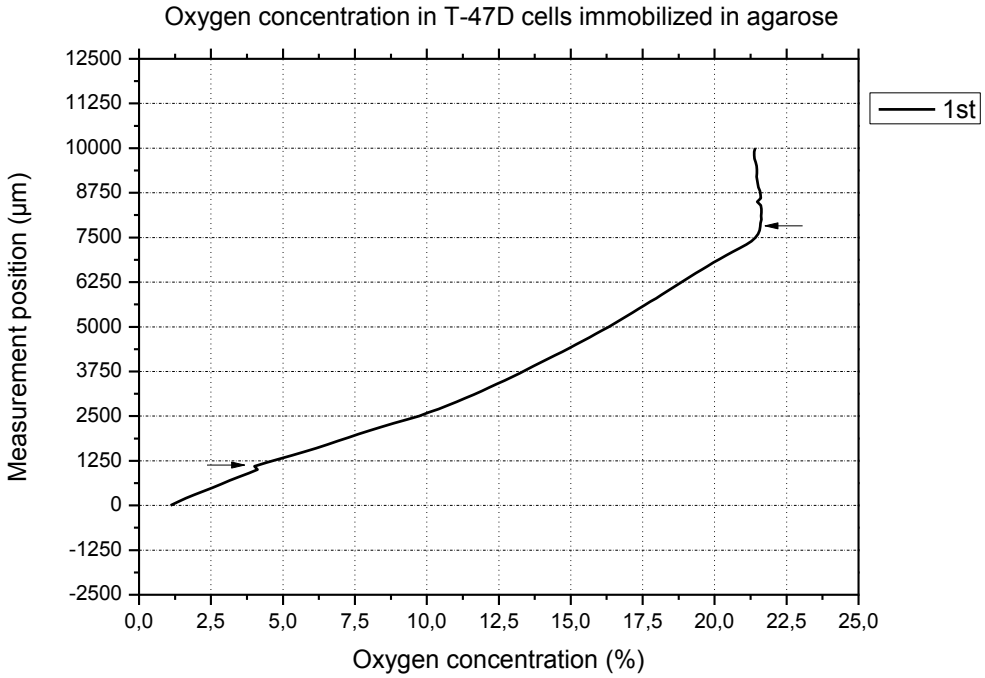

Figure 4.18: Illustration of the first oxygen profile measurement. The two arrows, indicate the upper and the lower boarders of the 0.75% cell-free agarose layer placed on the top of the cell-containing agarose layer. The zero-point on the ordinate axis is just the stop-point for the sensor, Which was was 1230 µm below the border between the two agarose layers. As observed by the figure, the cells consumed rapidly the oxygen available at the surrounding agarose layers and an oxygen gradient established, at least in the two agarose columns. During the first acquisition , oxygen concentration measured to be relatively constant in the growth medium downmost part.

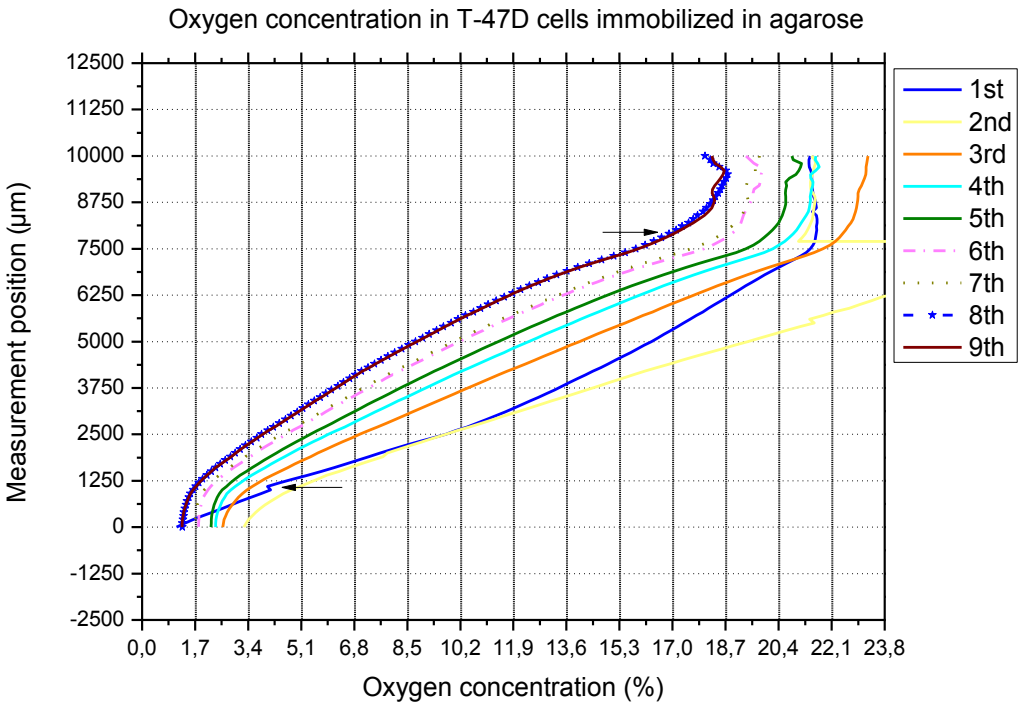

Figure 4.19: Illustration of the first nine oxygen profile measurements. Arrows indicate the upper and lower border of the 0.75% cell-free agarose. There is a trend to decrease the oxygen concentration from the first to the seventh oxygen measurement if a specific position in the glass tube is considered.

Due to an unexpected, software problem the microsensor stopped the oxygen acquisition after the ninth profile and no more profiles obtained until the next morning. The oxygen acquisition resumed as soon the software problem was solved and 12 new profiles were acquired (figure 4.20). The difference between the 9th and the 10th profile is about 14 hours. There are interesting observations when the two figures, 4.19 and 4.20, are compared. The oxygen content in the medium is kept relatively stable at about 16.5% at the medium-agarose border from the 8th profile until the 21st which means that a steady-state has been reached. The oxygen gradient is homogenous after the 8th profile and we see that this homogeneity remains in all the acquired profiles afterwards.

Moreover the oxygen concentration remains at about 1.7% on the interface of the two agarose layers if we compare the profiles 8 to 21. From the 1st profile until the 7ththe steady-state had not been established yet which resulted to instability of the oxygen

content in the two boarders of the cell-free agarose. After the steady state situation was obtained no difference in the steepness of the oxygen reduction gradient was observed.

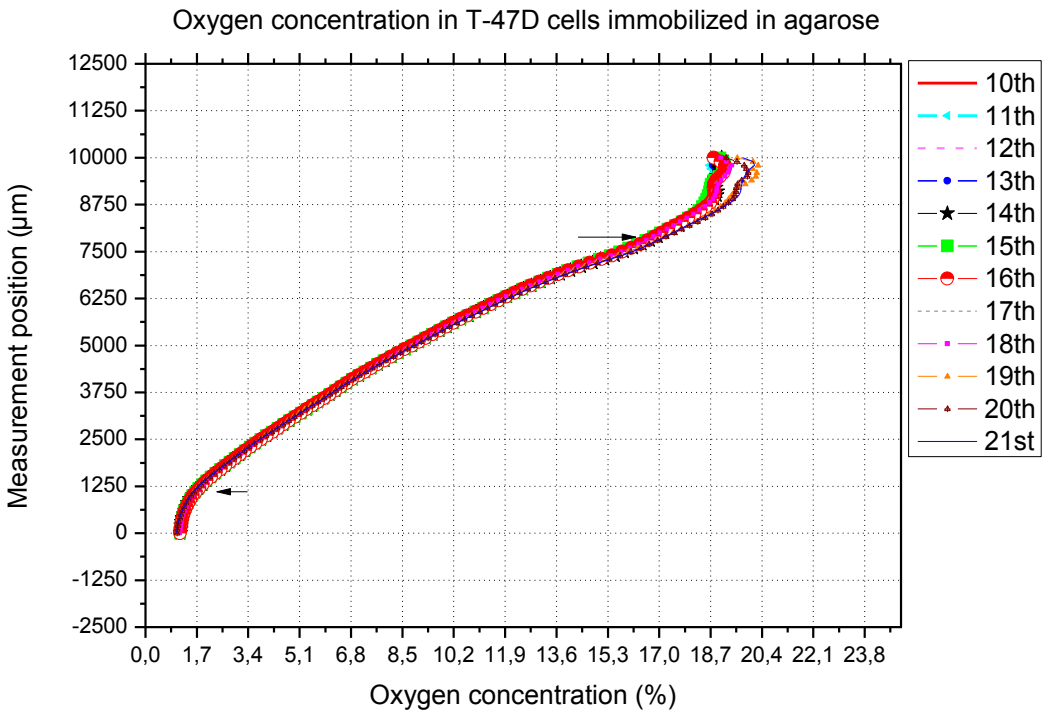

Figure 4.20: Illustration of the following 12 oxygen profile measurements. Arrows indicate the upper and lower border of the 0.75% cell-free agarose. The oxygen concentration in medium and cell-free agarose remained relatively stable through the acquisition sequences 10th to 21st.

5. Discussion

5.1 Spheroid formation

5.1.1 Spheroid generation method

In the present thesis, a new technique for spheroid culturing was tested in 4 cell lines (T-47D, HT29, MCF-7, and T98G) which have been proven to be able to form spheroids as reported in the literature (Sutherland, Sordat et al. 1986, Ronen and Degani 1989, Gamcsik, Millis et al. 1995, Eley, Benedict et al. 2002). The method proposed, tested and successfully established in the present work can be characterized as combination of the spinner flask (Gamcsik, Millis et al. 1995,Ronen and Degani 1989, Eley, Benedict et al. 2002,Marchal, Fadloun et al. 2005) and the liquid-overlay spheroid culturing methods(Sutherland, Sordat et al. 1986,Rouhani, Goliaei et al. 2014,(Ho, Yeap et al. 2012),(Sabanciota, Erguven et al. 2014)). In the proposed method,the spherically-shaped cellular aggregates formation is based upon 2 characteristic features of the experimental set up.

- Firstly, the inhibition of the cell-substrate interaction by the use of a minimally adhesive material, agarose in our case. This is the principle of the liquid-overlay technique.
- Secondly the induction of continuous rotating motion to the suspension of single cells and cellular aggregates which results in the enhancement of the cell-cell interaction and to the formation of aggregates which are characterized by nearly perfect spherical symmetry. This is the prime characteristic of the spinner flask spheroid cultures.

Spheroid culturing has been used in many laboratories but the transition from the simple and well established 2D monolayer culture to the more complicated and sophisticated 3D was never a simple process. Essential for the use of spheroid cultures in cancer research is the ability to form and maintain the spheroids with the minimum cost of material and labor. The method established in the present work combines those two very important features.

Our method has proven capable of producing spheroids with only portions of 8ml of growth medium per flask, a volume close to that used in the conventional 2D monolayer cell culture. The medium exchange was performed every alternative day meaning that the total volume utilized to produce spheroids 7 days old was not much greater than the total growth medium used in conventional monolayer cell culture for the same time period. This gives a clear advantage to our method over the spinner flask technique as the production of spheroids with this technique involves much greater volumes of growth medium with typical values ranging between 150 ml – 250 ml.

The spinner flask method is capable of production of more spheroids than the method proposed in present thesis. That comes, however with the cost of increased starting cell density and growth medium used. Furthermore, there are significant differences also on the cost between the 25 cm^2 cell culture flasks used in our method and the spinner flasks used for spheroid culturing.

On the other side, the traditional liquid overlay technique involves typically less volume of growth medium used as smaller flasks than the 25 cm^2 cell culture flasks are used. The traditional liquid overlay technique is not capable though of production of large amount of spheroidswithout the use of plates that involve a certain number of wells on it. In the case of involvement of such plates, the cost per spheroid produced is higher for the liquid overlay technique than for our method.

However, the method proposed in this thesis has also disadvantages. Damage induced to the agarose layer by the stirring movement has been noticed, meaning that the aggregates should be transferred to a new flask once per week. Furthermore, extensive cell attachment on the agarose layer has been spotted for some cell lines and there is need for further optimization of the agarose content of the layer or even substitution with other material.

Moreover the formation of large, irregularly-shaped aggregates was one of the main characteristics of our method and their presence have been proven negative to the final spheroid formation and the regular observation of the culture is mandatory in order to get those aggregates removed. From the results presented in this thesis it is clear that there is a need for individual optimization of the growth environment for each cell line. Each cell type has different characteristics regarding interaction

between cells as well as with the agarose matrix. The need of walk-in incubator or the use of a shaker that can be maintained in the regular incubator is mandatory for the application of the spheroid culturing method proposed in current thesis.

With the culturing environment tested in the present thesis, successful spheroid formation was achieved for all the 4 cell lines utilized in the experiments. However, the HT29 cells generated the largest spheroids, with good spheroid formation consistency compared to the other cell lines. From the experiments performed, it was well understood the need for individual cell-type optimization of the growth environment so as the best possible result to be achieved in the spheroid formation for all the 4 cell lines.

5.1.2 Experiments utilizing non-agarose containing flasks

In the experiments performed in 25 cm^2 cell culture flasks without any agarose coating, the results were not successful for 3 cell lines (T-47D,T98G and MCF-7) and were successful for HT29 cells. The complete absence of agarose layer on the bottom of the flask, in which the cells were seeded, led to cell attachment to the flasks bottom surface indicating that the cell-substrate force was greater than the cell-cell interaction force for the T-47D,T98G and MCF-7. In the culturing method used that did involve 25 cm^2 cell culture flasks without agarose coating, the basic principle behind the possible prevention of the cell-substrate interaction and enhancement of the cellular aggregates formation was the stirring motion induced by the orbital shaking. On this principle is also based the spinner flask spheroid culture technique where the generation of a dynamic cell suspension results in successful spheroid formation even in flasks without any agarose coating.

However, there are articles in the literature reporting successful spheroid generation with all the cell lines used in this thesis (Ronen and Degani 1989, Gamcsik, Millis et al. 1995, Eley, Benedict et al. 2002, Marchal, Fadloun et al. 2005). In all these experiments spinner flasks, with no agarose coating present, were utilized for the spheroid culture. The basic differences between the experiments reported in literature and the experiments reported in the present thesis are: The stirring speed and the utilized flasks geometry. Particularly for the two last cell lines (T98G and MCF-7)

there is a marked difference between the stirring speed used in our experiments and in the literature, with the stirring speeds utilized in literature being in the range of 120-180 rpm in contrast to the 60 and 75 rpm utilized in the our experiments.

For the T-47D-cell spheroids, there is minimal difference at the stirring speed used by Ronen and Degani (1989) and the experiments performed in our laboratory. Moreover, there was small difference in the cell density used by Ronen and Degani (1989) and the cell density utilized in our experiments. Despite the small differences in stirring speed and starting cell density, a completely different result was achieved. A possible explanation for the difference in the final result could be the use of flasks characterized by different geometry than the 25 cm^2 used in the present thesis. Furthermore, the use of different type of growth medium was noticed, with Ronen and Degani (1989) utilizing DMEM supplemented with 10% FCS, 100 u/ml penicillin, 100 μm/ml streptomycine and 10 u/ml mycostatin (Ronen and Degani 1989).

HT29-cell spheroids were generated in the experiments preformed in 25 cm^2 cell culture flasks without agarose coating. Successful spheroid formation was achieved by other researchers (Marchal, et al. 2005) using the spinner flask technique. Marchal et al. transferred (2005) HT29 cells to spinner flask with stirring at 75 rpm to generate spheroids, a stirring speed which was utilized also in the experiments reported in section 4.1.3. The successful formation of only HT29-cell spheroids by this method indicates that the experimental features utilized were more favorable for HT29 cells than for T-47D, MCF-7 and T98G, indication that if the stirring speed and/or the medium composition were optimized individually for these cells, then successful result could be achieved even with these. From the experiments performed and reported in both agarose-coated and non-agarose-coated flasks, we can conclude that there are differences in cell-cell to cell-substrate interaction forces ratio for HT29 cells and the other 3 cell lines used.

5.1.3 HT29 growth rate curves

In the experiments performed in the present thesis for the HT29-cell spheroid generation, spheroid volume growth rate curves were obtained and presented in figure 4.9. The growth rate for spheroids formed with a high starting cell number (2.7×10^6) was lower than the growth rate for spheroids formed with a low starting cell number (1.4×10^6) as presented in table 4. This result agrees with what was expected because the low starting cell number resulted in smaller spheroids than the high starting cell number. In big spheroids, a greater part of the spheroid interior is hypoxic and necrotic compared to small spheroids, meaning that the smaller spheroid should in principle grow at a faster rate than the big ones.

A main characteristic of the spheroid formation method utilized in the present thesis was the presence of single cells floating in the culture suspension. Some of those cells derive from the initially seeded single cells which are transferred over to new flasks with the transfer of spheroids. However there is reason to expect that also single cells are liberated from the surface of the spheroids simply due to cell proliferation. When a cell enters mitosis, it detaches from the surrounding cells and is prone to lose attachment to the substrate. The cells contained in the outer rim of the spheroid then, can be easily detached from the spheroid due to the stirring movement of the culture flask.

Doubling times of the cell number as measured for 2D monolayer cultures are different from the volume doubling times of the spheroids. This difference becomes more extensive for larger spheroids as it was observed for the HT29-cell spheroids. In our experiments, doubling times were obtained for two experiments reported in the chapter 4.1.2. As it was observed for the culture generating smaller spheroids, the value of the doubling time of the cell number was 34.7 hours being 8 hours lower than the value obtained for the culture generating large spheroids (table 6 and figure 4.9). Comparison can be made with the doubling time of the HT29 cell number in monolayer which is about 25 hours (personal communication with N. Edin).

Differences in the doubling times were observed by Sutherland and Durand (1984) in EMT6/Ro spheroids. Reports have also shown that the increase in doubling times is observed in both small and large spheroids. This increase in doubling times is probably associated with an increase in the cell-cycle time when the cells growing as

part of a spheroids instead of being attached on the flasks substrate (Sutherland and Durand 1984).Another possible explanation could be associated with contact inhibition of cells at the innermost part of the spheroids. For those cells the lack of space and the extensive contact with other cells could cause inhibited proliferation resulting in an increase of the mean volume doubling time of the spheroid. Furthermore, the presence of nutrient gradient at the spheroids could result in reduced nutrient supply for the cells at the central part of the spheroids. Those two situations are more extensive and severe in larger spheroids than in smaller and could explain the increase of the doubling time for large spheroids.

Moreover, the diffusion limited supply of growth factors to cells in the innermost part of the spheroid could result in limited cell cycling for those cells which would remain in the G0 phase as long as they do not get access to growth factors derived from the growth medium. Such limited supply with growth factors to cells is expected to be more extensive in the bigger spheroids than in the smaller ones.

5.2 Oxygen profiles

Oxygen concentrations have been recorded in HT29-cell spheroids using the microsensor described in chapter 3.4. The oxygen concentration measurements were characterized by high resolution, low oxygen consumption by the microsensor itself and least possible damage to the tissue.

The 2 successful oxygen acquisition experiments are presented in chapter 4.2. Both 2 spheroids had a diameter above 1 mm (1182.43 μm and 1072 μm) and both had developed a large necrotic region at the innermost part of the spheroid. As shown in the figures 4.14, 4.15 and 4.16 a large difference in the oxygen concentration of the spheroid surface was observed between the first and the subsequent profiles. The same feature was indicated in both experiments. For the 1072 μm-diameter HT29 spheroid, the oxygen concentration on the spheroid surface was measured to be 2.2% in the first profile acquired. The oxygen concentration on the same point was increased to 5% in the second oxygen profile acquired and did not change considerably thereafter (7 oxygen profiles were run). For the 1182.43 μm-diameter HT29 spheroid, the situation was very similar, with 2.5% oxygen concentration

measured on the spheroids surface in the first acquisition. In the second acquisition, there was an increase in the oxygen concentration at the same point reaching about 5.5%. The oxygen concentration value did not change significantly until the 7th profile.

The spheroids were cultured under air environment at 19% O_2 and the same oxygen concentration level was kept in the InVivo hypoxia cabinet during the oxygen profiles acquisition. For that reason the decrease of oxygen concentration on the spheroid surface to 2-2.5% and 5-5.5% was not expected. Such oxygen concentrations are significantly different from the oxygen concentration recorded by Sutherland et al. (1986) when he measured 18% for the surface of HT29 spheroid of 1116 μm diameter (Sutherland, Sordat et al. 1986). These differences can be explained by the different experimental set up that Sutherland et al. (1986) used compared to the one utilized in the present thesis. More specifically, the presence of the agarose layer, used as immobilization material for the HT29 spheroids, was the significant difference between Sutherland's experimental set up and ours. Sutherland et al. (1986) performed the oxygen measurements with the spheroids being in touch with well controlled growth medium at 19% oxygen.

The use of agarose layer in our experiments as immobilization material could be responsible for that dramatic drop of the spheroids surface oxygen concentration. In the chapter 3.5 a rather simple experimental system using a manipulator-controlled sensor system allowed for careful determination of the oxygen concentration as a function of the position of the detector. The experiment was performed, for the purpose of examination of the differences in the diffusion properties of oxygen in agarose compared to the growth medium.

As the cells consumed oxygen in a higher rate than the diffusion process of the oxygen could supply them, an oxygen concentration gradient was established through the agarose layer and the medium. A difference in the oxygen gradient in agarose and growth medium was recorded which was caused due different oxygen transport limitations. Such observations have been recorded in more experiments performed in our laboratory which have indicated also that the agarose content of such a gel can influence the oxygen diffusion through the gel (unpublished observations and personal communication with Joe Sandvik). By taking into account these results, it can be concluded that in the time interval that the oxygen profiles of the HT29

spheroids were acquired, the available oxygen in the upper agarose layer containing the spheroids, was rapidly metabolized and the presence of agarose caused reduced supply of oxygen to the spheroid due to oxygen transport limitation induced by the upper agarose layer. These limitations in oxygen supply may have to do with some form of binding of oxygen to the agarose material.

In both 2 experiments involved oxygen profile acquisition of HT29 spheroids, an oxygen concentration gradient was formed in the agarose matrix surrounding the spheroid due to high local oxygen consumption by the spheroid. The same characteristic was reported by Sutherland et al. (1986) in his experiments (Sutherland, Sordat et al. 1986) meaning that the presence of agarose instead of medium did not affect the formation of such zone in the surrounding material of the spheroid despite the fact that the oxygen gradient in the two materials are not the same as discussed before.

In both 2 experiments performed for measurement of oxygen concentration profiles in the present thesis, significant difference in the oxygen concentration on the surface of the spheroid between the first and the other 6 acquisition sequences was reported. The level of that difference is about 3% as illustrated in the figures 4.14, 4.15, and 4.16. That significant difference was not observed to the following oxygen profiles. This difference could possibly occur due to the piercing process which would involve oxygen to diffuse faster to the spheroid using the path that the sensor created through the agarose matrix during movement. As this path does not change due to the fact that the sensor does remain in the upper agarose matrix during the whole duration of the acquisitions, the difference in oxygen concentration does not change significantly after the second oxygen concentration profile.

The values of the thickness of the viable cell rim surrounding the necrotic core in the 2 oxygen concentration acquisition experiments, performed and reported in the present thesis, are presented in the table 7. Moreover, measurements of the thickness of the viable rim of HT29-cell spheroids, cultured with the same method but they were not part of the same culture as the ones measured, were obtained by the use of histological sectioning for Pimonidazome binding. Those data are also presented in table 7. The viable rim thickness values derived by the oxygen profiles are not very different from the values Sutherland et al.(1986) have reported which values are

presented in figure 5.1 (Sutherland, Sordat et al. 1986). Photographs of histological sections for Pimonidazole binding are presented in the figures 5.2 and 4.17.

Table 7: Presentation of the values describing the HT29 spheroids being used in the oxygen concentration measurements.

		Viable rim thickness (μm)		
Cell type	Spheroid diameter (μm)	Histology	Oxygen profile measurements	Difference μm
HT29	1182.4	160	216.2	56.2
HT29	1072.0	138	186	48

For spheroids of comparable size, Sutherland et al. (1986) had come up with a value of 186 μm which is not very different than the one obtained by the 2 experiments performed in the present thesis. In figure 5.2 is illustrated photograph of the histology section indicating for Pimonidazole binding. The brown colored areas indicate cells that are hypoxic but they are still alive belonging to the viable rim. In figure 5.2 the necrotic region is presented with white color surrounded by the cell viable rim. Sometimes the sections do not represent the situation at the center of the spheroid. It is a usual phenomenon during sectioning of spheroids that sections could be obtained from an outer part of the spheroid indicating thicker viable rim than the central sections.

	Spheroid diameter (μm)	Rim thickness (μm)		Hypoxic rim thickness (μm)
		Histology[a]	Microelectrode[b]	Histology-microelectrode
Co112	1035	211	160	51
	1203	193	150	43
	1335	244	110	134
	1360	210	160	50
	1504	228	140	88
	1532	208	125	83
	2011	156	200	−44
	2051	179	150	29
	2857	177	200	−23
	2271	176	150	26
	1716 ± 566[c]	198 ± 27	155 ± 29	44 ± 52
HT29	1026	257	160	97
	1039	248	186	62
	1310	237	150	87
	1324	189	250	39
	1415	196	174	22
	1532	203	200	3
	1631	215	150	65
	1751	235	180	55
	1887	226	155	71
	2035	266	250	16
	2739	203	199	4
	1608 ± 494	225 ± 26	178 ± 31	47 ± 33

[a] Measured on histological sections through centers of spheroids as in Figs. 1 and 2.
[b] Measured as the distance from where the electrode enters the spheroid to where the PO_2 profile begins to plateau as in Fig. 4.
[c] Mean ± SD.

Figure 5.1: Table illustrating the measured values for the thickness of the viable rim of HT29-cell spheroids. The values that are presented in the table by Sutherland et al. (1986) are very similar to the values presented in the table 7 (Sutherland, Sordat et al. 1986).

The extent of the viable rim's thickness was expected to be lower than the values reported by Sutherland et al. (1986) due to the fact that the oxygen concentration on the surface of the spheroid in the experiments performed in the present thesis, was significantly lower than the values Sutherland et al. (1986) measured in their experiments (18% vs 2-5%) (figures 4.14, 4.15, and 4.16). The values for the thickness of the viable rim were expected much lower due to the lower diffusion distance of the oxygen in the spheroid. However, the viable rim values obtained by the experiments performed in the present thesis and presented in table 7 are very similar to the values Sutherland et al. (1986) obtained in their experiment. Such a fact leads to the thought that the transfer of the spheroids from their growth conditions in

the spheroid culture (19%) in the upper agarose matrix before the measurements took place, did not immediately cause the death of the severely hypoxic cells near the necrotic core due to the luck of oxygen such deep in the spheroid.

It might be the case that the severely hypoxic cells in the innermost part of the spheroids viable rim get no oxygen supply after the transfer and immobilization of spheroids in the upper agarose layer with a spheroids surface oxygen concentration around 2-5%. However during the time interval that the experiment took place (about 7 hours) the length of the viable rim did not fall, indicating that the severely hypoxic cells contained in the innermost part of the viable rim survived even without any oxygen supply. Situation in which the exposure of viable cells to extreme hypoxia did not cause the imminent death of the cells, have been shown by Amellem and Pettersen (1991) who have shown that the after 6 hours of exposure to extreme hypoxia the surviving fraction of the exposed cells was about 80% (Amellem and Pettersen 1991).

By taking this fact into consideration, the similarity between the values obtained from the experiments in the present thesis and the values Sutherland et al. (1986) have measured can be explained. Furthermore, it could be part of a future research the examination of the effect of a longer oxygen acquisition length could have in the thickness of the viable rim of spheroids which would be immobilized in agarose matrix.

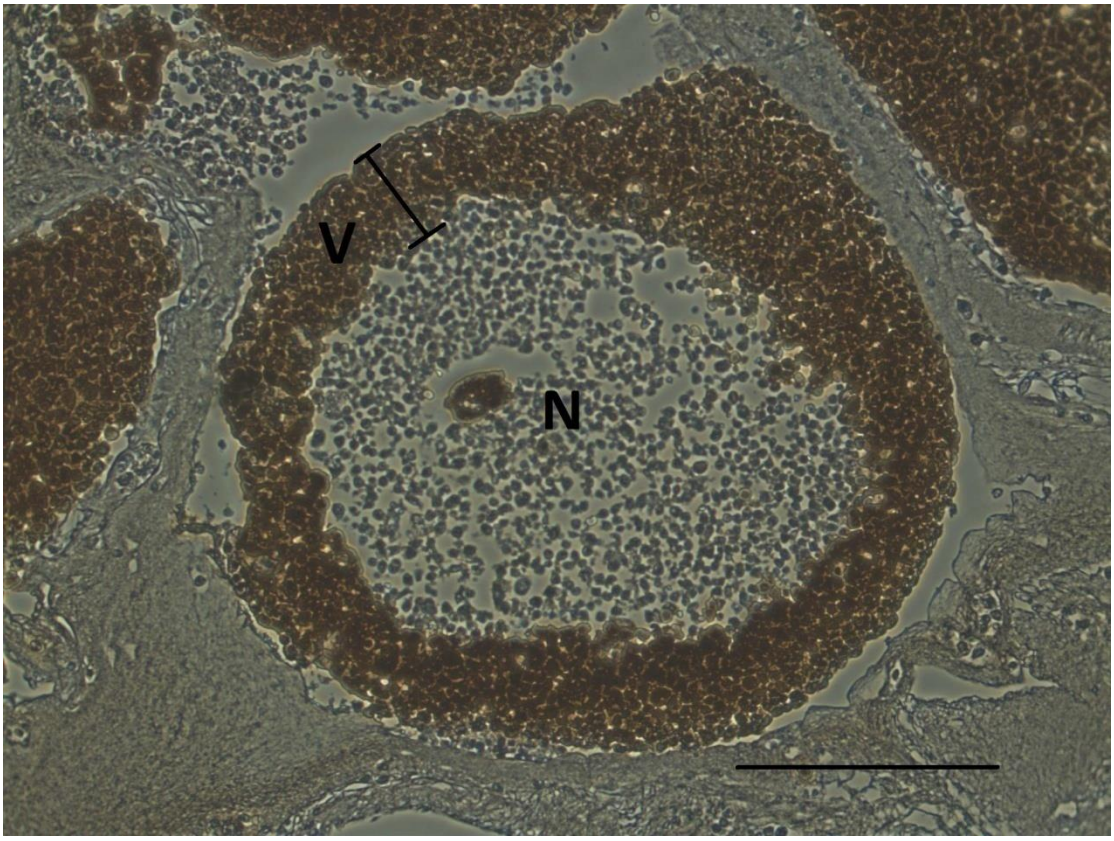

Figure 5.2: Histology section for Pimonidazole binding of HT29-cell spheroid. The cell ring illustrated with brown color indicates the region containing normoxic and hypoxic cells which are still alive (Viable rim) and denoted with the letter V. The development of necrotic core at the inner part of the spheroid can be observed in the photograph where the letter N stands for the necrotic region. The scale bar stands for distance of 333.33 μm

The use of agarose layer as a material that could ensure a stable positioning for the spheroids for the scope of oxygen profiles acquisition was successful as oxygen profile measurements were obtained. However the oxygen concentration acquisition experiments were not successful at each attempt as technical problems raised in some experiment. As illustrated in figure 5.3, there were cases when the piercing of the spheroid resulted in the distruction of the spheroid with release of cells and extracellular fluid. In such cases the whole spheroid was destroyed and the acquisition was stopped. Moreover, the process for determination of the center of the spheroid could be influenced by agarose gel inhomogeneities and compression of the agarose gel due to the progression of the sensor in the process. In such cases, the acquired oxygen profiles were not symmetric around the center of the spheroid. Moreover, the poor calibration of the oxygen sensor could induce problematic measurements.

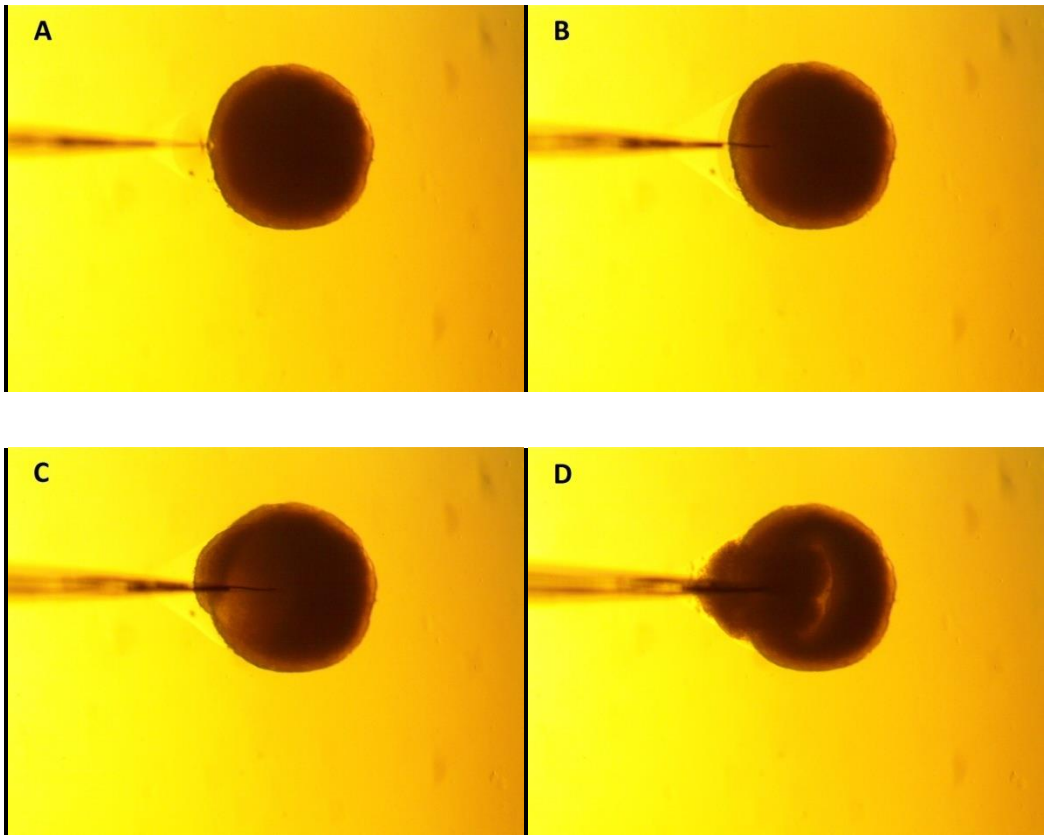

Figure 5.3: Photographic illustration of a situation of spheroid damage in the process of piercing by the oxygen sensor during an oxygen concentration profile measurement. The oxygen sensor propagation process starts in the photograph A and ends to the photograph D. Such phenomenon was observed in several cases, with the destruction of the spheroid with the release of cells and fluid immediately after the piercing of the spheroid.

6. Conclusion and further work

6.1 Conclusion

The spheroid culture method proposed and tested in the present thesis was successful in spheroid formation with all 4 cell lines used. The HT29 cells though formed the largest spheroids and thus seems best suited for this technique without further optimization.

Successful T-47D-cell spheroid formation was achieved with spheroids cultured to diameters up to about 300 μm. MCF-7 spheroids were also successfully generated with formed spheroids grow to diameter about 250 μm. HT29-cell spheroids were cultured until they reached to mean diameter of 840 μm. Moreover, T98G-cell spheroid formation was achieved with their size growing to diameter range between 150 and 200 μm.

Two successful oxygen profile sequences were obtained for HT29-cells spheroids immobilized in agarose. The agarose matrix induced increased transportation limitations to oxygen diffusion than the growth medium did, which is the main reason why the oxygen concentration on the spheroid surface is so low (at 2- 2.5%) for spheroids immobilized in agarose.

The values of the viable rim for the two HT29-cell spheroids measured from the oxygen profiles (figures 4.15 and 4.16) do not differ greatly from the values measured using the histology sections for Pimonidazole staining, as presented in the table 7. Thickness values of the viable rim range from 138 to 216.2 μm for HT29-cell spheroid of diameter above 1 mm.

6.2 Further work

The work that was performed in the current thesis has plenty room for improvement and potential use in the future studies. The spheroid formation method proposed and tested in the current thesis, requires optimization for the individual cell line that will be applied. The different culture environments tested in all 4 cell lines used in the present thesis, it was proven to be optimum for HT29 than for the other cell lines. Positive results were obtained from all the cell lines but HT29-cell spheroids were by far the spheroids with the best results in matters of consistency of successful spheroid generation and in matters of size of spheroids. The proposed spheroid formation method, could be adopted by various researchers in the cancer research involve in vitro tumor modeling.

As far as the oxygen concentration profiles acquisition experiments are concerned, the immobilization of spheroids in agarose matrix while a microsensor penetrates into the spheroid's inner part measuring oxygen concentration, was successfully applied in the experiments performed in the present thesis. There are few researchers who have used agarose matrix for spheroid immobilization in experiments involving oxygen profiles acquisition in vitro and this thesis can provide other researchers with vital information about the advantages and the disadvantages of such a technique.

Due to some technical problems faced during the last year, only two experiments were successfully accomplished for the acquisition of oxygen concentration profiles in HT29-cell spheroids. In the future, such experiments could be also performed for spheroids of a wider range of diameters. Furthermore, it could be a challenge for the future researchers to perform such experiments with spheroids of various cell lines.

The mathematical model simulating the oxygen consumption and the oxygen concentration was based on the assumptions which Grimes et al. (2014) did in their work and the final expression for the oxygen concentration was similar to the one Grimes at al. reached (Grimes, 2014). This model could be used so as mathematical analysis to be performed for the determination of the consumption rate and the oxygen diffusion distance in cancer spheroids for plenty of cell lines as both consumption rate and oxygen diffusion constant in spheroids are cell-dependent quantities.

7. Bibliography

Amellem, O. and E. O. Pettersen (1991). "Cell inactivation and cell cycle inhibition as induced by extreme hypoxia: the possible role of cell cycle arrest as a protection against hypoxia-induced lethal damage." Cell Prolif**24**(2): 127-141.

An, W. G., M. Kanekal, M. C. Simon, E. Maltepe, M. V. Blagosklonny and L. M. Neckers (1998). "Stabilization of wild-type p53 by hypoxia-inducible factor 1alpha." Nature**392**(6674): 405-408.

Bakkenist, C. J. and M. B. Kastan (2003). "DNA damage activates ATM through intermolecular autophosphorylation and dimer dissociation." Nature**421**(6922): 499-506.

Bedford, J. S. and J. B. Mitchell (1974). "The effect of hypoxia on the growth and radiation response of mammalian cells in culture." Br J Radiol**47**(562): 687-696.

Brown, J. M. (1990). "Tumor hypoxia, drug resistance, and metastases." J Natl Cancer Inst**82**(5): 338-339.

Brown, J. M. and A. J. Giaccia (1998). "The unique physiology of solid tumors: opportunities (and problems) for cancer therapy." Cancer Res**58**(7): 1408-1416.

Brown, J. M. (1999). "The hypoxic cell: a target for selective cancer therapy--eighteenth Bruce F. Cain Memorial Award lecture." Cancer Res**59**(23): 5863-5870.

Brown, J. M. and W. R. Wilson (2004). "Exploiting tumour hypoxia in cancer treatment." Nat Rev Cancer**4**(6): 437-447.

Chaplin, D. J., R. E. Durand and P. L. Olive (1986). "Acute hypoxia in tumors: implications for modifiers of radiation effects." Int J Radiat Oncol Biol Phys**12**(8): 1279-1282.

Chaplin, D. J., P. L. Olive and R. E. Durand (1987). "Intermittent blood flow in a murine tumor: radiobiological effects." Cancer Res**47**(2): 597-601.

CLARK, L. C., R. WOLF, D. GRANGER and Z. TAYLOR (1953). "Continuous recording of blood oxygen tensions by polarography." J Appl Physiol**6**(3): 189-193.

Del Duca, D., T. Werbowetski and R. F. Del Maestro (2004). "Spheroid preparation from hanging drops: characterization of a model of brain tumor invasion." J Neurooncol**67**(3): 295-303.

Dewhirst, M. W., H. Kimura, S. W. Rehmus, R. D. Braun, D. Papahadjopoulos, K. Hong and T. W. Secomb (1996). "Microvascular studies on the origins of perfusion-limited hypoxia." Br J Cancer Suppl**27**: S247-251.

Edin, N. J., D. R. Olsen, J. A. Sandvik, E. Malinen and E. O. Pettersen (2012). "Low dose hyper-radiosensitivity is eliminated during exposure to cycling hypoxia but returns after reoxygenation." Int J Radiat Biol**88**(4): 311-319.

Eley, K. W., S. H. Benedict, T. D. Chung, B. D. Kavanagh, W. C. Broaddus, R. K. Schmidt-Ullrich and P. S. Lin (2002). "The effects of pentoxifylline on the survival of human glioma cells with continuous and intermittent stereotactic radiosurgery irradiation." Int J Radiat Oncol Biol Phys**54**(2): 542-550.

Fogh, J., J. M. Fogh, T. Orfeo (1977). "One hundred and twenty-seven cultured human tumor cell lines producing tumors in nude mice"J Natl Cancer Inst**59**(1): 221-226.

Friedrich, J., C. Seidel, R. Ebner and L. A. Kunz-Schughart (2009). "Spheroid-based drug screen: considerations and practical approach." Nat Protoc**4**(3): 309-324.

Gamcsik, M. P., K. K. Millis and O. M. Colvin (1995). "Noninvasive detection of elevated glutathione levels in MCF-7 cells resistant to 4-hydroperoxycyclophosphamide." Cancer Res**55**(10): 2012-2016.

Griemes, D. R., C. Kelly, K. Bloch, M. Partridge (2014). "A method for estimating the oxygen consumption rate in multicellular tumour spheroids." J R Soc Interface **11**(92): 20131124.

Hall E. J., A. J. Giaccia.*Radiobiology for the Rdiologist*. Lippincott Williams & Wilkins, seventh edition, 2012.

Hammond, E. M., M. J. Dorie and A. J. Giaccia (2003). "ATR/ATM targets are phosphorylated by ATR in response to hypoxia and ATM in response to reoxygenation." J Biol Chem**278**(14): 12207-12213.

Ho, W. Y., S. K. Yeap, C. L. Ho, R. A. Rahim and N. B. Alitheen (2012). "Development of multicellular tumor spheroid (MCTS) culture from breast cancer cell and a high throughput screening method using the MTT assay." PLoS One**7**(9): e44640.

Keydar, I., L. Chen, S. Karby, F. R. Weiss, J. Delarea, M. Radu, S. Chaitcik, J. H. Brenner (1979). "Establishment and characterization of a cell line of human breast carcinoma origin." Eur J Cancer**15**(5): 659-670.

Koch, C. J., J. Kruuv, H. E. Frey and R. A. Snyder (1973). "Plateau phase in growth induced by hypoxia." Int J Radiat Biol Relat Stud Phys Chem Med**23**(1): 67-74.

Kraggerud, S. M., J. A. Sandvik and E. O. Pettersen (1995). "Regulation of protein synthesis in human cells exposed to extreme hypoxia." Anticancer Res**15**(3): 683-686.

Lin, R. Z., L. F. Chou, C. C. Chien and H. Y. Chang (2006). "Dynamic analysis of hepatoma spheroid formation: roles of E-cadherin and beta1-integrin." Cell Tissue Res**324**(3): 411-422.

Marchal, S., A. Fadloun, E. Maugain, M. A. D'Hallewin, F. Guillemin and L. Bezdetnaya (2005). "Necrotic and apoptotic features of cell death in response to Foscan photosensitization of HT29 monolayer and multicell spheroids." Biochem Pharmacol**69**(8): 1167-1176.

Obacz, J., S. Pastorekova, B. Vojtesek and R. Hrstka (2013). "Cross-talk between HIF and p53 as mediators of molecular responses to physiological and genotoxic stresses." Mol Cancer**12**(1): 93.

Pettersen, E. O. and T. Lindmo (1983). "Inhibition of cell-cycle progression by acute treatment with various degrees of hypoxia: modifications induced by low concentrations of misonidazole present during hypoxia." Br J Cancer**48**(6): 809-817.

Pettersen, E. O., N. O. Juul and O. W. Ronning (1986). "Regulation of protein metabolism of human cells during and after acute hypoxia." Cancer Res**46**(9): 4346-4351.

Pettersen, E. O., L. H. Larsen, N. B. Ramsing, P. Ebbesen (2005). " Pericellular oxygen depletion during ordinary tissue culturing, measured with oxygen microsensors." Cell Proliff**38**(4): 257-267.

Radiobiology for the Radiologist , 7.edition,Eric J. Hall and Amato J. Giaccia , Lippincott Williams &Wilkins, 2012.

Ronen, S. and H. Degani (1989). "Studies of the metabolism of human breast cancer spheroids by NMR." Magn Reson Med**12**(2): 274-281.

Sabanciota, P. A., M. Erguven, N. Yaziotahan, E. Aktas, Y. Aras, E. Civelek, A. Aydoseli, M. Imer, M. Gurtekin and A. Bilir (2014). "Sorafenib and lithium chloride combination treatment shows promising synergistic effects in human glioblastoma multiforme cells in vitro but midkine is not implicated." Neurol Res**36**(3): 189-197.

Smith, T. G., P. A. Robbins and P. J. Ratcliffe (2008). "The human side of hypoxia-inducible factor." Br J Haematol**141**(3): 325-334.

Soule, H. D., J. Vazquez, A. Long, S. Albert, M. Brennan (1973). "A human cell line from a pleural effusion derived from a breast carcinoma."J Natl Cancer Inst**51**(5): 1409-1416

Stein, G. H. (1979). "T98G: an anchorage-independent human tumor cell line that exhibits stationary phase G1 arrest in vitro" J Cell Physio**99**: 43-54.

Stenersen Espe, E. K. (2009). "The effect of chronic hypoxia and low dose-rate β-irradiation on the MCF-7 human cancer cell." Master's Thesis, Universitetet i Oslo.

Sutherland, R. M., J. A. McCredie, W. R. Inch (1971)."Growth of multicell spheroids in tissue culture as a model of nodular carcinomas."J Natl Cancer Inst**46**(1): 113-120.

Sutherland, R. M. and R. E. Durand (1984). "Growth and cellular characteristics of multicell spheroids." Recent Results Cancer Res**95**: 24-49.

Sutherland, R. M., B. Sordat, J. Bamat, H. Gabbert, B. Bourrat and W. Mueller-Klieser (1986). "Oxygenation and differentiation in multicellular spheroids of human colon carcinoma." Cancer Res**46**(10): 5320-5329.

Thomlinson, R. H. and L. H. Gray (1955). "The histological structure of some human lung cancers and the possible implications for radiotherapy." Br J Cancer**9**(4): 539-549.

Varia, M. A., D. P. Calkins-Adams, L.H. Rinker, A. S. Kennedy, D.B. Novotny, W. C. Jr Fowler, J. A. Raleigh (1998). "Pimonidazole: a novel hypoxia marker for complementary study of tumor hypoxia and cell proliferation in cervical carcinoma."Gynecol Oncol**71**(2):270-277

Vaupel, P. (2008). "Hypoxia and aggressive tumor phenotype: implications for therapy and prognosis." Oncologist**13 Suppl 3**: 21-26.

Vinci, M., S. Gowan, F. Boxall, L. Patterson, M. Zimmermann, W. Court, C. Lomas, M. Mendiola, D. Hardisson and S. A. Eccles (2012). "Advances in establishment and analysis of three-dimensional tumor spheroid-based functional assays for target validation and drug evaluation." BMC Biol**10**: 29.

Wartenberg, M., F. Donmez, F. C. Ling, H. Acker, J. Hescheler and H. Sauer (2001). "Tumor-induced angiogenesis studied in confrontation cultures of multicellular tumor spheroids and embryoid bodies grown from pluripotent embryonic stem cells." FASEB J**15**(6): 995-1005.

Yuan, J. and P. M. Glazer (1998). "Mutagenesis induced by the tumor microenvironment." Mutat Res**400**(1-2): 439-446.

Zhao, Y., R. Yao, L. Ouyang, H. Ding, T. Zhang, K. Zhang, S. Cheng and W. Sun (2014). "Three-dimensional printing of Hela cells for cervical tumor model in vitro." Biofabrication**6**(3): 035001.

Appendix A

T-47D-cell spheroid formation experiments

A.1

A.1.1

In this experiment, 1.6 x 10^6 cells were seeded, on day 0, in a 25 cm^2 spheroid culture flask without agarose coating. The flask was continuously orbital rotated at 60 rpm. Photographs were taken during all stages of the culture and are presented in figure A.1. It was noticed that the vast majority of the T-47D cells attached to the bottom surface of the flask rather than attach to other T-47D cells. This is clearly demonstrated by the photographs shown in figure A.1. As soon as day 1, most cells had attached to the flask's substrate and not many cell aggregates had formed. At the following days, 100% confluence was reached and not any successful spheroid formation was observed. The cells were maintained in the same flask during the whole duration of the experiment and after day 5 the experiment was stopped. In chapter 3.2 can be found more information regarding the cell cultivation and maintenance method. The spheroids were constantly kept in an atmosphere with 19% O_2 and 4% CO_2 in N_2.

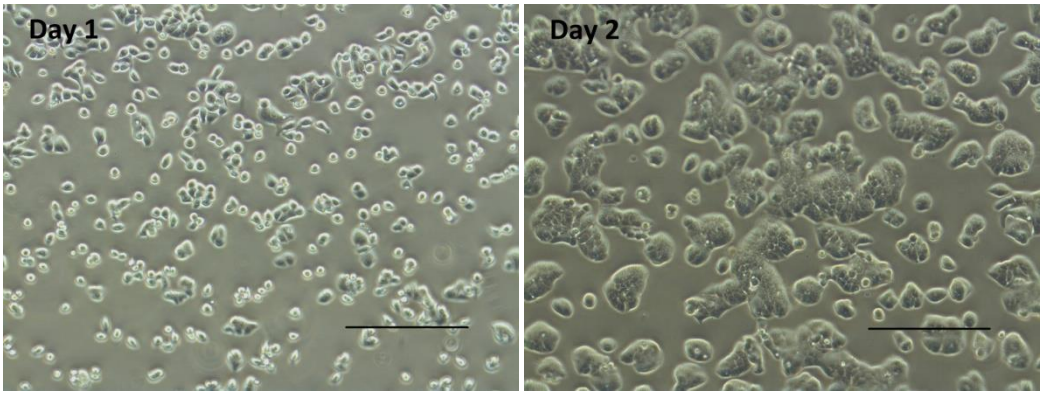

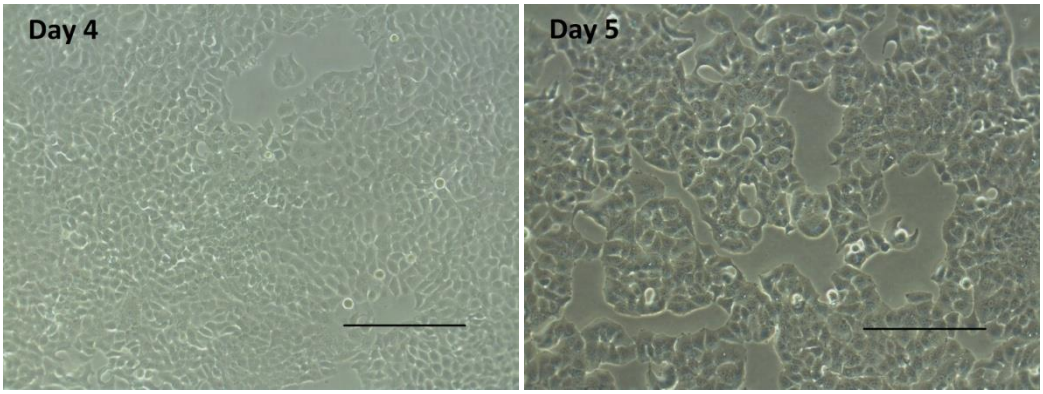

Figure A.1: Illustration of the an experiment for spheroid formation with T-47D cells in 25cm^2 cell culture flask without any agarose coating. The initial number of the cells seeded was 1.6 x 10^6 using stirring speed of 60 rpm. The cell attachment to the substrate of the flask was obvious from day 1 of the culture and no successful spheroid formation was observed in any stage of the experiment. The degree of attachment did not change at all in the whole duration of the experiment. The scale bar stands for distance of 333.33 μm.

Day 1

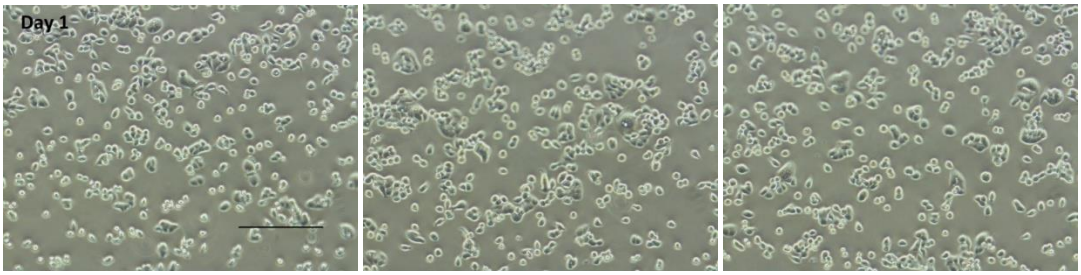

Day 2

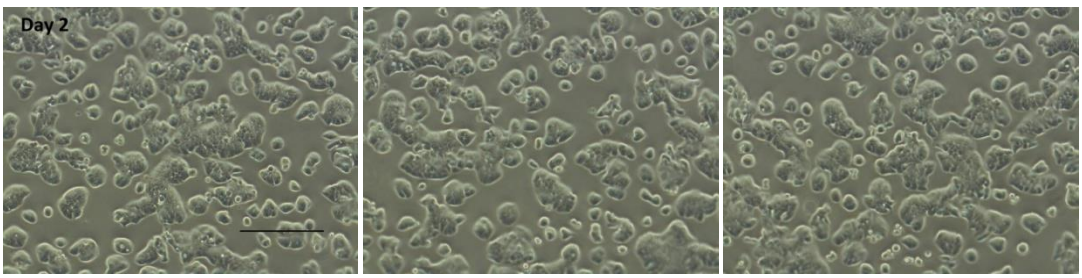

Day 4

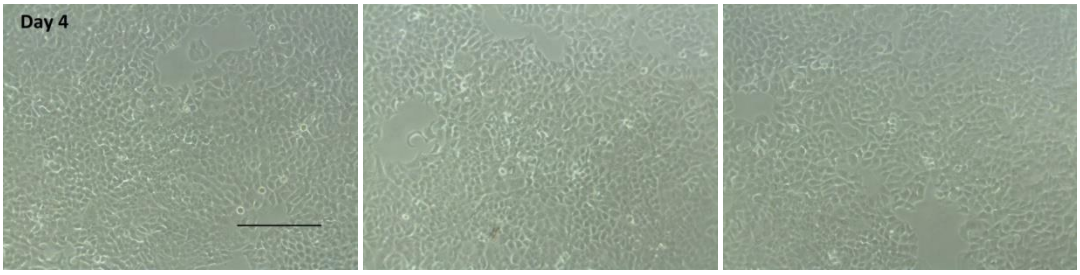

Day 5

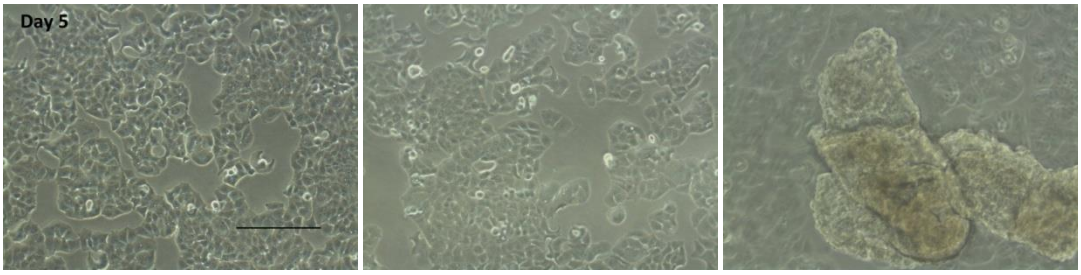

A.1.2

The description of the present experiment is reported in the chapter 4.1.1.

Day 2

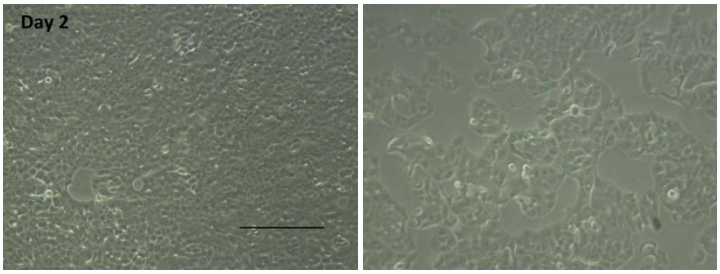

Day 3

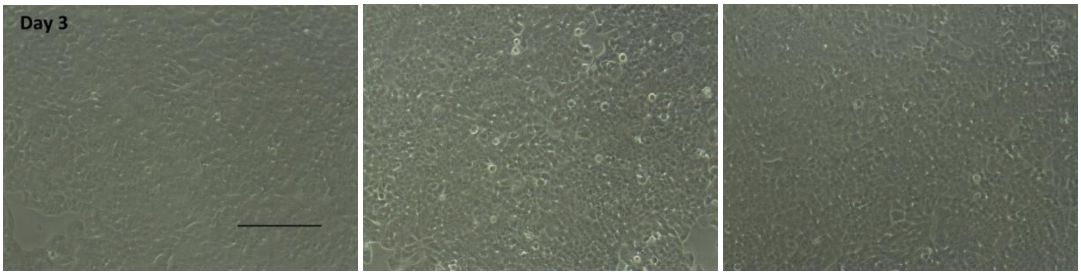

Day 5

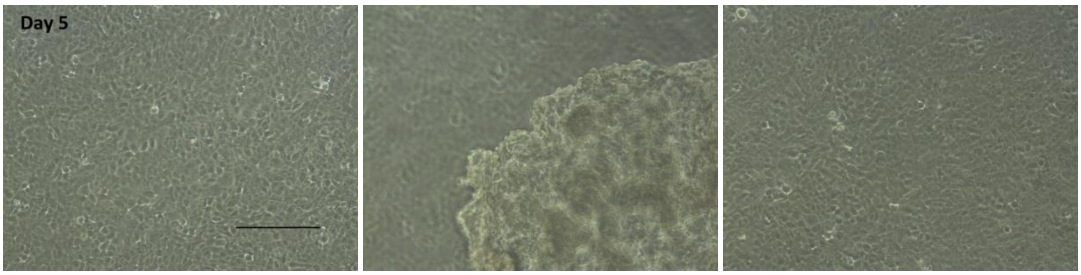

A.1.3

For the present experiment, still using a flask without agarose coating, the stirring speed was increased to 75 rpm with the starting cell number reduced to 1.6 x 10^6 T-47D cells seeded on day 0. In figure A.2 photographs are shown, which were taken during the experiment. In the first days, the cell attachment to the flask bottom was reduced compared to the first experiment as a result of the increase of stirring speed. Moreover, more cell aggregates were formed in the first days of the experiments than in the previous two experiments. However, at the next days, most of the single cells adher on the flasks substrate and the growth of the aggregate was minimal. On day 5, there were few aggregates and those that existed were irregularly shaped. The irregular shape and size of those aggregates was the reason that they cannot be considered as spheroids. After the day 5, the experiment stopped and was characterized as unsuccessful. As in the previous two experiments, the cells and cellular aggregates were not transferred to a new flask during the 6 days of the experiment. As described in chapter 3.2, the growth medium exchange was performed every alternative day with the first exchange performed on day 2. The spheroids were constantly kept in an atmosphere with 19% O_2 and 4% CO_2 in N_2.

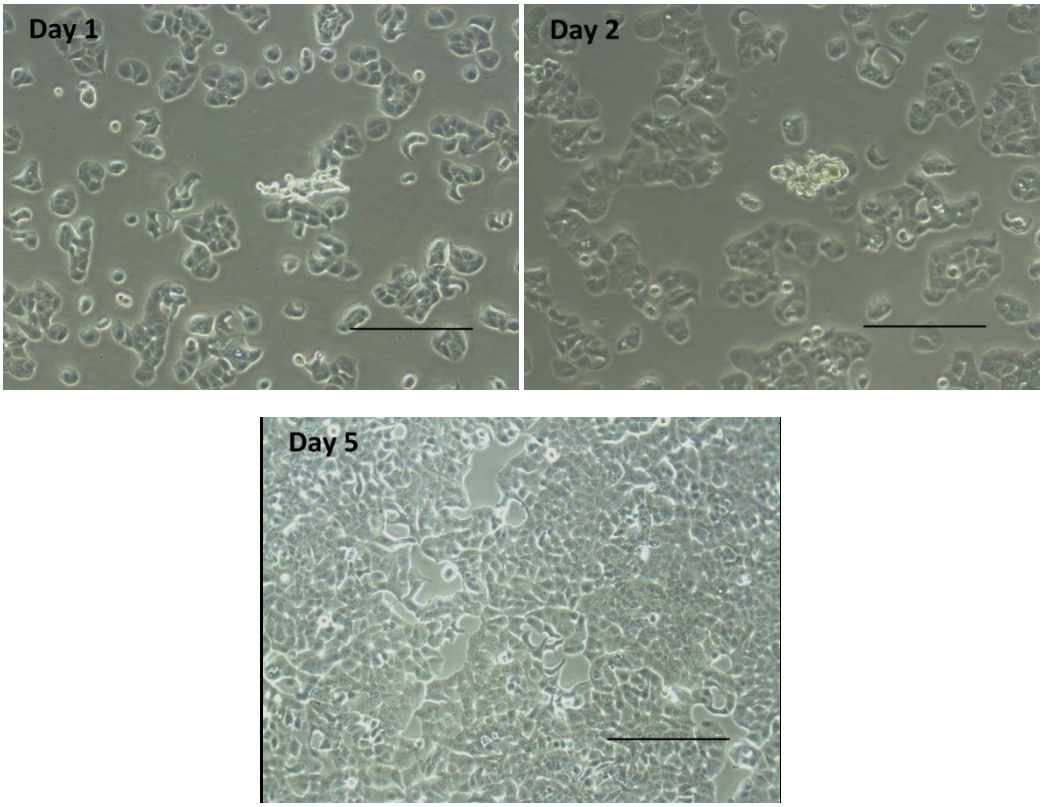

Figure A.2: Illustration of photographs from the present experiment for spheroid culture and growth with T-47D cells in 25 cm^2 cell culture flask without any agarose coating. The starting cell number used in this experiment was the same as in the first experiment (Appendix A.1.1) (1.6 x 10^6) but the stirring speed was increased to 75 rpm. The increase of the orbital speed seemed to reduce cell attachment to the bottom of the culture flask for the first days. Some small aggregates can be observed in the photographs taken on day 1 and day 2. However, during the following days most cells were driven to substrate attachment and at the day 5 no spheroid was successfully formed. The scale bar stands for distance of 333.33 µm.

Day 1

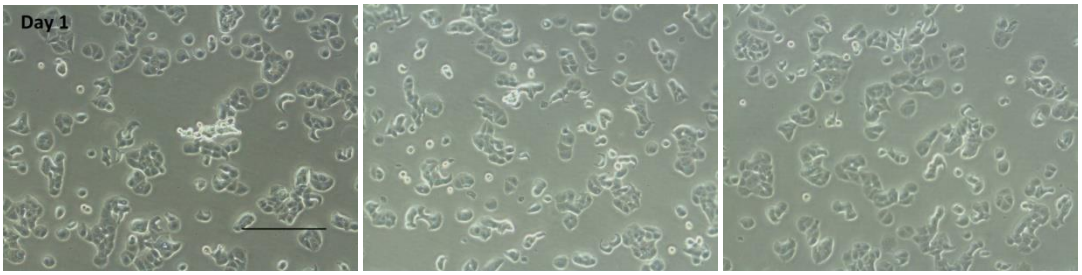

Day 2

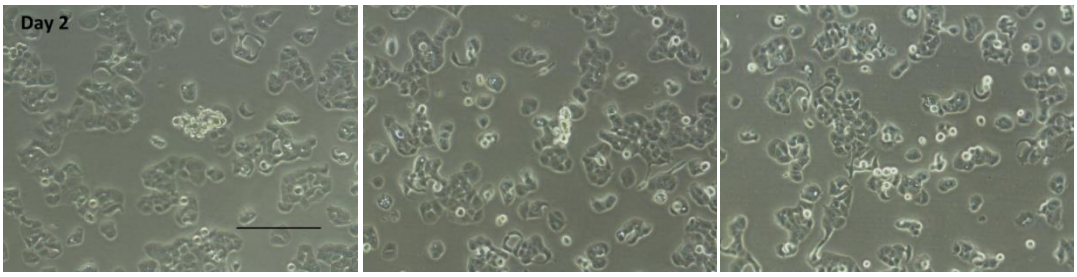

Day 4

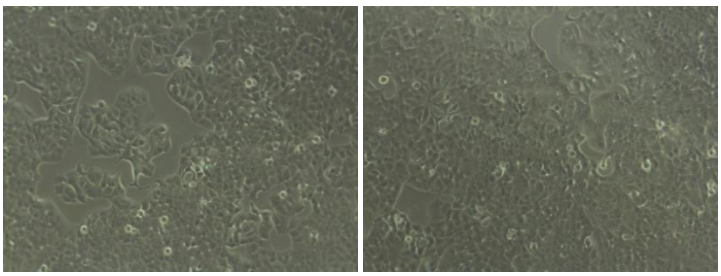

Day 5

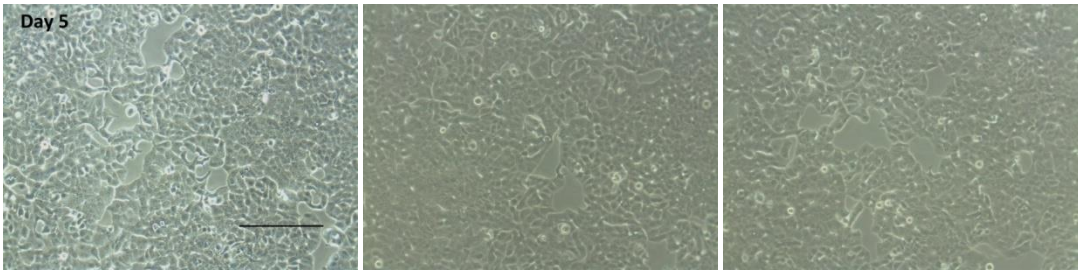

A.1.4

In the last experiment in this series, 4.1 x 10^6 T-47D cells were seeded, day 0, in a flask without agarose coating which was maintained under continuous stirring motion at 75 rpm. At the first days of the culture, the dominating interaction was the cell-substrate interaction with the vast majority of the total amount of the cells to adhere on the flasks bottom. Not any significant cell aggregate formation was noticed during the whole duration of the attempt. In that experiment the cellular aggregates and the single cells were kept in the same 25 cm^2 cell culture flask from day 0 (cell seeding day) to day 5. After day 5 the experiment terminated without any successful result. As described in chapter 3.2, the growth medium exchange was performed every alternative day with the first exchange performed on day 2. The spheroids were constantly kept in an atmosphere with 19% O_2 and 4% CO_2 in N_2.

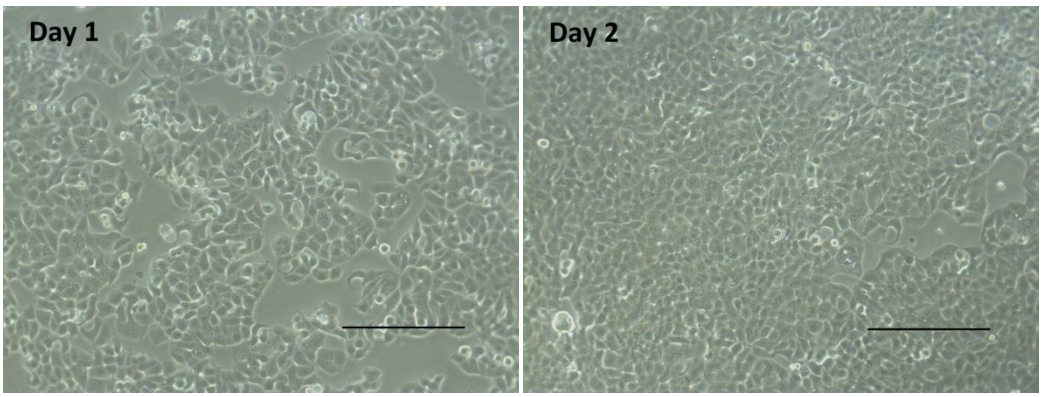

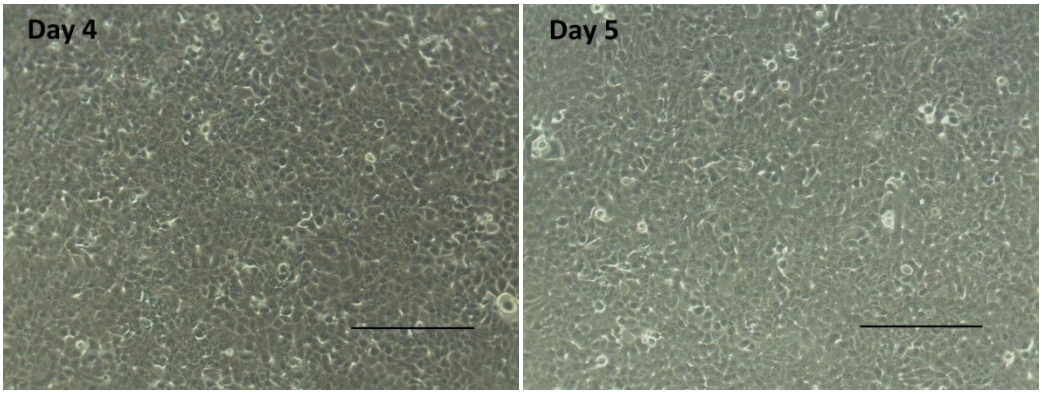

Figure A.3: Illustration of the last attempt for spheroid formation with T-47D cells in 25 cm^2 cell culture flask without any agarose coating. In this attempt 4.1 x 10^6 cells were seeded on day 0 of the experiment. The cells were kept in a uninterrupted stirring motion at 75 rpm speed. It is noticeable that the most cells attached to the flasks bottom from the first days of the attempt. The confluence of the flask reached about 95% at day 2. There were no cellular aggregates formed in this experiment The scale bar stands for distance of 333.33 μm.

Day 1

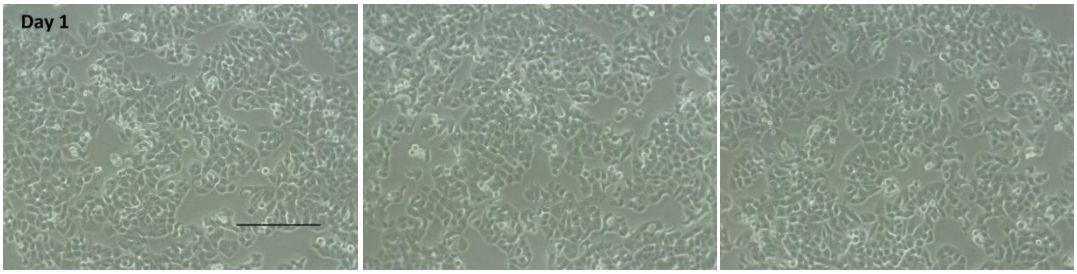

Day 2

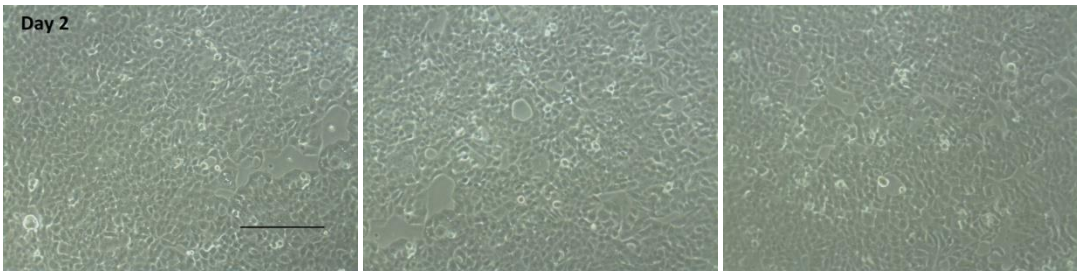

Day 4

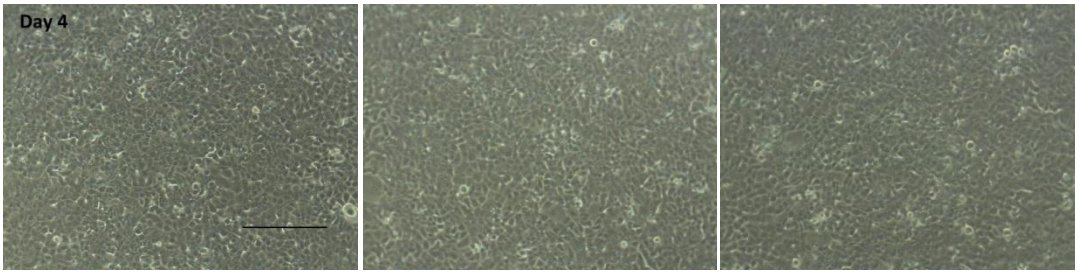

Day 5

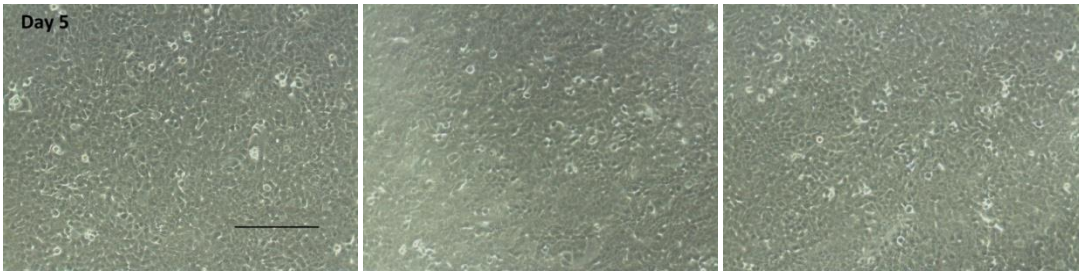

Table A.1: All the different combinations of stirring speed and initial cell number tested in 25 cm^2 cell culture flasks without any agarose

	T-47D cells seeded on day 0	
Stirring speed (rpm)	1.6 x 10^6	4.1 x 10^6
60	A.1.1	A.1.2
75	A.1.3	A.1.4

A.2

A.2.1

The description of the present experiment is reported in the chapter 4.1.1.

Day 1

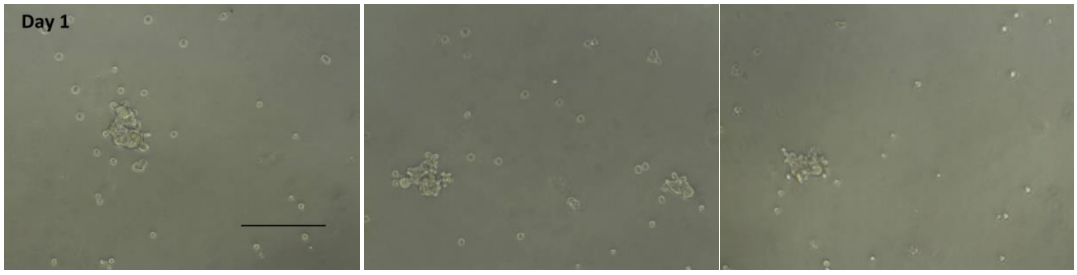

Day 2

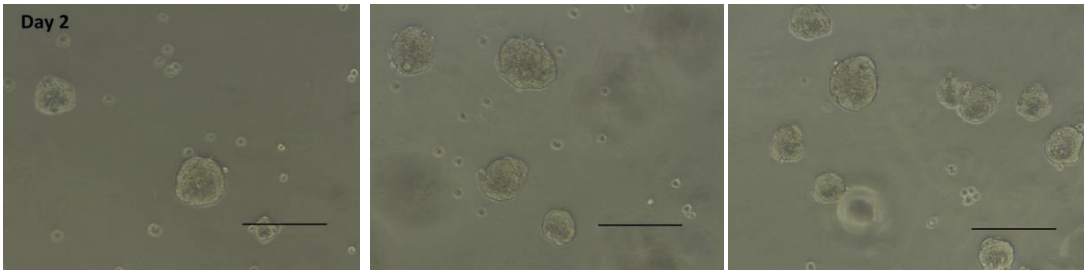

Day 3

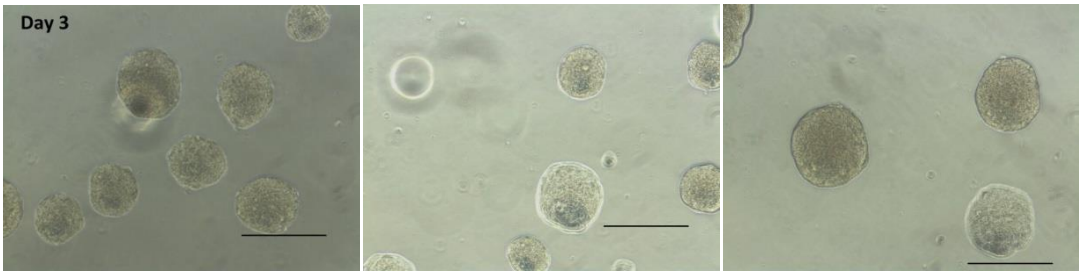

Day 4

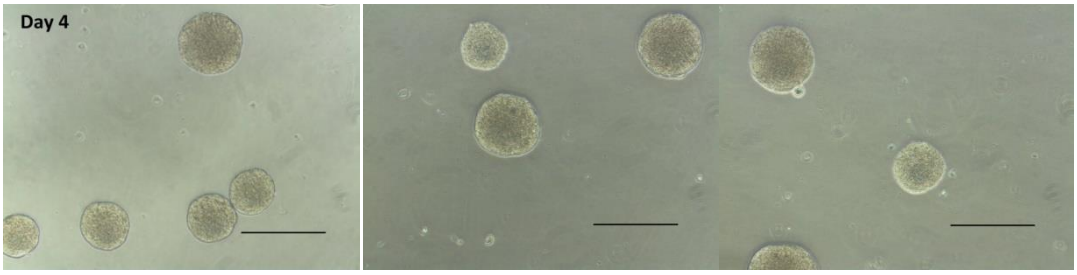

Day 5

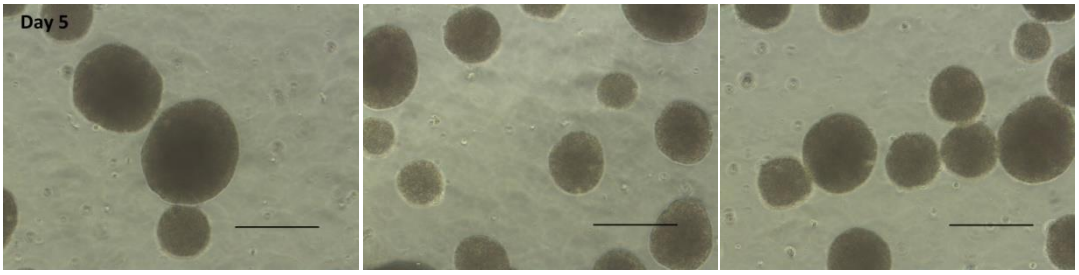

Day 7

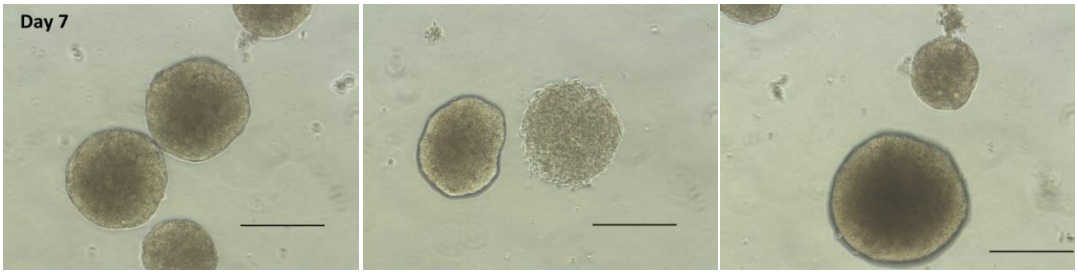

Day 11

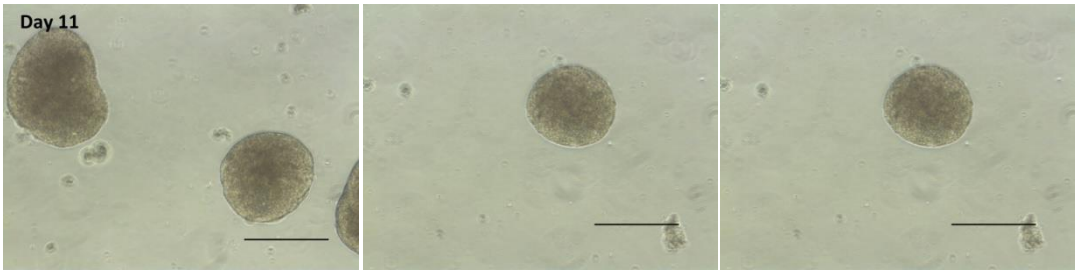

A.2.2

In the present experiment using agarose-coated 25 cm^2 cell culture flask, the cell number was 1.6 x 10^6 T-47D cells and the stirring speed was at 75 rpm. The spheroids were transferred to a new cell flask at day 3 of the experiments and the growth medium was exchanged every second day thereafter. Cellular aggregates were successfully formed but they lacked of any spherical symmetry as it is illustrated in figure A.4. The shape of most cellular aggregates was irregular with some very large aggregates formed at day 7 as is visualized in the figure A.4. Those large aggregates were formed in most of the attempts independently of the cell type used and can be declared as a basic characteristic of the culturing method in question. As described in chapter 3.2, the growth medium exchange was performed every alternative day with the first exchange performed on day 2. The spheroids were constantly kept in an atmosphere with 19% O_2 and 4% CO_2 in N_2.

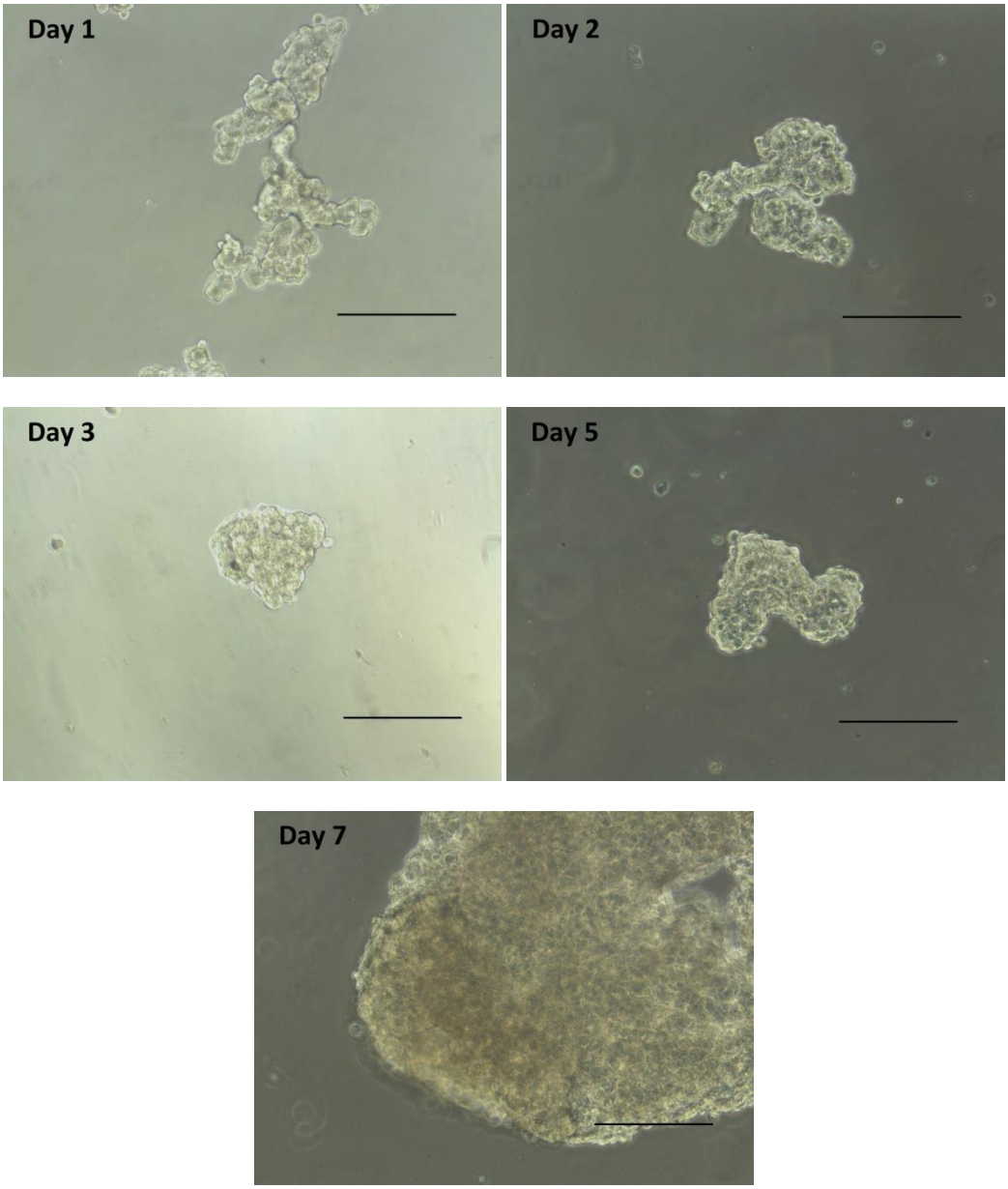

Figure A.4: Illustration of the photographs acquired at the second experiment for spheroid formation with T-47D cells in agarose-coated 25 cm^2 cell culture flask. 1.6 x 10^6 cells seeded in the flask on day 0 and mantained under continuous stirring speed of 75 rpm. The only difference between this experiment and the one illustrated in figure 4.3 was the increased stirring speed used in this experiment (75 rpm) compared to 60 rpm utilized in the one described in Chapter 4.1.1 (section 2). The vast majority of the aggregates obtained and retained an irregular shape. The irregular shape of the formed aggregates was the main drawback in this attempt. A large aggregate is illustrated in the photograph taken at day 7. The scale bar stands for distance of 333.33 μm.

Day 1

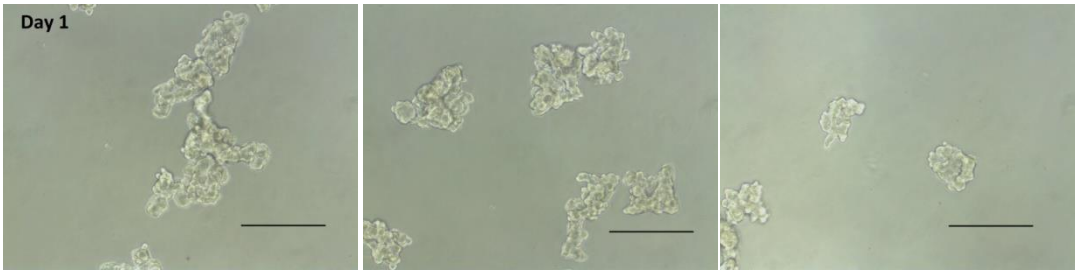

Day 2

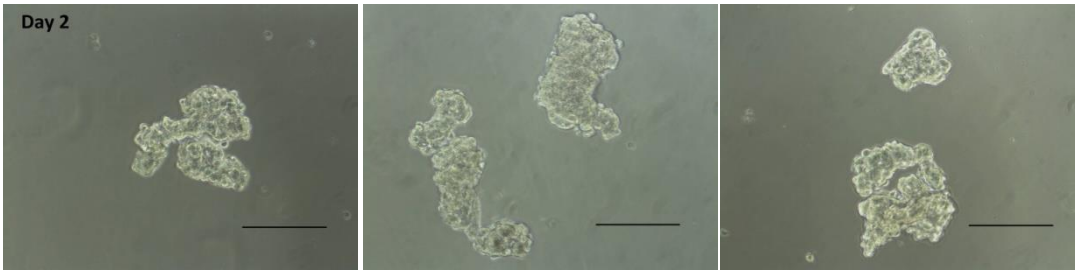

Day 3

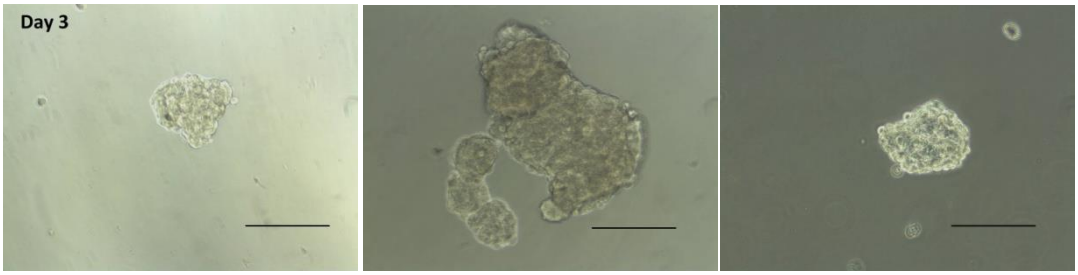

Day 5

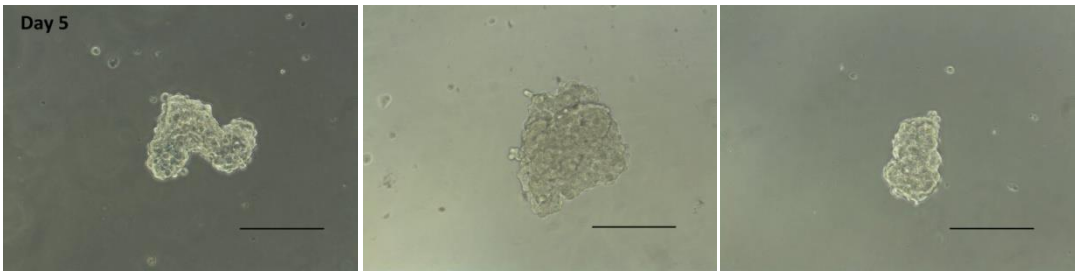

Day 7

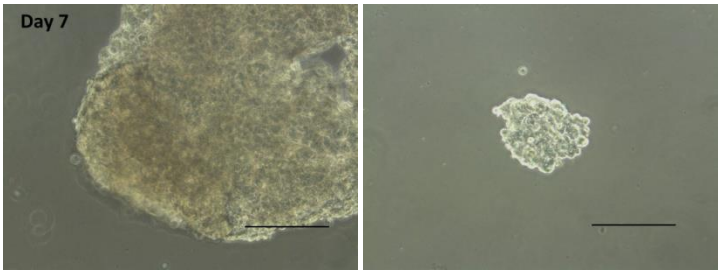

A.2.3

In the third and last experiment in this series the stirring speed was kept at 75 rpm while the initial number of seeded cells was increased to 4.1 x 10^6 cells. As in the previous case the agarose-coated flask, containing the suspension with aggregates, was kept under constant orbital motion promoting the formation of cellular aggregates. In figure A.5 can be observed photographs acquired from day 1 to day 7 of the culture. The resulting aggregates were irregularly shaped, a result which is similar to that obtained in the previous experiment (shown in figure A.4). Large aggregate clusters showed up on day 7 as in the previous case. This attempt failed to produce any spheroid and it was stopped after day 7. As described in chapter 3.2, the growth medium exchange was performed every alternative day with the first exchange performed on day 2. The spheroids were constantly kept in an atmosphere with 19% O_2 and 4% CO_2 in N_2.

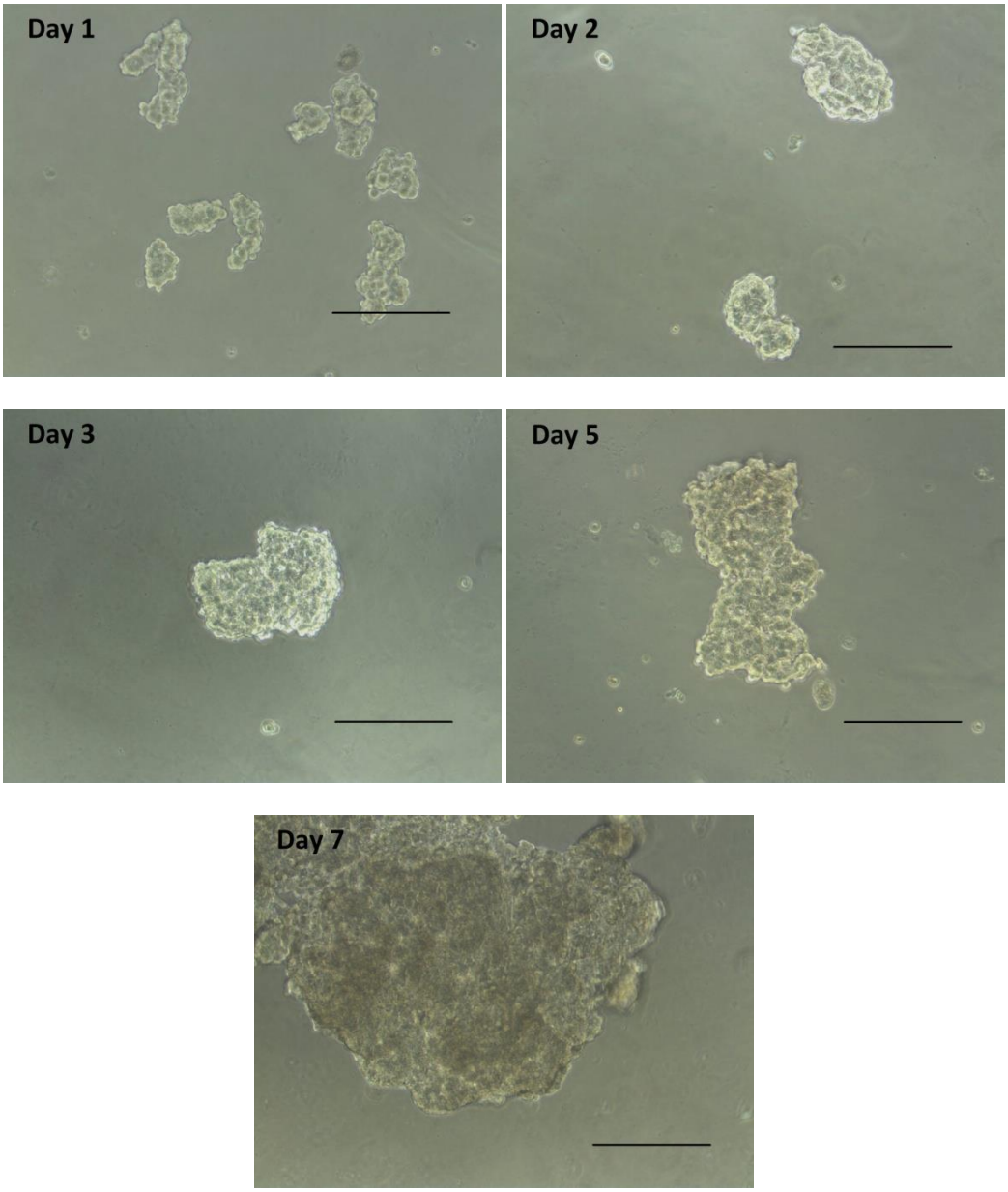

Figure A.5: Visualization of the third experiment of spheroid formation by using T47-D cells. 4.1 x 10^6 T47-D cells, suspended in 8 ml of RPMI, were seeded in the agarose-coated 25 cm^2 flask. The uninterrupted shaking motion (75 rpm) of the flask boosted the cellular aggregates formation with the first ones formed at the first two days of the culture. The vast majority of the cellular aggregates were not characterized by spherical symmetry and so they were not considered as spheroids. The scale bar stands for distance of 333.33 μm.

Day 1

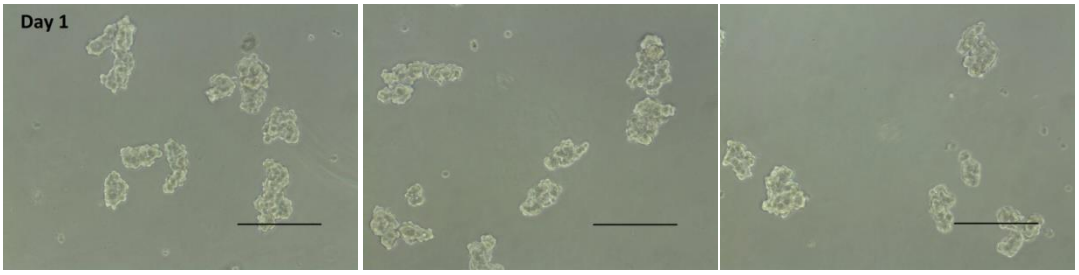

Day 2

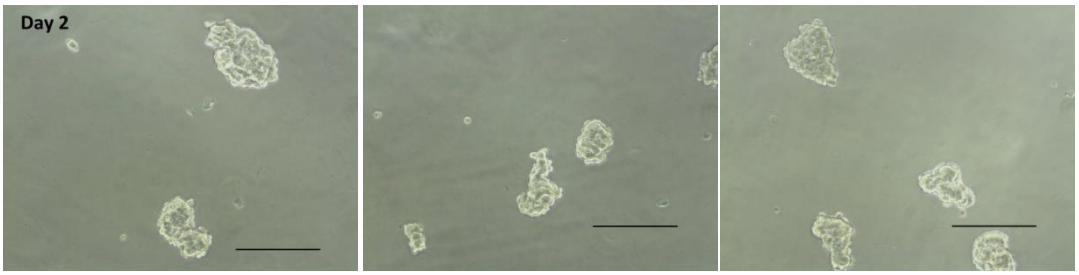

Day 3

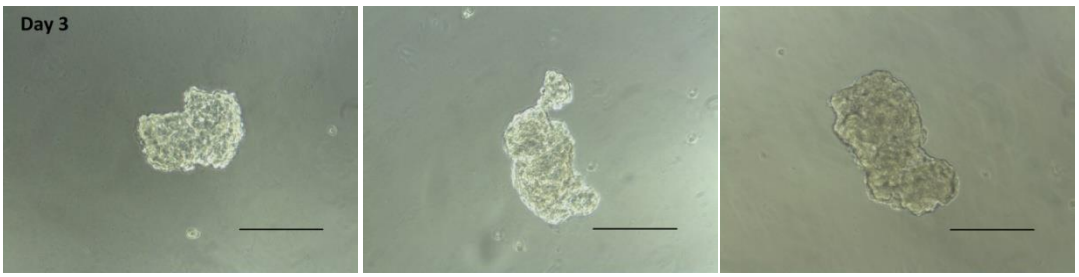

Day 5

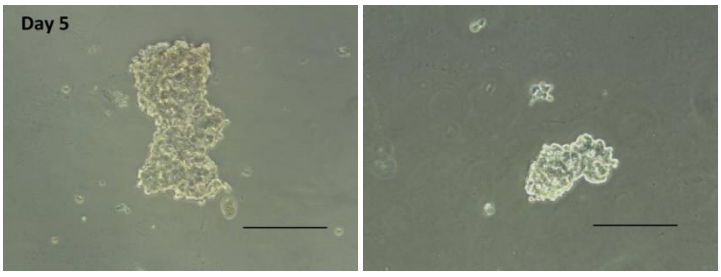

Day 7

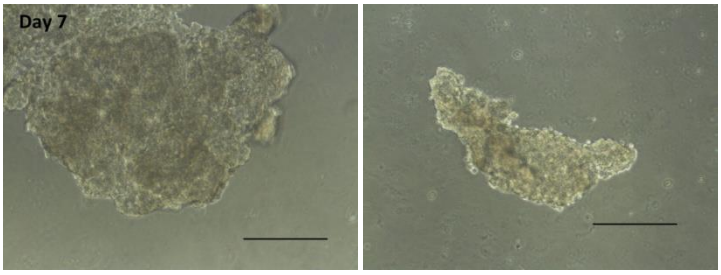

Table A.2: The dedicated chapter in the Appendix A.2 for all the different combinations of stirring speed and initial cell number tested in agarose-coated 25 cm^2 cell culture flasks

	T-47D cells seeded on day 0	
Stirring speed (rpm)	1.6×10^6	4.1×10^6
60	A.2.1	--
75	A.2.2	A.2.3

A.3

Overview of the optimal parameters for the T-47D-cell spheroids generation.

Cell type	**T-47D**
Starting cell number	1.6×10^6
Stirring speed	60 rpm
Agarose-coating	Yes
Thickness of agarose layer	1 mm
Diameters of spheroid formed	300 µm
Day that this diameter reached by the spheroids	Day 7-Day 11
Medium volume	8 ml

Appendix B

HT29-cell spheroid formation experiments

B.1

B.1.1

The description of the present experiment is reported in the chapter 4.1.2.

Day 2

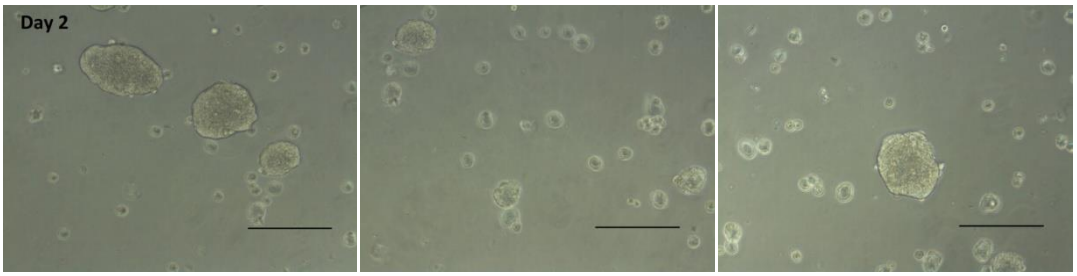

Day 5

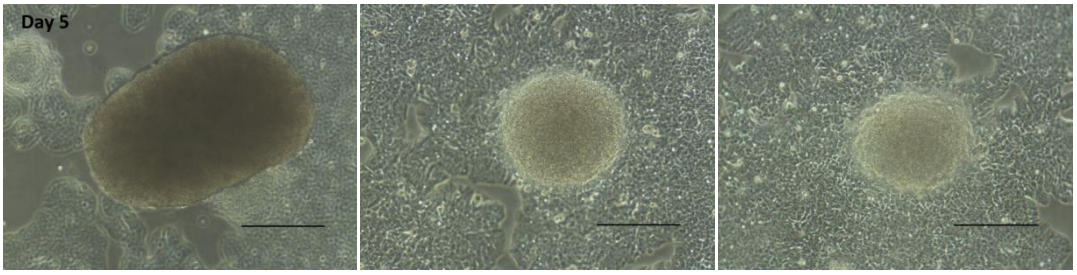

Day 7

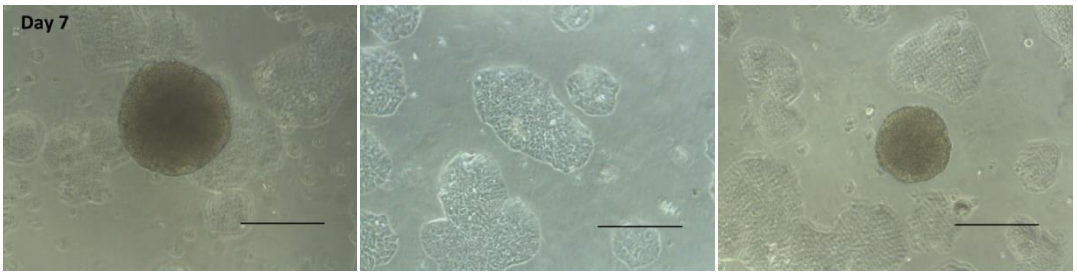

B.1.2

For the present experiment, 2.7 x 10^6 HT29 cells were seeded, on day 0, in 25 cm^2 cell culture flask without agarose coating. The flask was put on the shakers platform and was kept under continuous stirring movement at the speed of 60 rpm. On day 2, cellular aggregates were already formed even if the flask was not coated with agarose. The absence of agarose coating from the flask, used in this experiment, was the main reason for the cell attachment to the substrate of the flask and 2D monolayer culture occurrence, as visualized figure B.1. Spherical aggregates were successfully generated in this experiment as well. In this experiment the spherical and non-spherical aggregates were transferred to a new 25 cm^2 on day 6. After the end of day 7, the experiment was terminated. As described in chapter 3.2, the growth medium exchange was performed every alternative day with the first exchange performed on day 2. The spheroids were constantly kept in an atmosphere with 19% O_2 and 4% CO_2 in N_2.

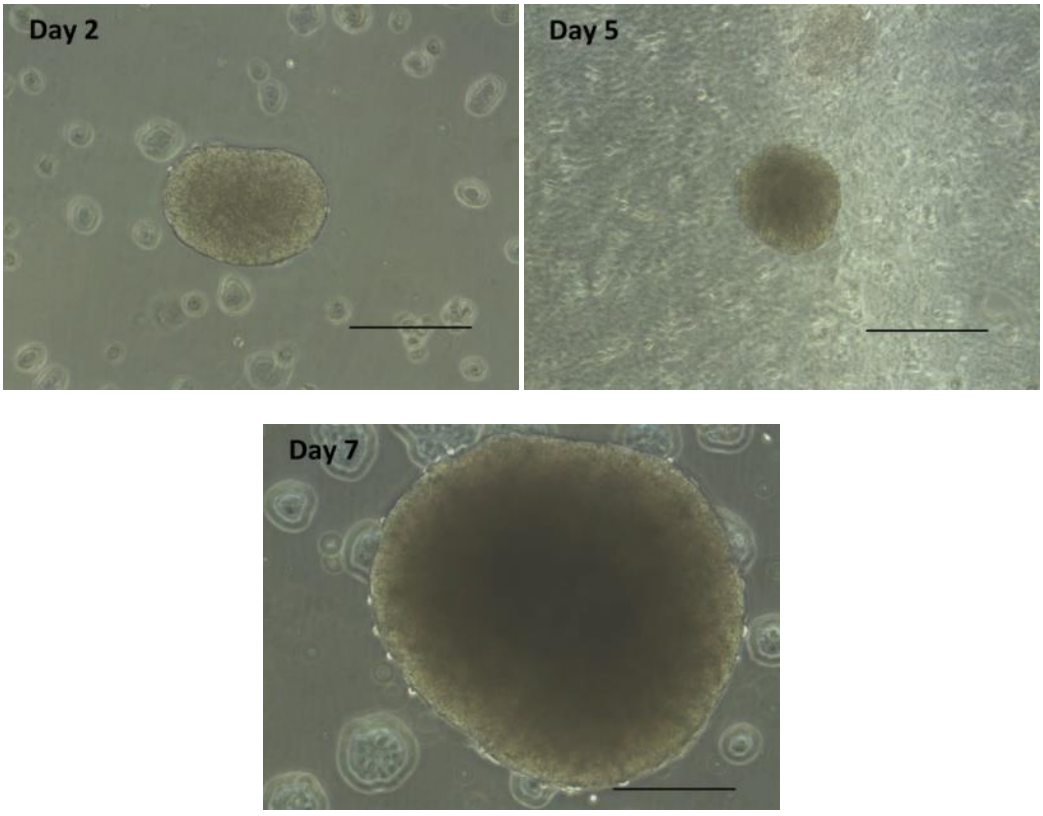

Figure B.1: Visualization of experiment for HT29-cell spheroids generation. 2.7 x 10^6 single cells were employed in day 0 and seeded in a 25 cm^2 cell culture flask. The culture was maintained under orbital stirring motion at 60 rpm. Successful spheroid formation was noticed in the experiment as well

with the cell attachment to the bottom surface of the flask. The scale bar stands for distance of 333.33 μm.

Day 2

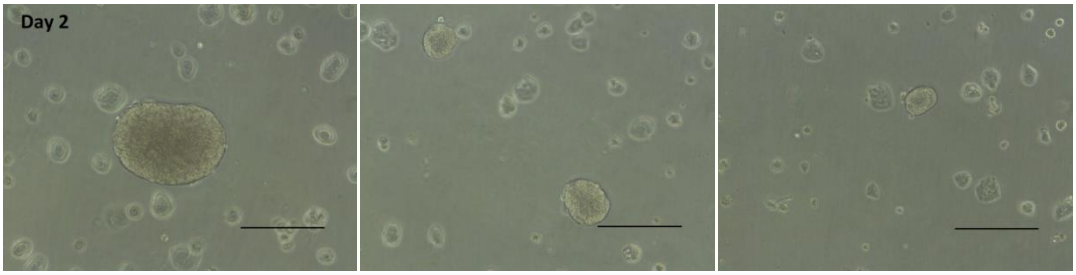

Day 5

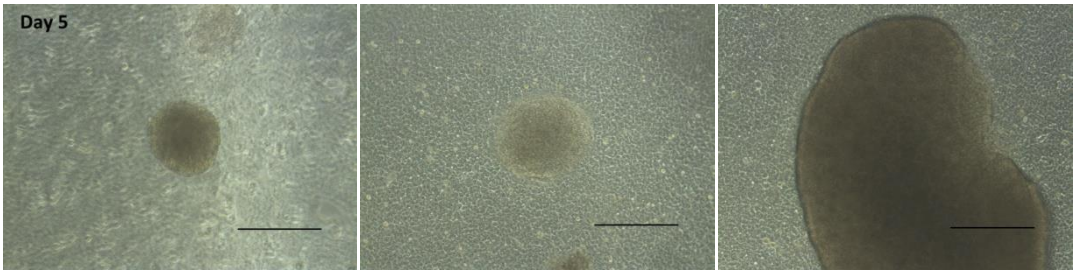

Day 7

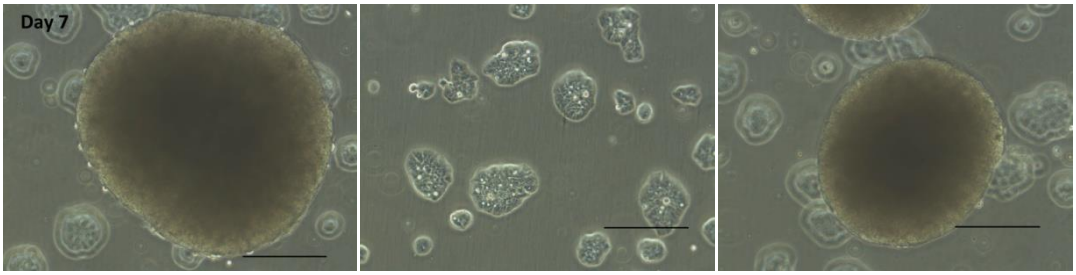

B.1.3

For the present experiment, 1.4 x 10^6 HT29 cells were seeded, on day 0, in 25 cm^2 cell culture flask without agarose coating. The flask was put on the shakers platform and was kept under continuous stirring movement at the speed of 75 rpm. Spherical aggregates were formed in various stages of the experiment, always along with some cell attachment to the flask. The increase of the stirring speed, compared to the experiment described in chapter 4.1.2 (section 1), had positive contribution in the spheroid formation as fewer cells attached on the flasks bottom surface on the first days of the culture. Illustration of photographs acquired on various days of the experiment is presented in figure B.2. The aggregates were maintained in the same flask until the end of the experiment on day 7. As described in chapter 3.2, the growth medium exchange was performed every alternative day with the first exchange performed on day 2. The spheroids were constantly kept in an atmosphere with 19% O_2 and 4% CO_2 in N_2.

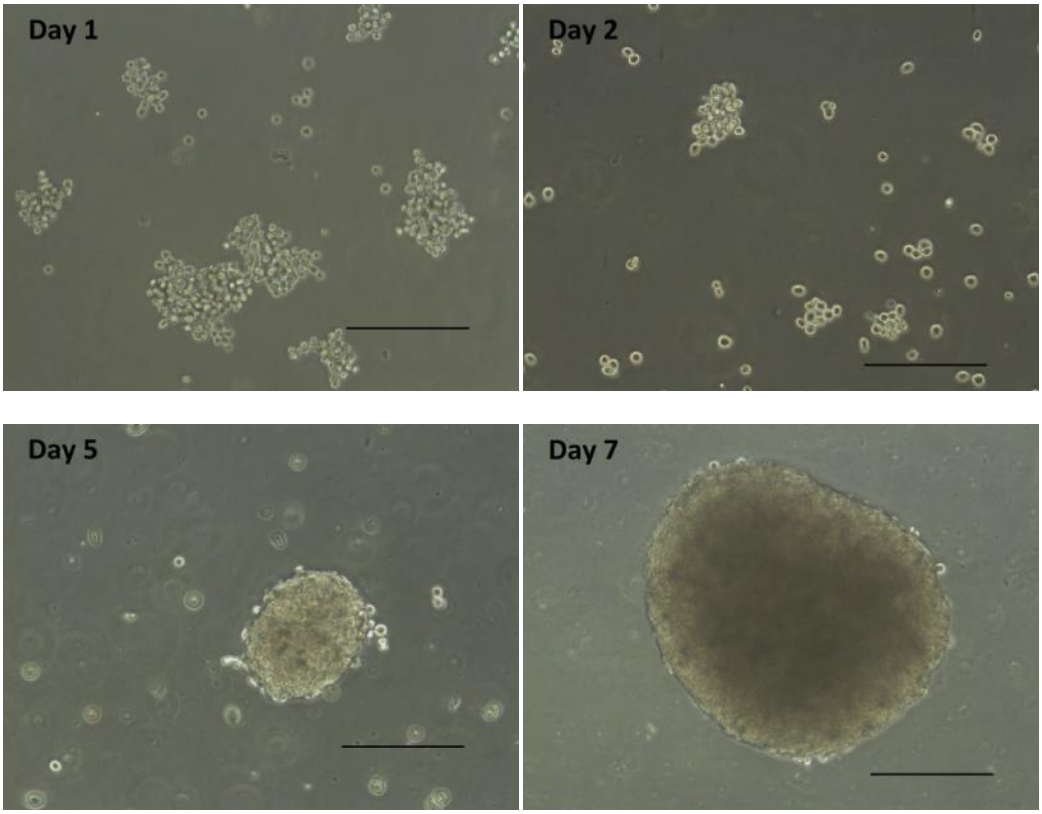

Figure B.2: Photographic illustration of experiment for HT29-cell spheroid generation. 1.4 x 10^6 cells were employed on day 0 and maintained in the culture flask under orbital motion at 75 rpm. Spheroids associated with irregularly-shaped cellular aggregates and single cells were present in the flask on day 5.The scale bar stands for distance of 333.33 μm.

Day 1

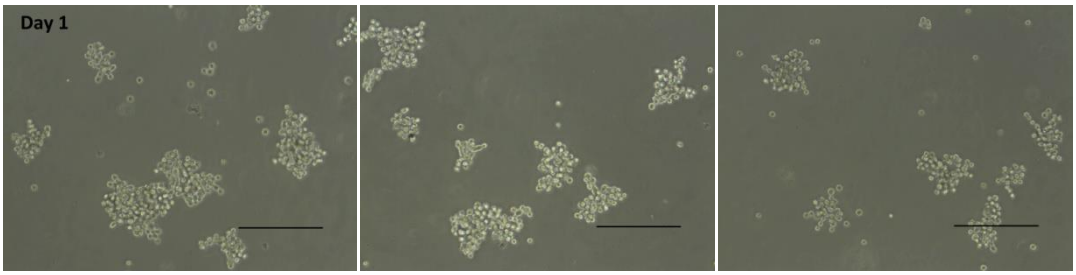

Day 2

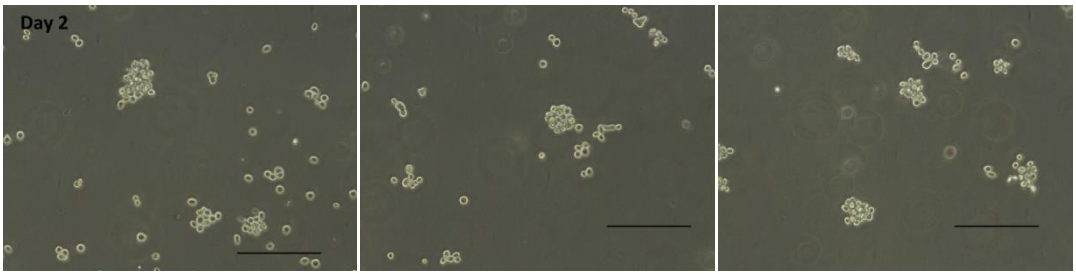

Day 5

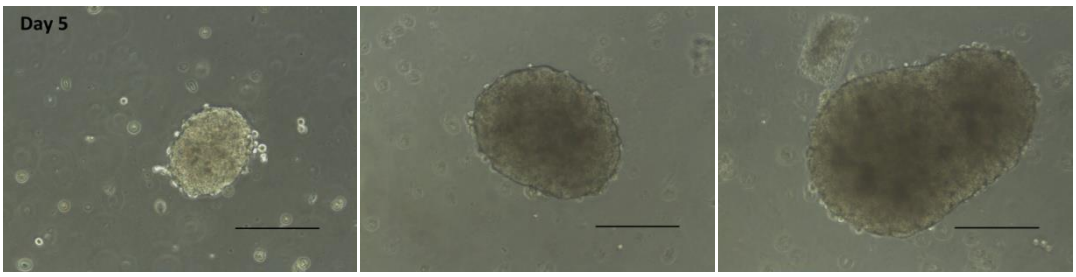

Day 7

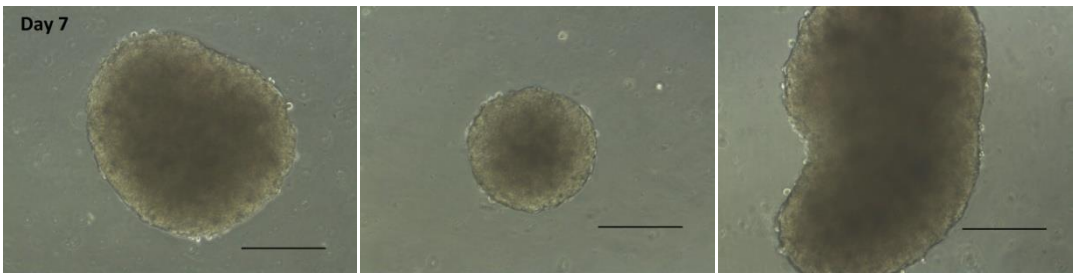

B.1.4

In the present experiment, 2.7 x 10^6 cells were seeded, on day 0, in a flask without any agarose coating and kept under continuous gentle stirring at 75 rpm. Spheroids were formed in the last experiments, as done in the previous three reported in appendix B.1. The increase of the initial cell number comparing to the experiment presented in chapter B.1.3 (Appendix B), led to increased cell attachment to the flasks bottom substrate. The culture was ended on day 7 with the spheroids remaining in the same flask for all the days of the experiments. Photographs illustrating the result of the experiment were taken during day 2, day 5 and day 7 and are presented in figure B.3. As described in chapter 3.2, the growth medium exchange was performed every second day with the first exchange performed on day 2. The spheroids were constantly kept in an atmosphere with 19% O_2 and 4% CO_2 in N_2.

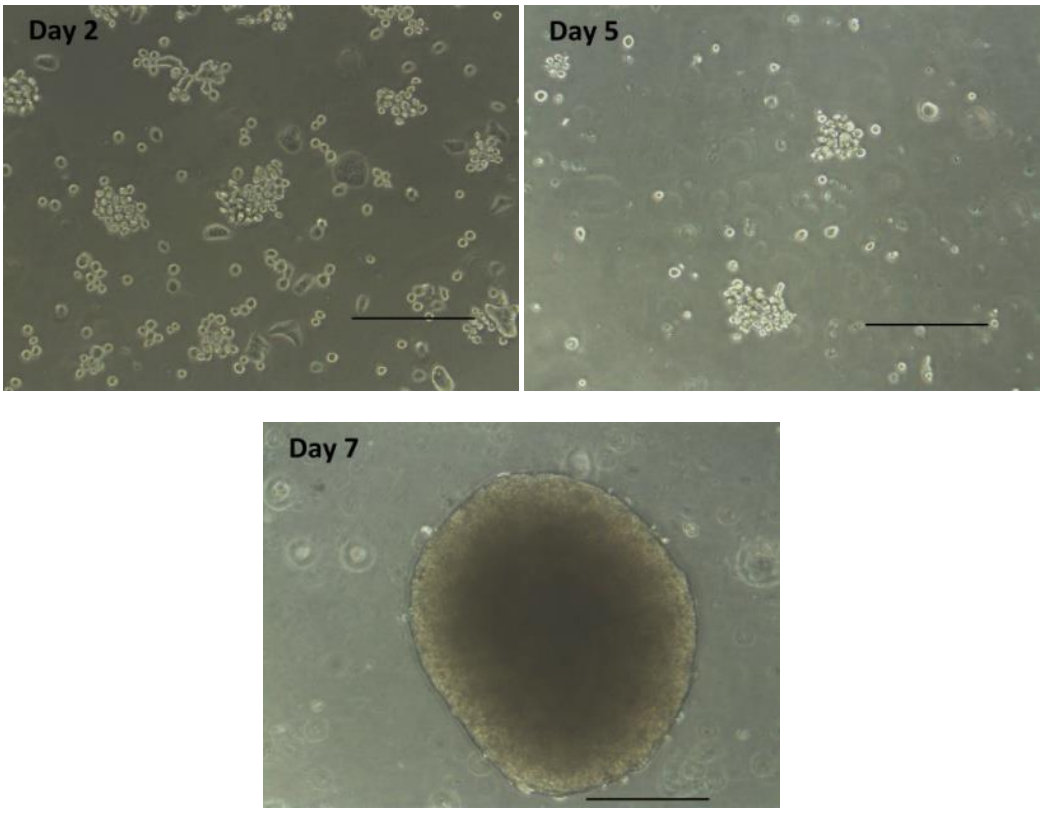

Figure B.3: Illustration of photographs taken during an experiment for generating HT29-cell spheroids using non-agarose-coated flask. 2.7 x 10^6 cells were seeded in a 25 cm^2 cell culture flask without agarose coating and maintained under orbital motion at 75 rpm. Spherical and non-spherical aggregates were formed during day 5 and 7. Worth to be mentioned that the cell attachment to the bottom surface

of the flask was increased compared to the experiment presented in chapter B.1.3. The scale bar presents distance of 333.33 μm.

Day 2

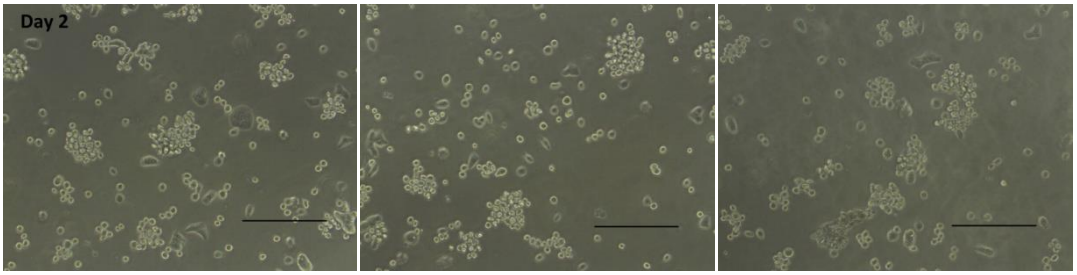

Day 5

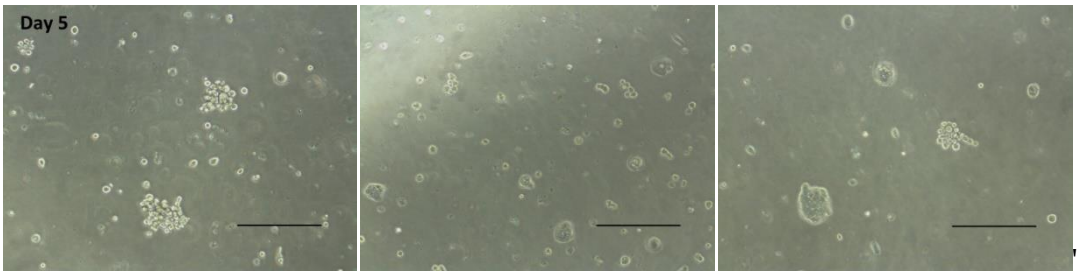

Day 7

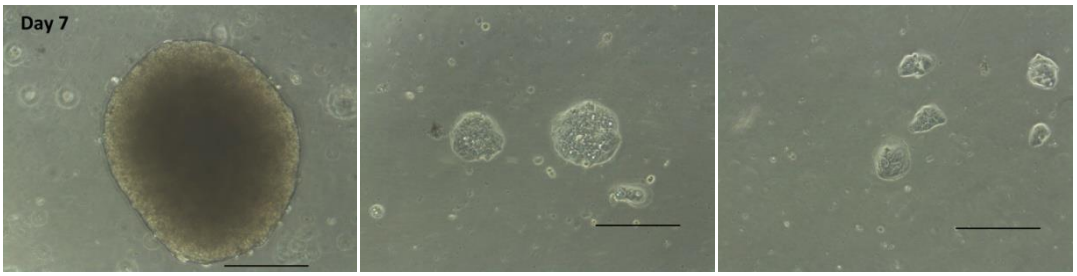

Table B.1: All the different combinations of stirring speed and initial cell number tested in 25 cm^2 cell culture flasks without any agarose

	HT29 cells seeded on day 0	
Stirring speed (rpm)	1.4 x 10^6	2.7 x 10^6
60	B.1.1	B.1.2
75	B.1.3	B.1.4

B.2

B.2.1

In the present experiment, 1.4 x 10^6 HT29 cells were seeded in an agarose-coated 25 cm^2 cell culture flask. The flask was placed on the platform of the shaker maintaining the cells under continuous stirring motion at the speed of 60 rpm. Photographs were taken in different days of the culture and they are presented in figure B.4. The first rather small, spherical cellular aggregates appeared at day 2 and it is probably better to be described as micro-spheroids so as to exist a distinction in the description term between the spherical aggregates present in the photographs taken from day 2 and day 3 illustrated in figure B.4, with day 0 to be the cell seeding day. The spheroids grew in size in the following days reaching to diameters up to about 600 μm on day 7. Many aggregates possessed spherically symmetric shapes as can be observed in figure B.4. The spheroids were transferred to a new agarose-coated flask on day 3. Large irregularly-shaped aggregates observed, were manually removed from the culture. The experiment stopped after day 7. More information about the spheroid culture are presented in chapter 3.2. The spheroids were constantly kept in an atmosphere with 19% O_2 and 4% CO_2 in N_2.

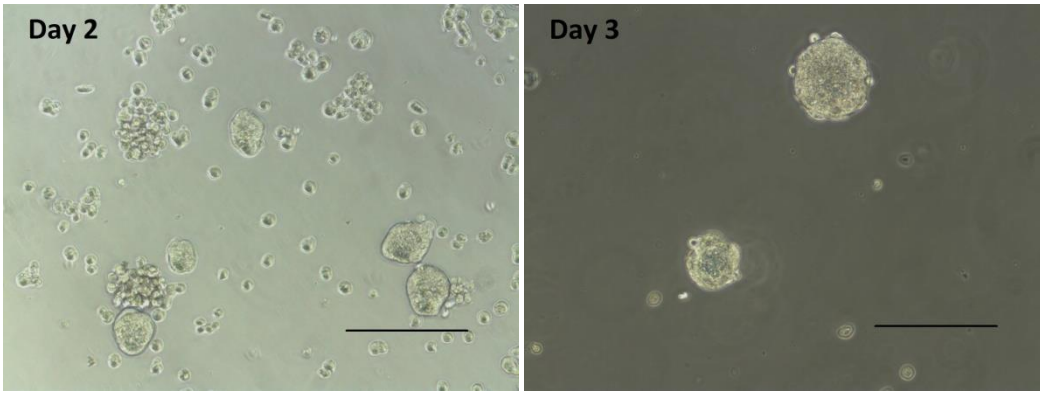

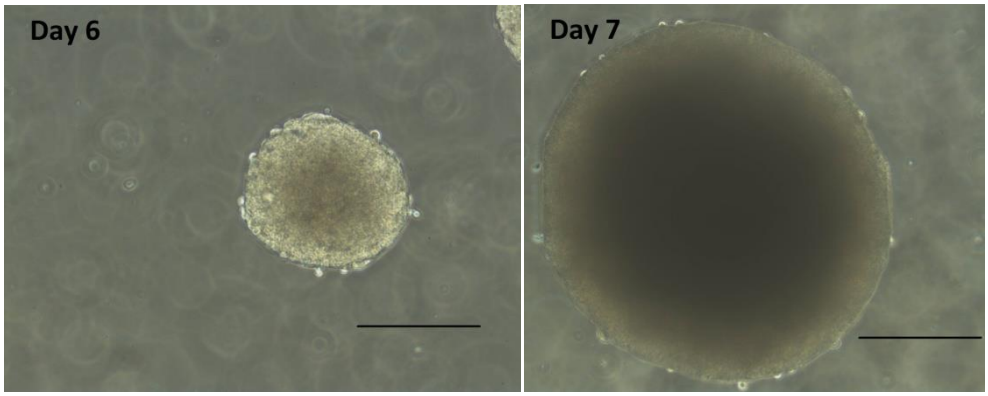

Figure B.4: Photographic illustration of the experiment for spheroid cultivation using HT29 cells where 1.4 x 10^6 HT29 cells were seeded, on day 0, in a 25 cm^2 agarose-coated cell culture flask and maintained under continuous shaking at 60 rpm. Spherical HT29 aggregates were successfully formed during this attempt with plenty spheroids being observed in different stages of the culture (day 3, day 6, day 7). The scale bar presents distance of 333.33 μm.

Day 2

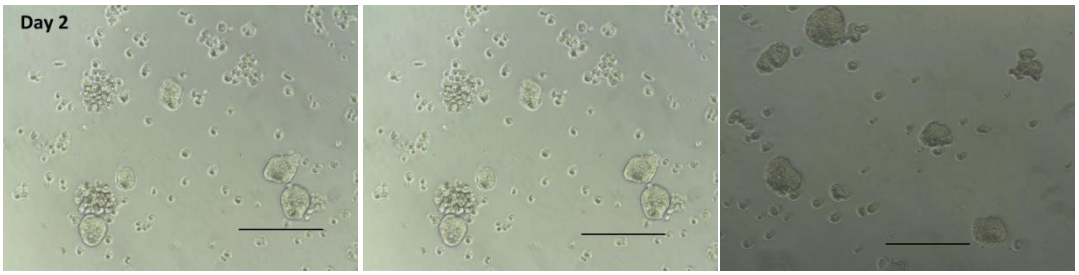

Day 3

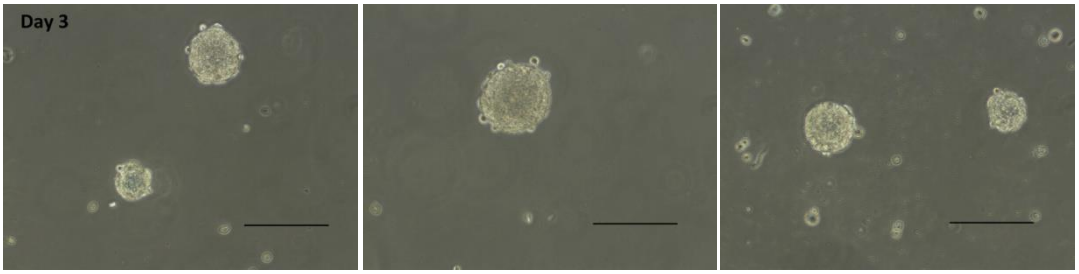

Day 6

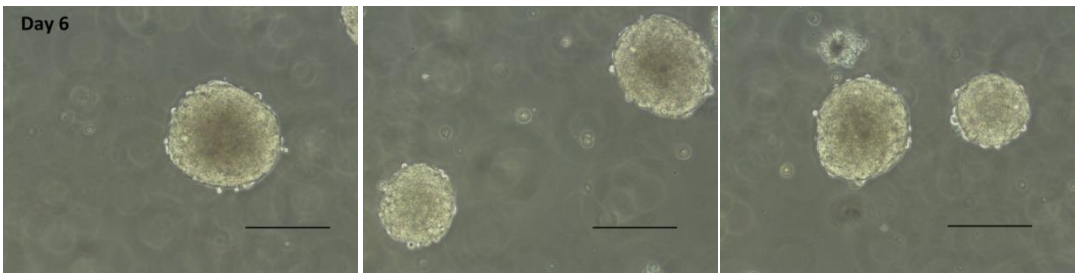

Day 7

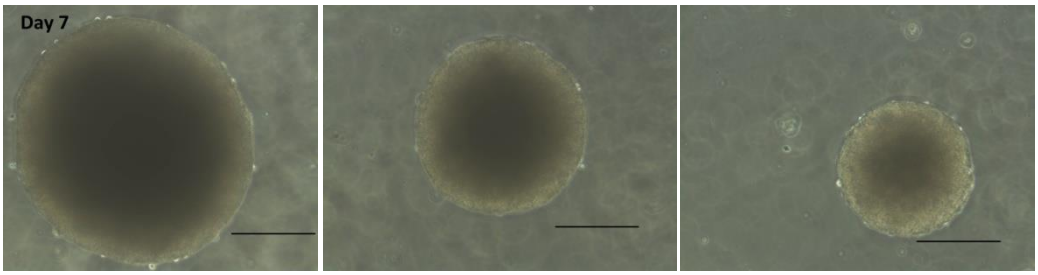

B.2.2

In the present experiment, 2.7 x 10^6 HT29 cells were seeded, on day 0, in a agarose-coated flask and maintained under continuous orbital stirring motion at 60 rpm. By increasing the starting cell number with a factor of 2 compared to the experiment reported in chapter B.2.1, the chance for cell-cell interactions become enhanced and the probability for cellular aggregates formation increases. In the figure B.5 photographs, taken from this experiment, are presented. Spheroids were successfully formed as in the previous case. As in the first experiment, micro-spheroids were formed already in day 2 when the first medium change was performed. In day 3, spheroids were present in the flask and they were transferred in a new 25 cm^2 cell culture flask. The spheroids continued to grow in the later days of the experiment. In the day 7, the experiment was ended after successful spheroid, with diameters up to 600 μm formation. As described in chapter 3.2, the growth medium exchange was performed every second day with the first exchange performed on day 2. The spheroids were constantly kept in an atmosphere with 19% O_2 and 4% CO_2 in N_2.

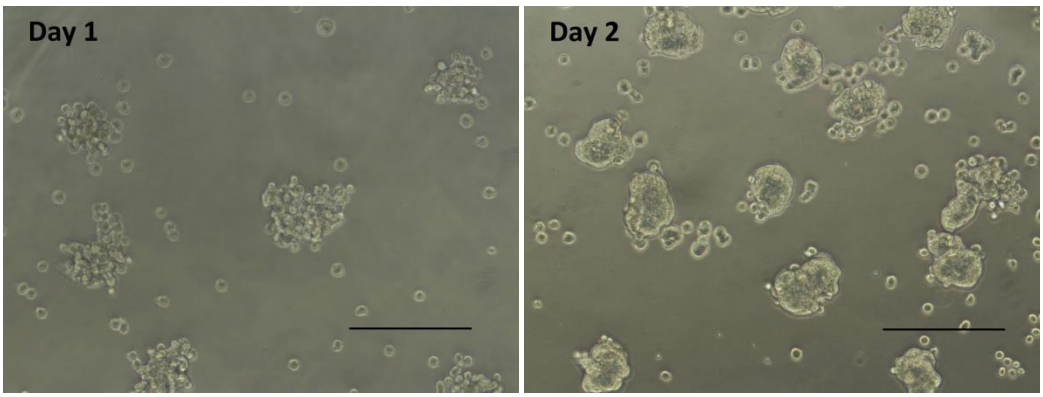

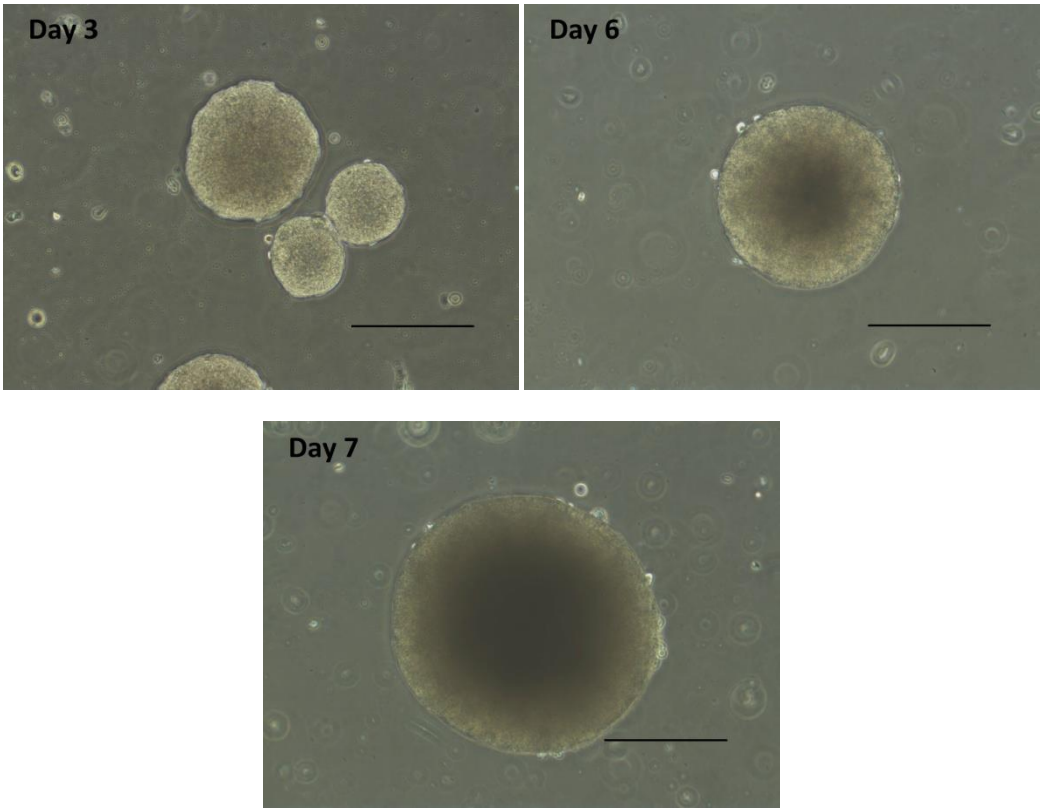

Figure B.5: Visualization of the experiment utilizing 2.7 x 10^6 HT29 cells seeded in a 25 cm^2 cell culture flask containing agarose coating which were kept under constant orbital motion of 60 rpm speed. Small spherical aggregates, which later were evolved into spheroids, could be observed after day 2 of the culture. The scale bar indicates distance of 333.33 μm

Day 1

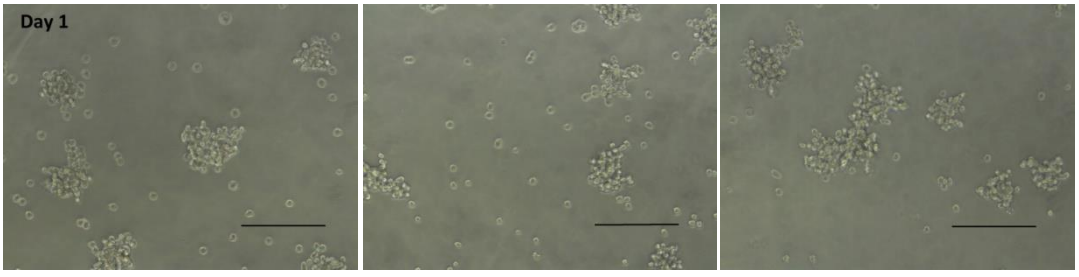

Day 2

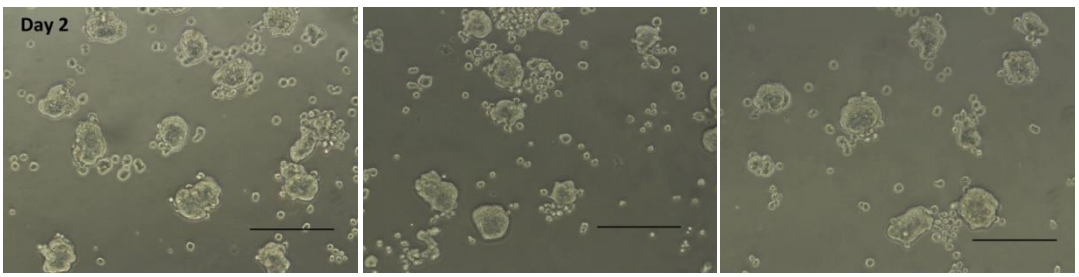

Day 3

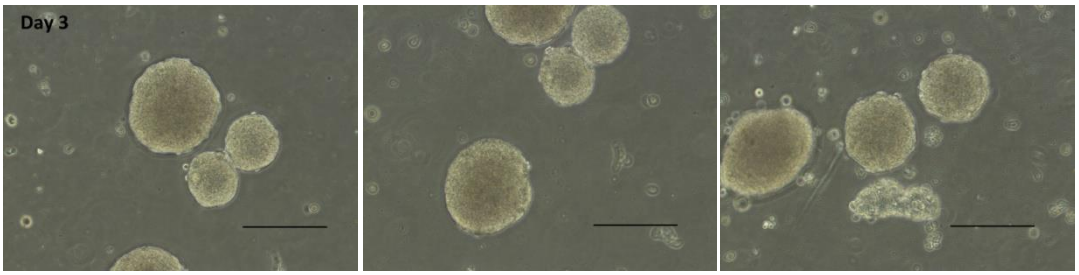

Day 6

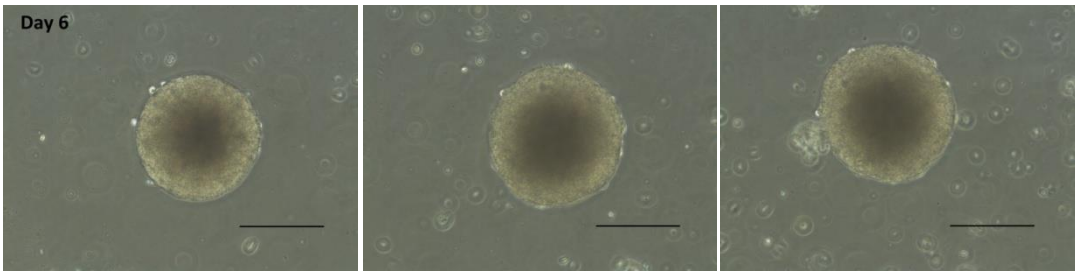

Day 7

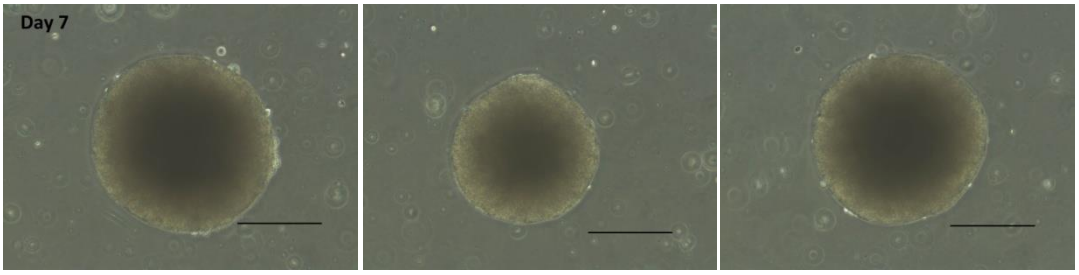

B.2.3

The description of the present experiment is reported in the chapter 4.1.2 (section 2).

Day 1

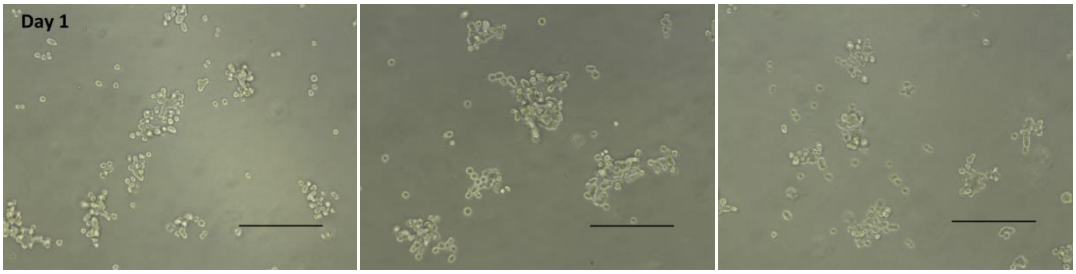

Day 2

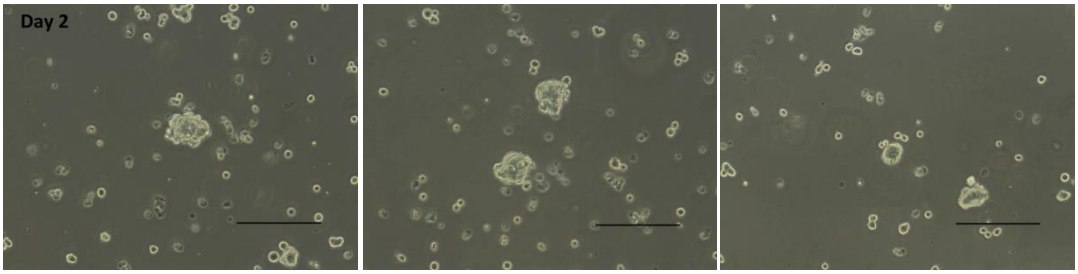

Day 3

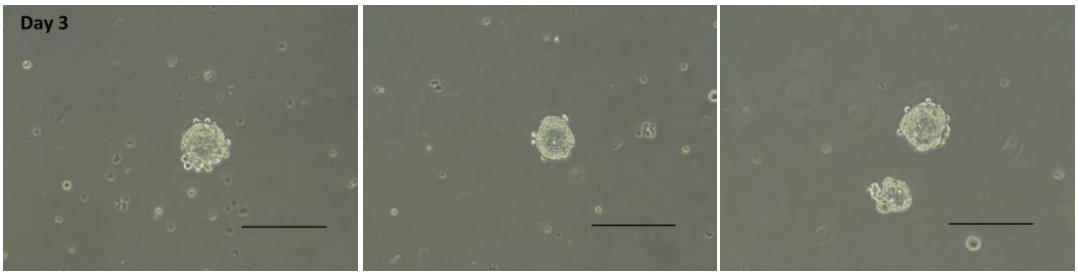

Day 4

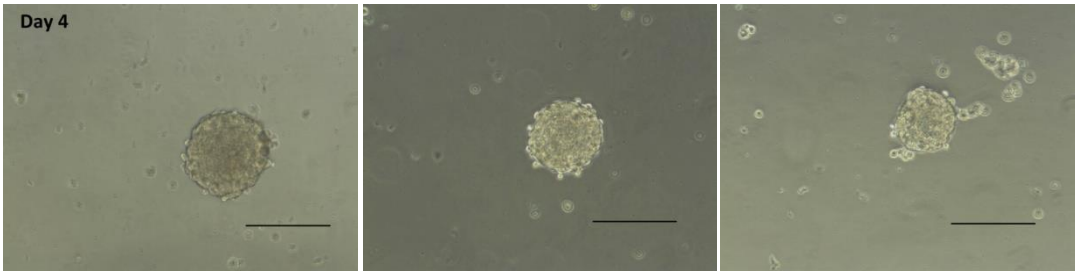

Day 5

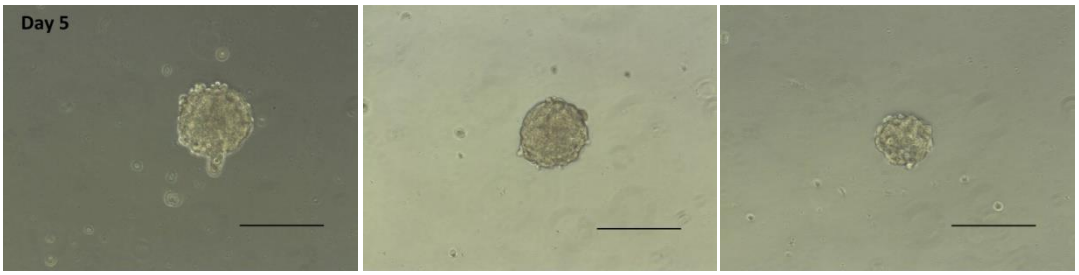

Day 6

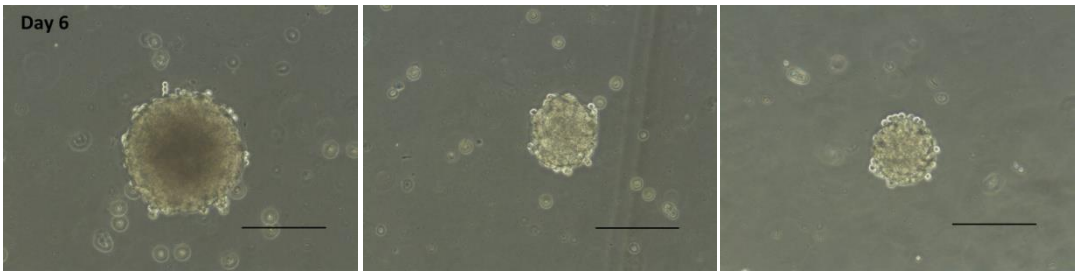

Day 7

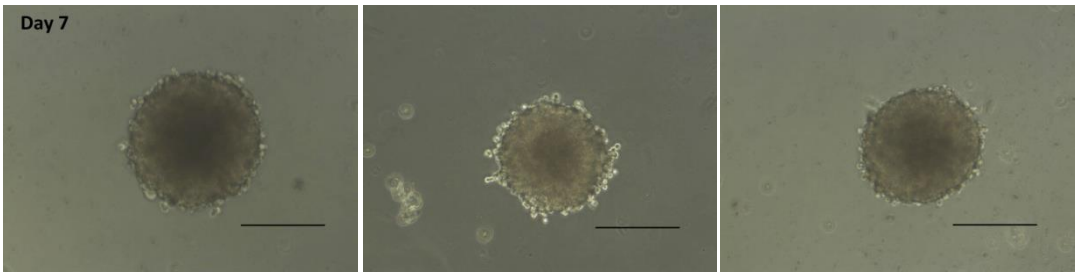

Day 8

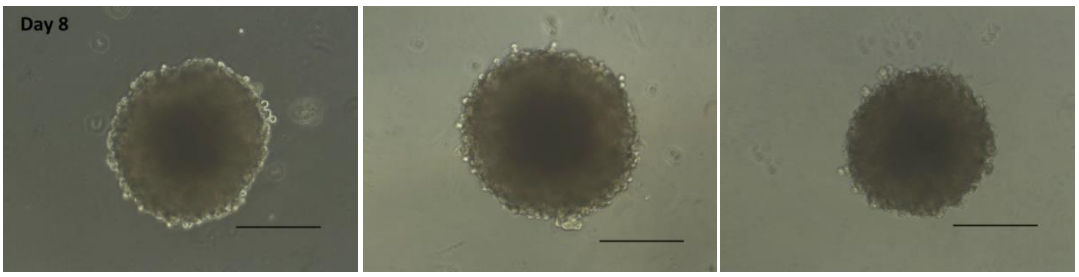

B.2.4

The description of the present experiment is reported in the chapter 4.1.2 (section 2).

Day 1

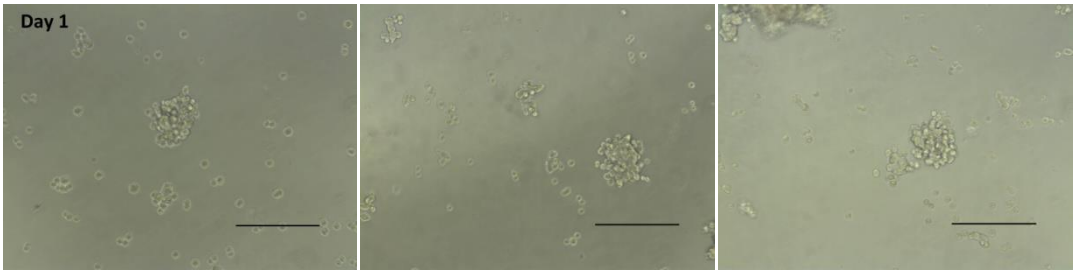

Day 2

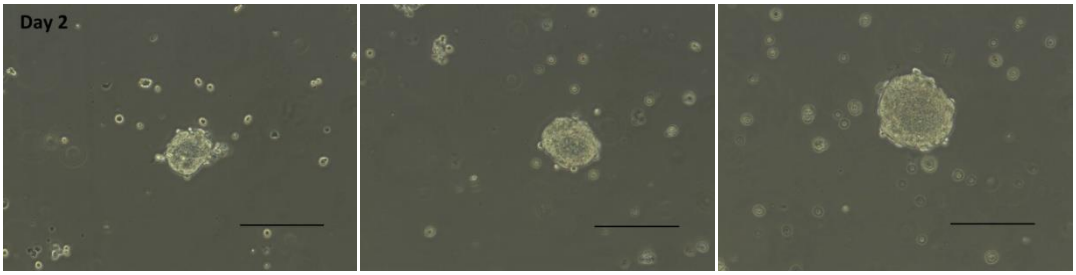

Day 3

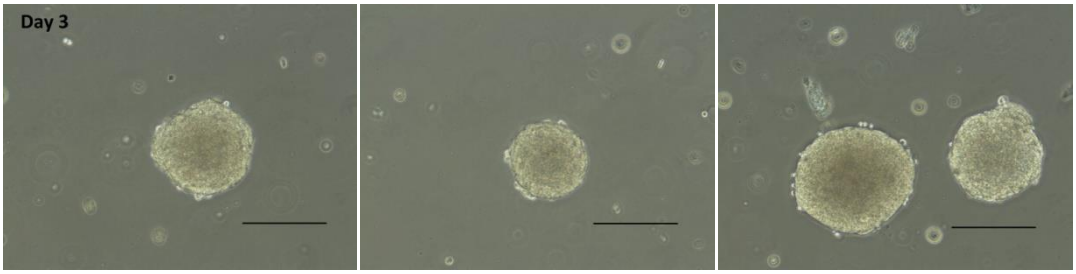

Day 4

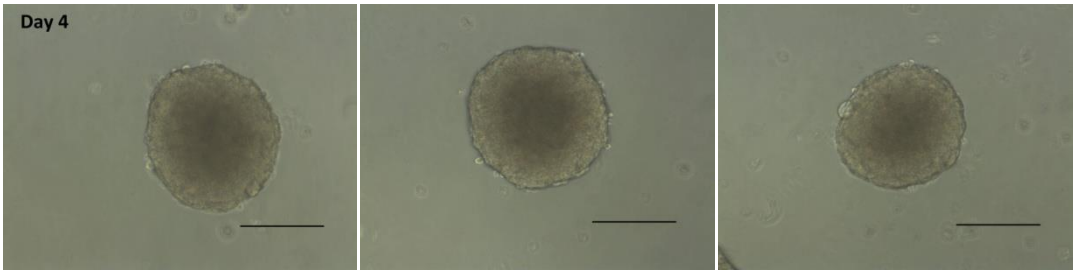

Day 5

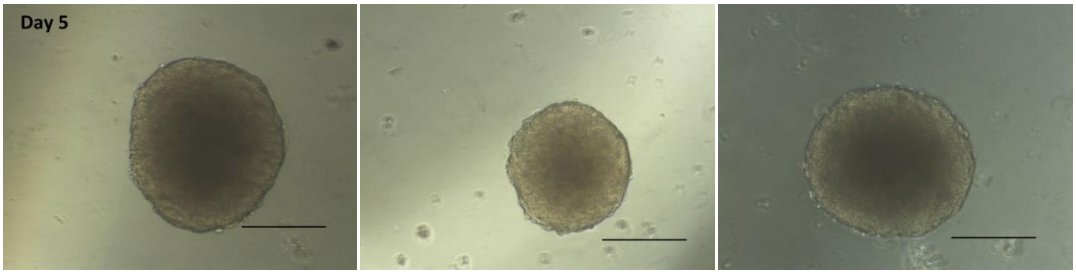

Day 6

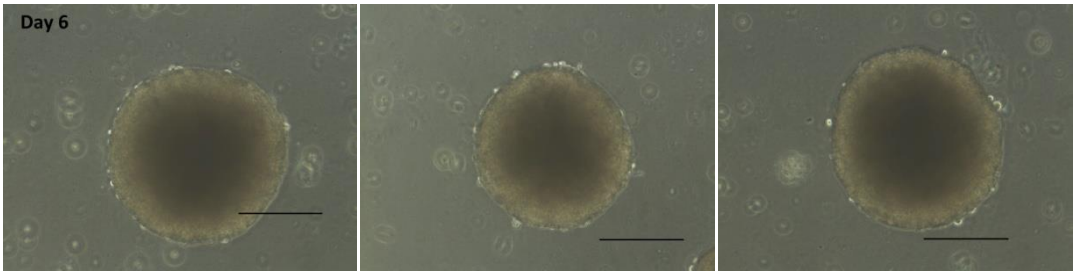

Day 7

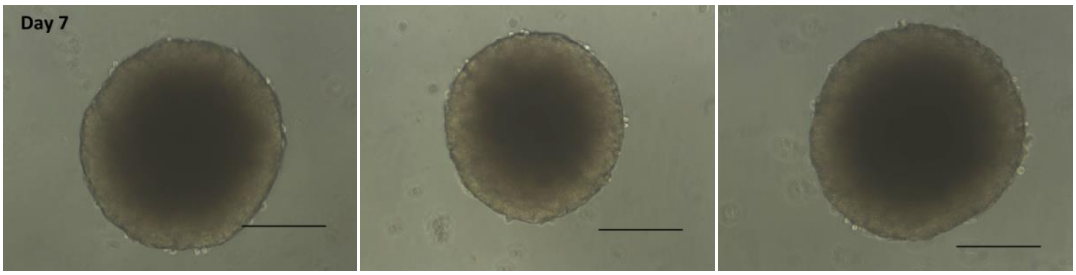

Day 8

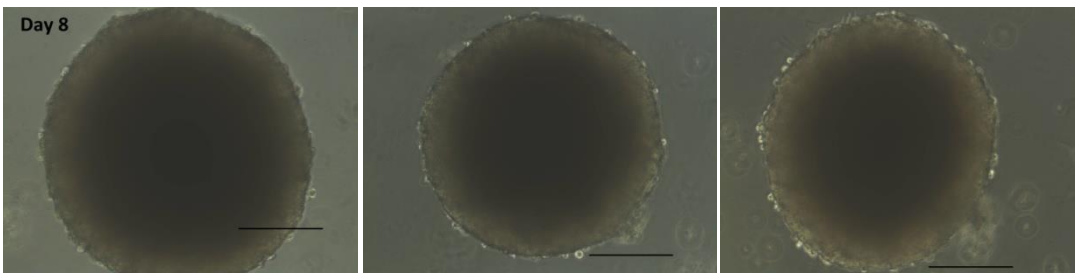

Table B.2: All the different combinations of stirring speed and initial cell number tested in agarose-coated 25 cm^2 cell culture flasks

	HT29 cells seeded on day 0	
Stirring speed (rpm)	1.4 x 10^6	2.7 x 10^6
60	B.2.1	B.2.2
75	B.2.3	B.2.4

B.3

Overview of the optimal parameters for the HT29-cell spheroids generation.

Cell type	**HT29**
Startingcellnumber	1.4 - 2.7 x 10^6
Stirring speed	75 rpm
Agarose-coating	Yes
Thickness of agarose layer	1 mm
Diameters of spheroid formed	400-800 µm
Day that this diameter reached by the spheroids	Day 7- Day 9
Medium volume	8 ml

Appendix C

MCF-7-cell spheroid formation experiments

C.1

C.1.1

The description of the present experiment is reported in the chapter 4.1.3 (section 1).

Day 1

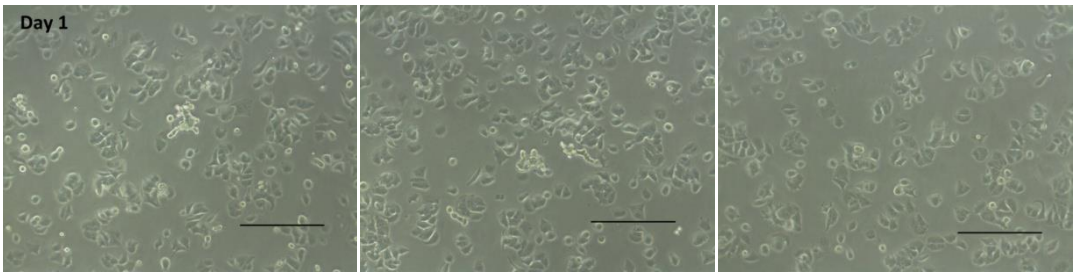

Day 3

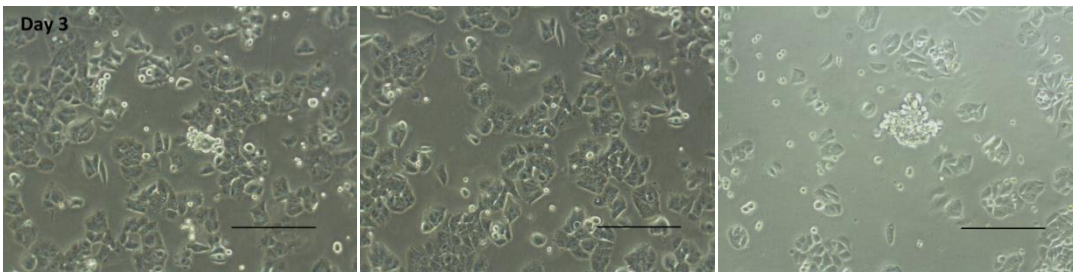

Day 5

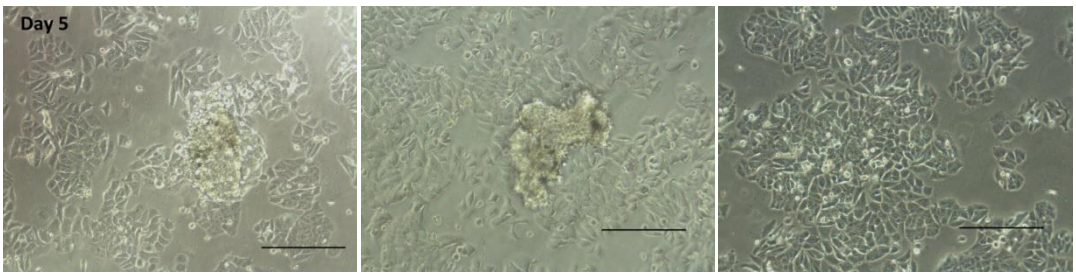

C.1.2

In the presented experiment, 4.5 x 10^6 MCF-7 cells were seeded in 25 cm^2 cell culture flask and were maintained under continuous stirring motion at the speed of 75 rpm. Presentation of photographs taken in various days of the experiment is visualized in figure C.1. As in the experiment presented in chapter 4.1.3 (section 1), formation of small and irregularly-shaped cell aggregates was observed until day 3. Single cells attachment to the bottom surface of the flask and formation of a monolayer cell culture was also observed. The increase of the cell seeded in day 0, led to the formation of more aggregates than in experiments of chapter 4.1.3 (section 1). The exchange of medium was performed every second day with the first medium change taking place on day 2. The aggregates were maintained in the same flask under the whole duration of the experiment. The shape and the size of the aggregates formed was the main reason that the experiment stopped on day 5. None of the 2 experiments described in section 1 was successful in spherical aggregates formation. The spheroids were constantly kept in an atmosphere with 19% O_2 and 4% CO_2 in N_2.

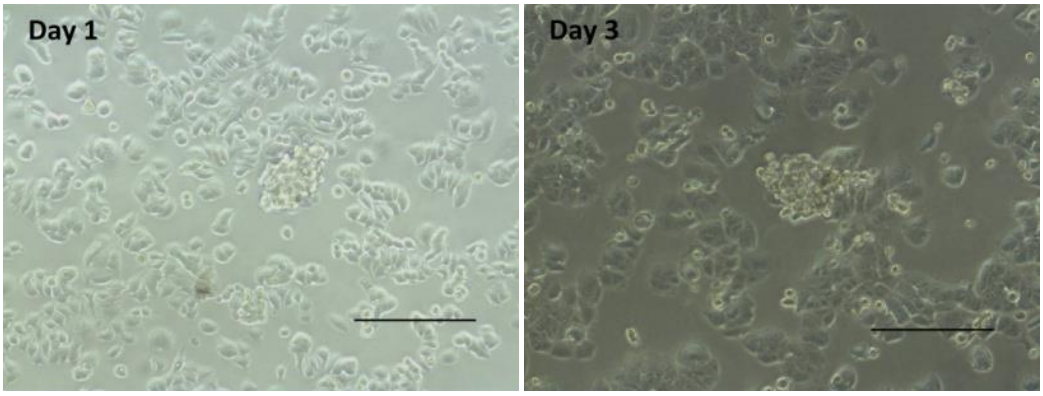

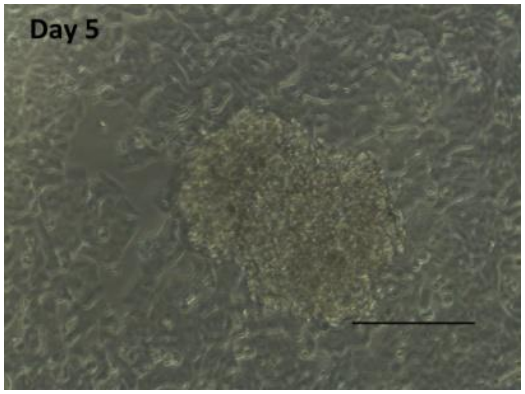

Figure C.1: Photographic illustration of an experiment using MCF-7 cells for spherical aggregates formation. 4.5 x 10^6 MCF-7 cells were seeded in a 25 cm^2 cell culture flask and maintained under orbital movement at 75 rpm. The culture was kept under air atmosphere and the change of growth medium was performed every second day. Small and irregularly shaped cell aggregates were also generated in this experiment, with many single cells attached to the substrate of the flask and formed monolayer cell culture. The result was the same as in the experiment presented in chapter 4.1.3 (section 1), meaning that the increase in the stating cell number was not enough to lead to successfully generated spheroid in the experiment. The scale bar stands for distance of 333.33 μm.

Day 1

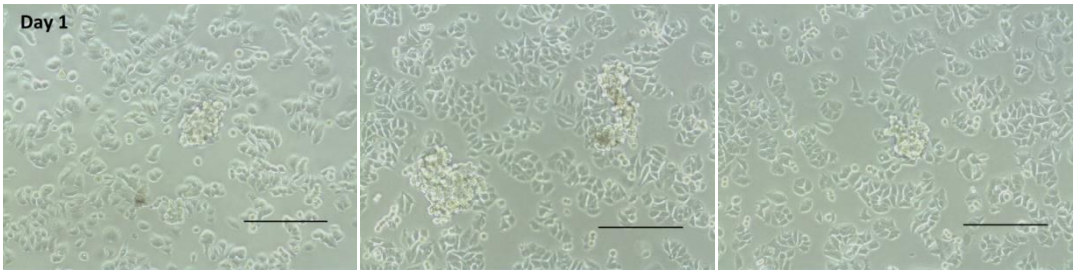

Day 3

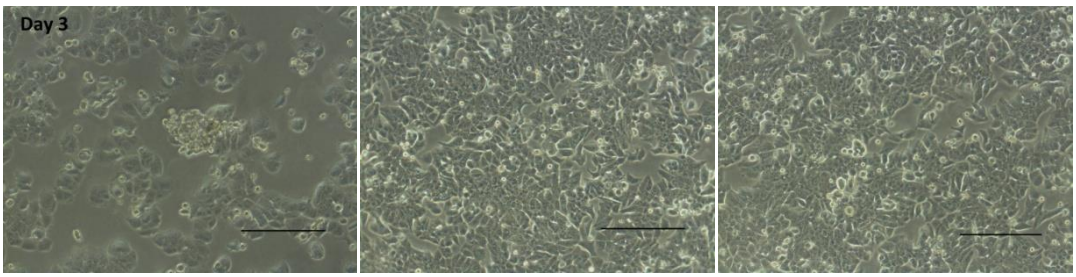

Day 5

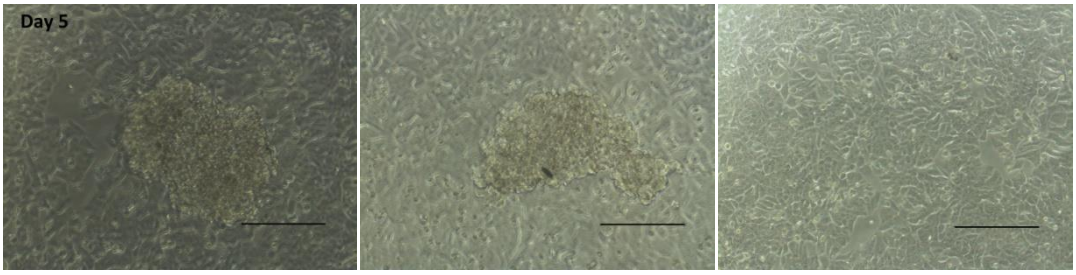

Table C.1: All the different combinations of stirring speed and initial cell number tested in 25 cm^2 cell culture flasks without any agarose

	MCF-7 cells seeded on day 0	
Stirring speed (rpm)	2.4 x 10^6	4.5 x 10^6
60	--	--
75	C.1.1	C.1.2

C.2

C.2.1

The description of the present experiment is reported in the chapter 4.1.3 (section 2).

Day 1

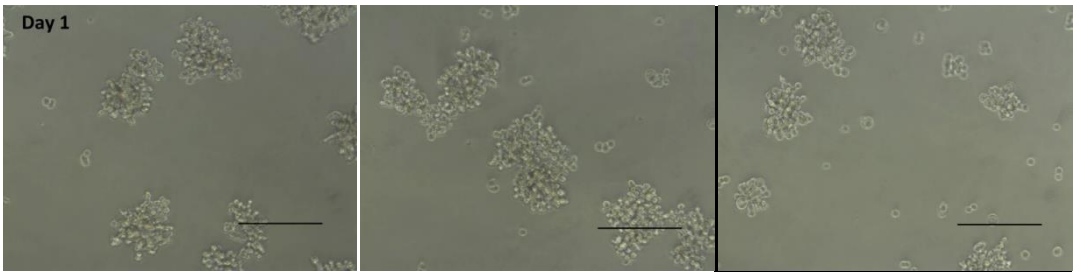

Day 3

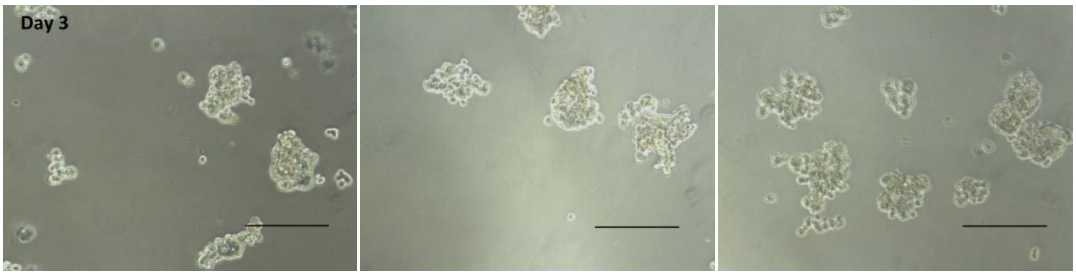

Day 5

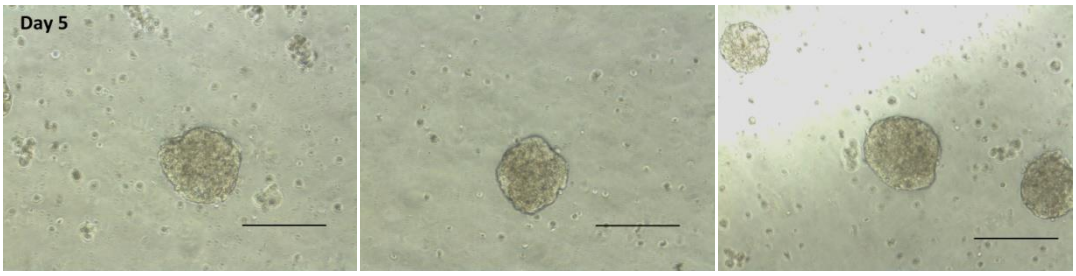

Day 7

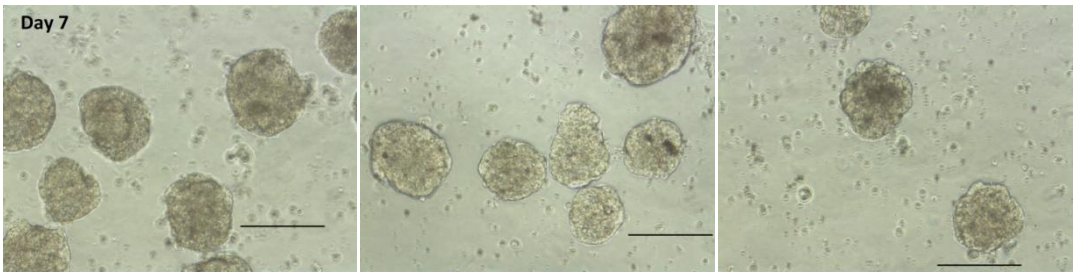

C.2.2

In the presented experiment, 4.5 x 10^6 MCF-7 cells were seeded, on day 0, in a pre-agarose coated 25 cm^2 cell culture flask and maintained under orbital stirring motion at 60 rpm. As in all the experiment presented in chapter 4.1.3 (section 2), the medium exchange was performed every second day, with the first exchange of growth medium performed in day 2. The pre-aggregates and some single cells were maintained under air environment and they were transferred in a new flask containing agarose coating on day 3. Spheroids were successfully generated in this experiment with some spherical aggregates reaching in diameters up to 300 μm, as it is illustrated in figure C.2. Spheroids can be observed in photographs acquired on day 6, 7 and 10. After day 10 the experiment was terminated. The spheroids were constantly kept in an atmosphere with 19% O_2 and 4% CO_2 in N_2.

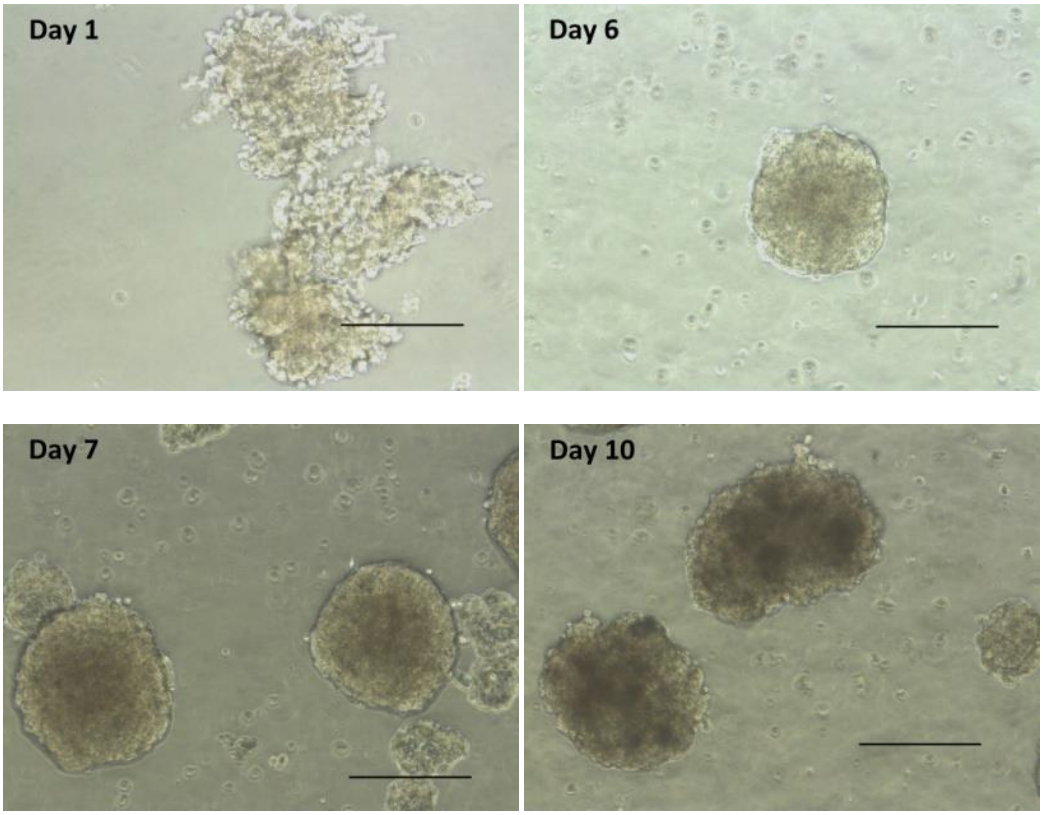

Figure C.2: Visualization of the cellular aggregates formed on different days of the experiment. 4.5 x 10^6 MCF-7 cells were seeded in a 25 cm^2 flask containing agarose coating and maintained under continuous orbital motion at 60 rpm. Successful spheroid formation was observed, with spheroids reaching diameters up to about 300 μm on days 7 and 10. The scale bar stands for distance of 333.33 μm.

Day 1

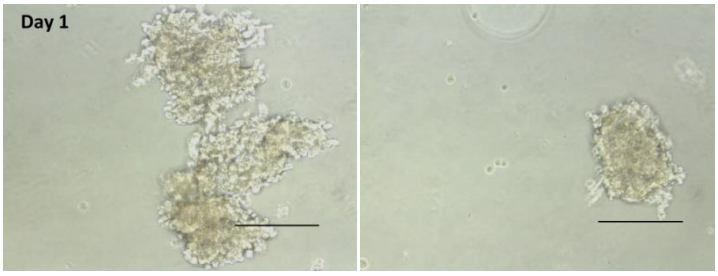

Day 6

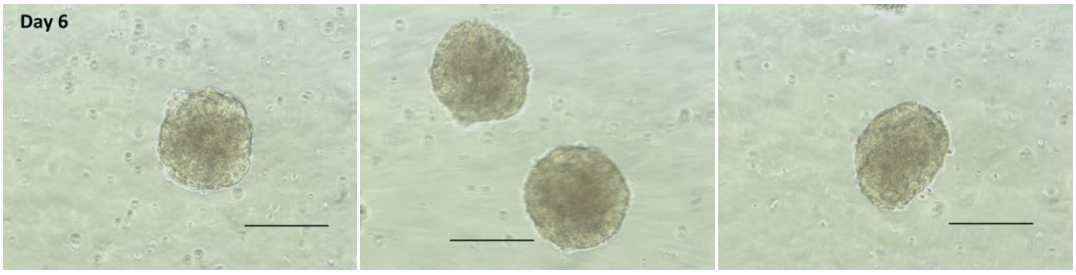

Day 7

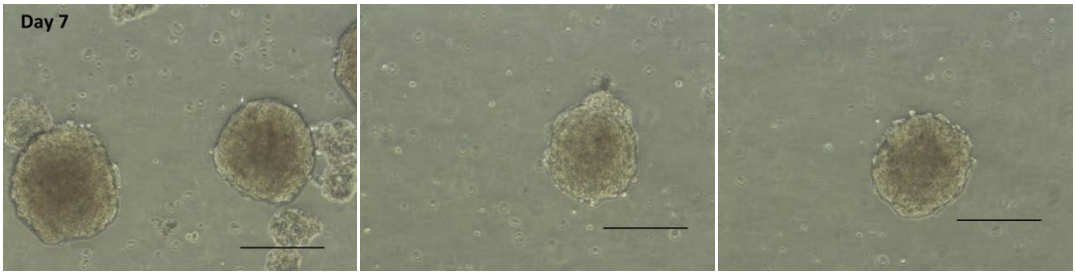

Day 10

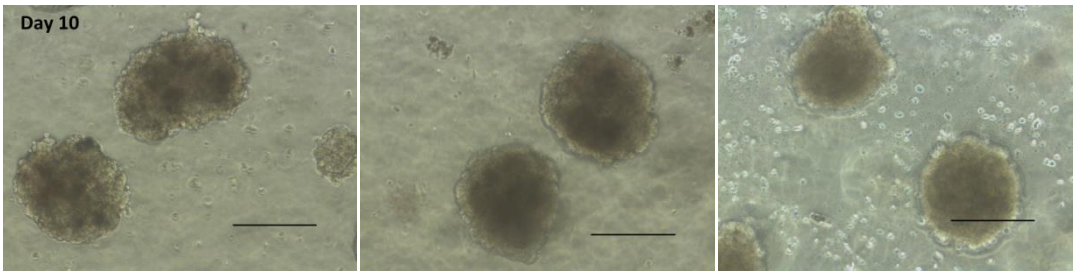

C.2.3

In the presented experiment, 2.4 x 10^6 MCF-7 cells were seeded, on day 0, in a pre-agarose coated 25 cm^2 cell culture flask and maintained under orbital stirring motion at 75 rpm. The increase of the stirring speed could, in principle, enhance the cell aggregates formation and growth. Photographs were taken from different stages of the experiment and are presented in figure C.3. Aggregates were transferred to a new flask on day 3. Aggregates were generated in this experiment. The aggregates formed in this experiment were small in size and they did not obtain as high level of spherical symmetry as spheroids generated in the two experiments presented in chapter 4.1.3 (section 2) and chapter C.2.2 (Appendix C). The culture terminated after day 5. The spheroids were constantly kept in an atmosphere with 19% O_2 and 4% CO_2 in N_2.

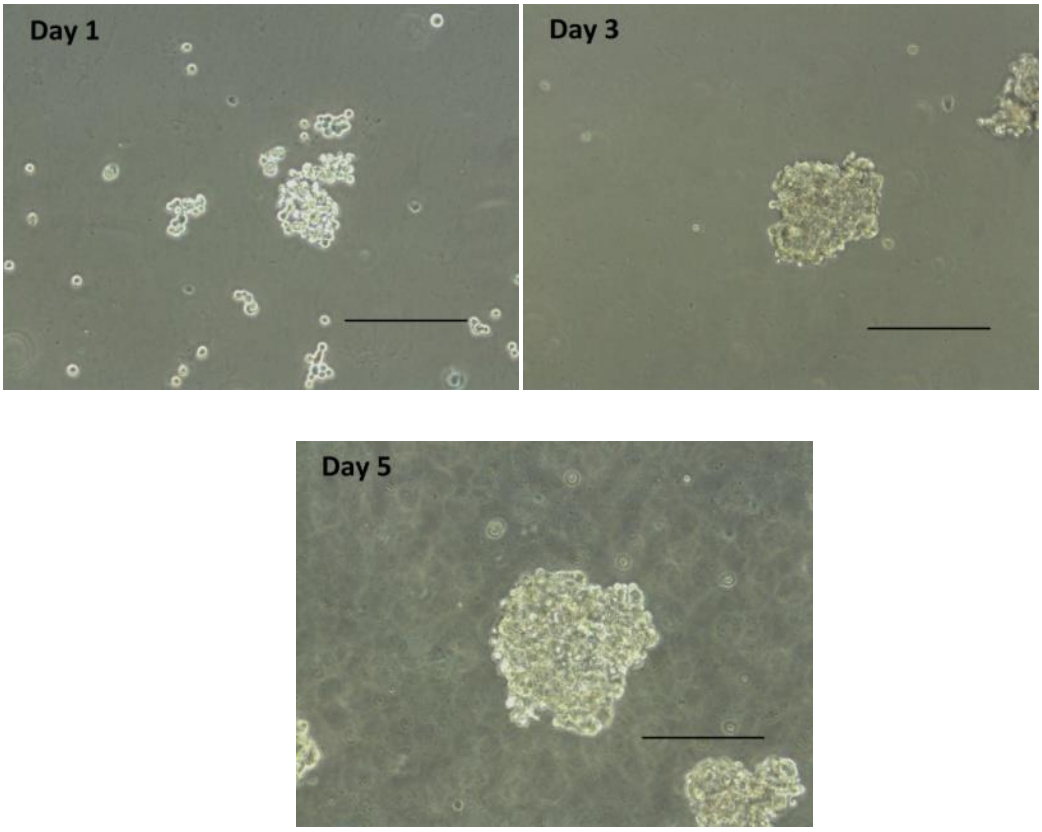

Figure C.3: Illustration of photographs taken at different stages of this experiment. 2.4 x 10^6 MCF-7 cells were seeded in an agarose-coated 25 cm^2 cell culture flask and maintained under orbital stirring motion at 75 rpm. Cell aggregates were successfully formed but there were not many aggregates that were characterized by spherical symmetry as in the previous two experiments. The scale bar stands for distance of 333.33 μm.

Day 1

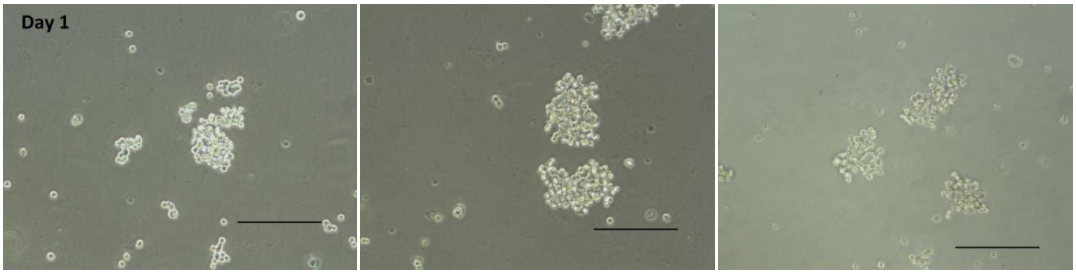

Day 3

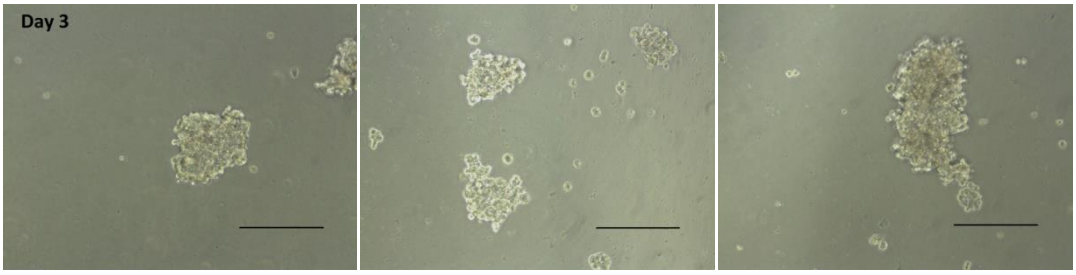

Day 5

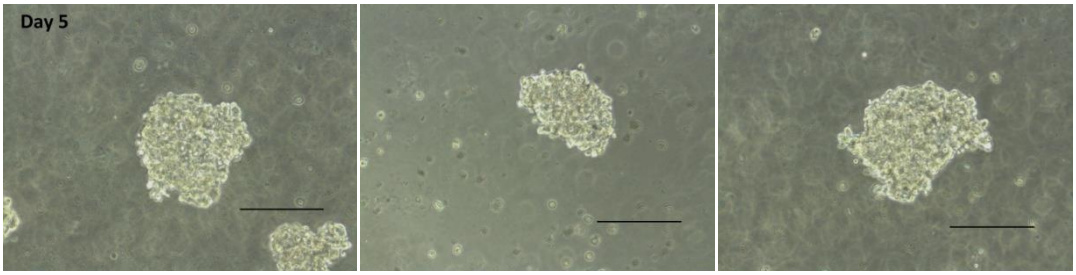

C.2.4

In the presented experiment, 4.5 x 10^6 MCF-7 cells were seeded, on day 0, in a pre-agarose coated 25 cm^2 cell culture flask and maintained under orbital stirring motion at 75 rpm. The exchange of growth medium was routinely performed every second day with the first medium change performed on day 2. Aggregates were generated in the experiment and photographs are presented in figure C.4. The aggregates were transferred to a new agarose coated flask on day 3. Due to the increase of the starting cell number from the experiment presented in chapter C.2.3, the spheroids were more in number and slightly bigger in size. The culture stopped after day 5. The spheroids were constantly kept in an atmosphere with 19% O_2 and 4% CO_2 in N_2.

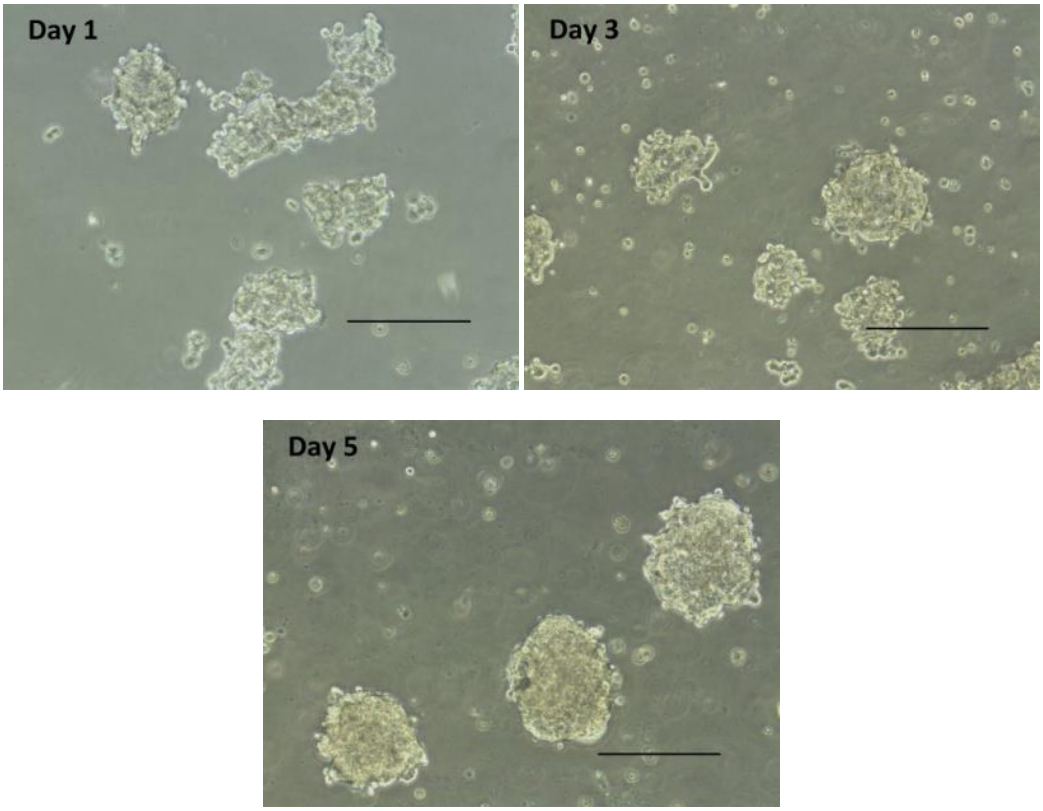

Figure C.4: Photographic presentation of the fourth and last experiment utilizing MCF-7 cells for spheroids generation. 4.5 x 10^6 cells were seeded in a flask containing agarose coating and kept under stirring movement at 75 rpm. Medium exchange were performed every second day and the cellular aggregates and single cells were maintained under air environment. Cellular aggregates were formed and were present on day 3 and day 5.The scale bar stands for distance of 333.33 μm.

Day 1

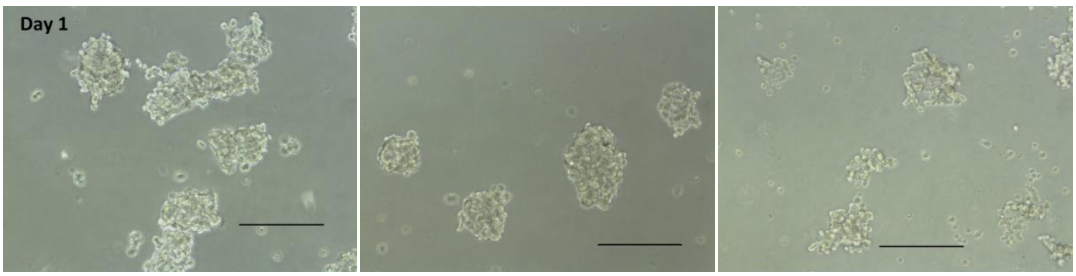

Day 3

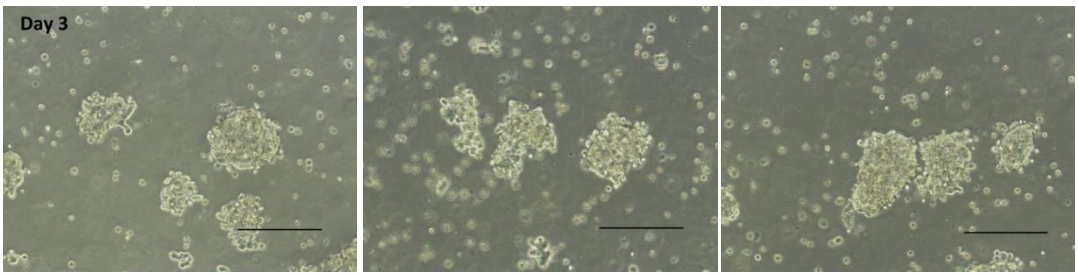

Day 5

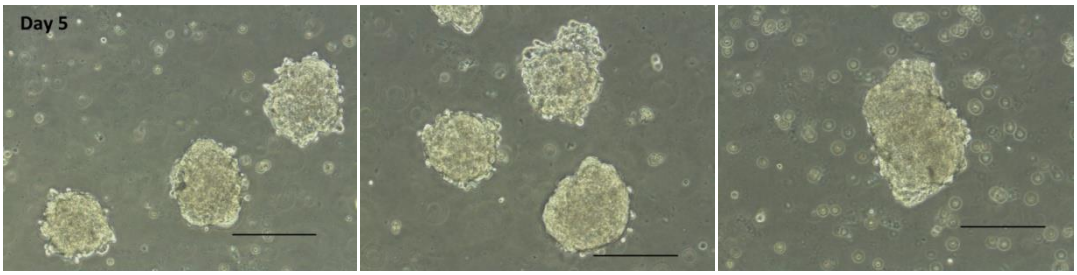

Table C.2: All the different combinations of stirring speed and initial cell number tested in agarose-coated 25 cm^2 cell culture flasks

	MCF-7 cells seeded on day 0	
Stirring speed (rpm)	1.4 x 10^6	2.7 x 10^6
60	C.2.1	C.2.2
75	C.2.3	C.2.4

C.3

Overview of the parameters for the MCF-7-cell spheroids generation.

Cell type	**MCF-7**
Startingcellnumber	4.5 x 10^6
Stirring speed	60 rpm
Agarose-coating	Yes
Thickness of agarose layer	1 mm
Diameters of spheroid formed	300 µm
Day that this diameter reached by the spheroids	Day 7- Day 9
Medium volume	8 ml

Appendix D

T98G-cell spheroid formation experiments

D.1

D.1.1

The description of the present experiment is reported in the chapter 4.1.4 (section 1).

Day 1

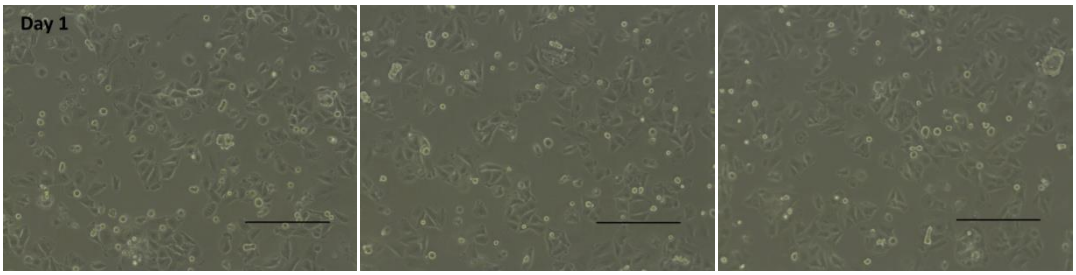

Day 4

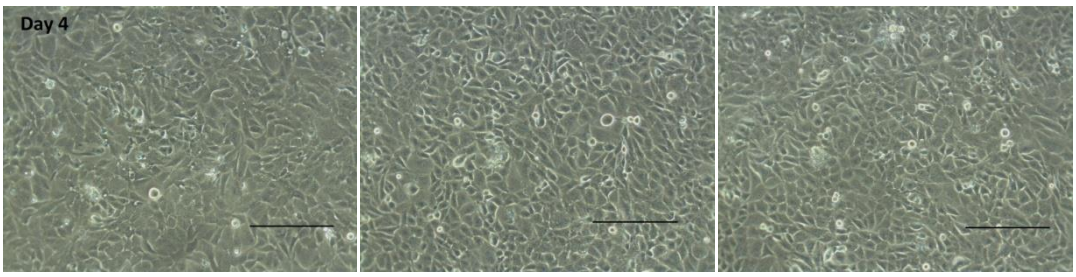

Day 6

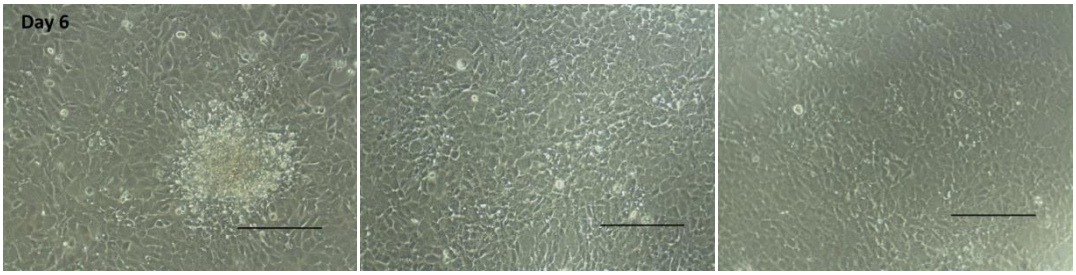

D.1.2

In the presented experiment, 0.9 x 10^6 T98G cells were seeded, on day 0, in a 25 cm^2 cell culture flask without agarose coating and maintained under orbital stirring motion at 75 rpm. Spheroids were not successfully formed in the present experiment. The cell-substrate interaction was dominating in the first days of the experiment. On the day 3, most part of the bottom surface of the flask was covered by monolayer cell culture. Characteristic photographs illustrating the second experiment can be observed in figure D.1. The experiment did not continued after day 7. The spheroids were constantly kept in an atmosphere with 19% O_2 and 4% CO_2 in N_2.

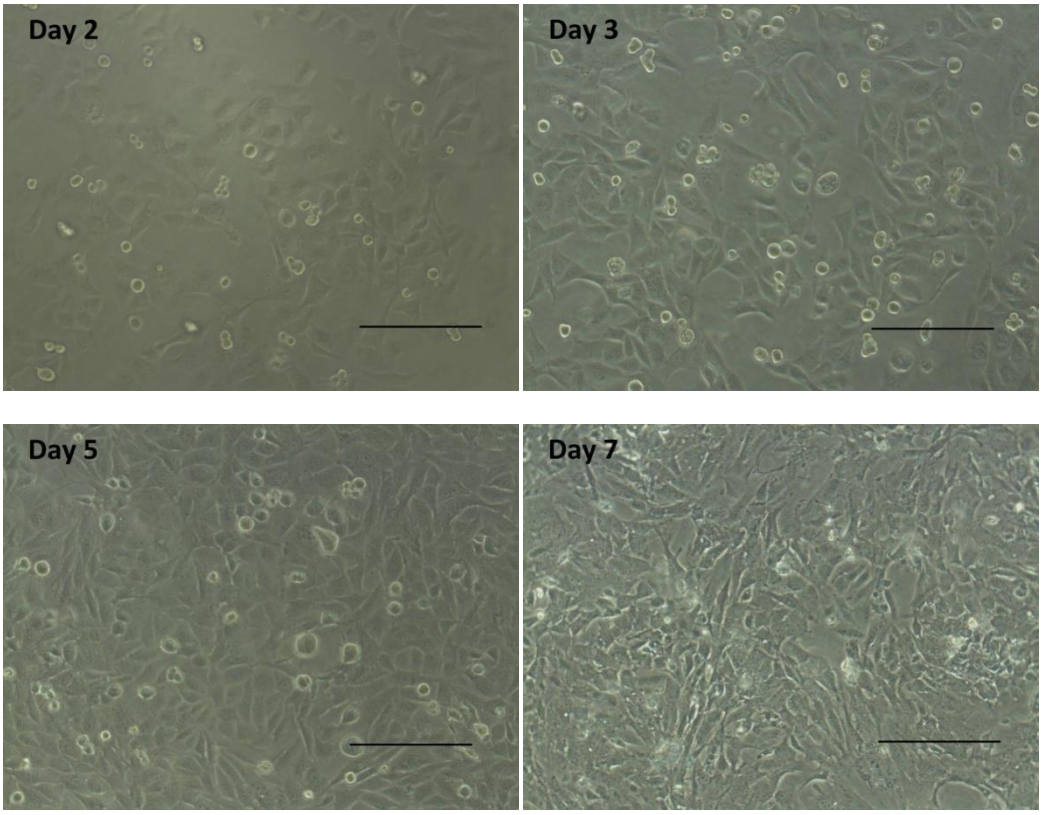

Figure D.1: Visualization of an experiment using T98G cells and flask without agarose coating. The stirring speed was kept at 75 rpm and the starting cell number was 0.8 x 10^6 cells. Spheroid were not formed in this experiment, neither cellular aggregates. Cell attachment to the bottom of the flask was the observed also in the present experiment. The scale bar stands for distance of 333.33 μm.

Day 2

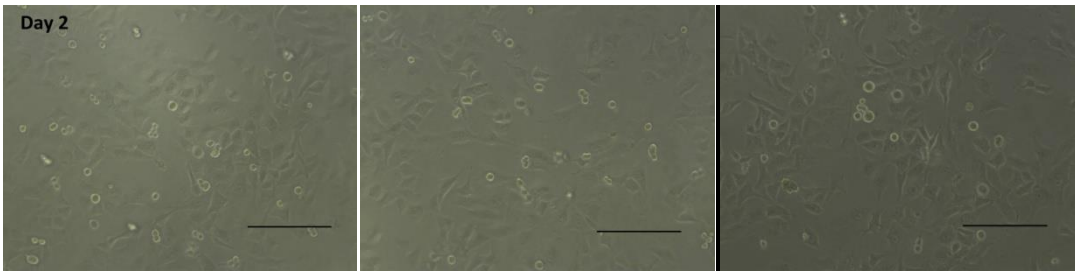

Day 3

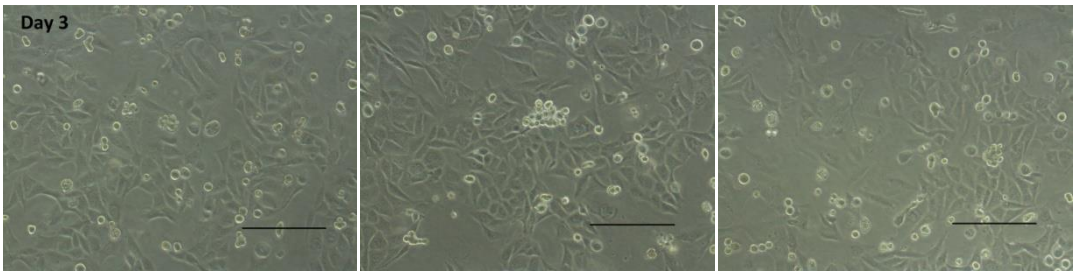

Day 5

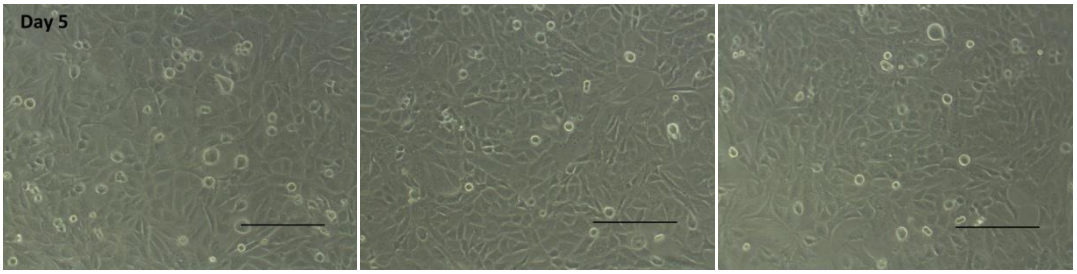

Day 7

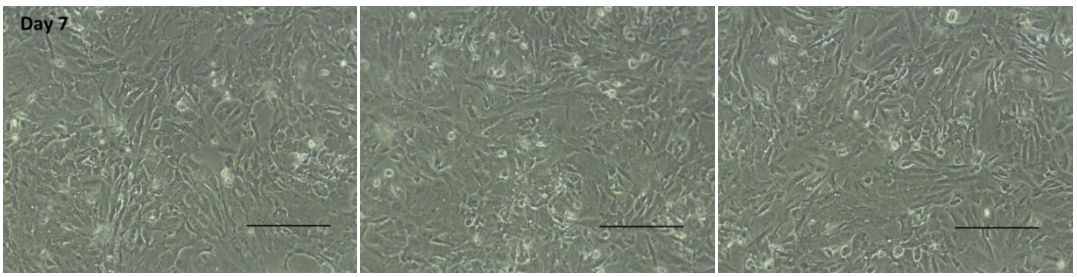

D.1.3

In the presented experiment, 1.3 x 10^6 T98G cells were seeded, on day 0, in a 25 cm^2 cell culture flask without agarose coating and maintained under orbital stirring motion at 75 rpm. Photographs illustrating the experiment are presented in figure D.2. An clear improvement of the cell attachment to the first days of the experiment was noticed. Some small aggregates, containing no more than 10 cells, were formed on day 2 and day 3. However, on the following days most cells had attached to the surface of the flask with no aggregates present on day 7 of the culture when the experiment was stopped. The spheroids were constantly kept in an atmosphere with 19% O_2 and 4% CO_2 in N_2.

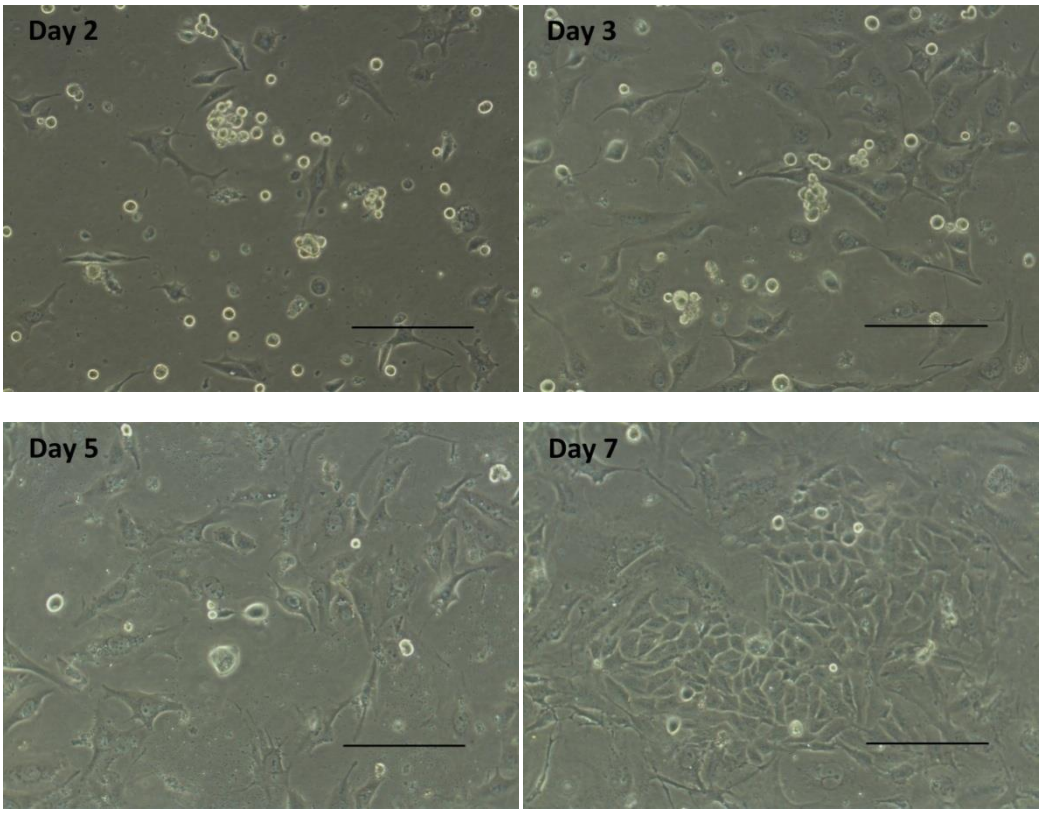

Figure D.2: Visualization of the experiment where 1.3 x 10^6 cells were seeded in a flask without any agarose coating. The flask was maintained under stirring movement at 75 rpm. Cell attachment was not so extensive on the first days of the culture with the some small cell aggregates formed on day 2 and day 3. There was some improvement compared to the first experiment (figure 4.26) indicating that the increase in stirring speed had small positive effect on the cellular aggregates formation. The scale bar stands for distance of 333.33 μm.

Day 2

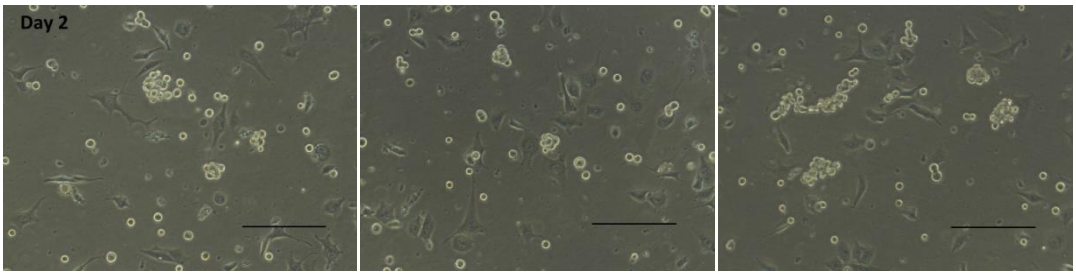

Day 3

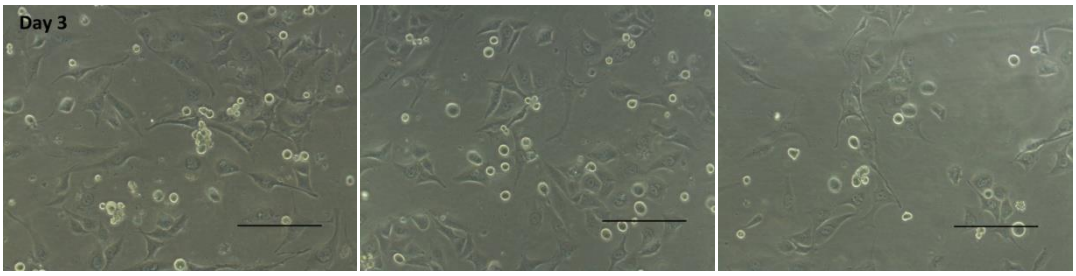

Day 5

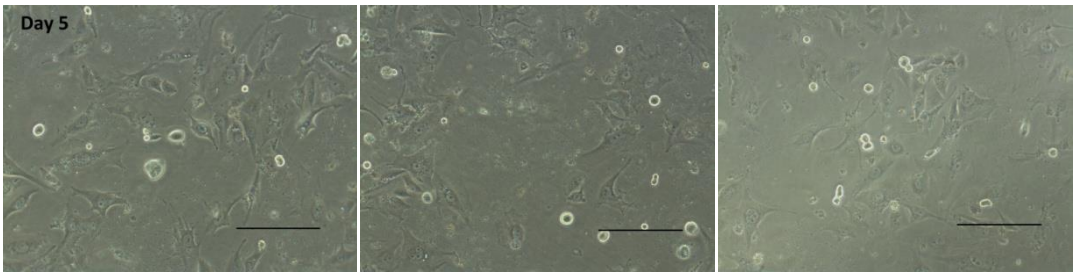

Day 7

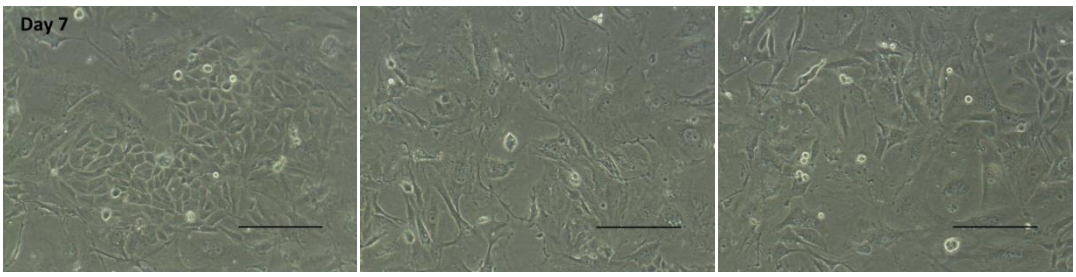

Table D.1: All the different combinations of stirring speed and initial cell number tested in 25 cm^2 cell culture flasks without any agarose.

	T98G cells seeded on day 0	
Stirring speed (rpm)	0.9 x 10^6	1.3 x 10^6
60	--	D.1.3
75	D.1.2	D.1.3

D.2

D.2.1

For the experiment reported in the present section, 0.9 x 10^6 T98G cells were seeded in a pre-agarose-coated flask and which was kept under orbital stirring at 60 rpm. The cell seeding took place on day 0 and the experiment ended on day 5. Successful spheroid formation was not observed during this experiment. Few small cellular aggregates were noticed in day 3 and day 5 of the experiment. On day 5 was observed an increasing cell attachment to the agarose matrix which is presented in the photographs illustrated on figure D.3. The cellular aggregates were maintained in the same agarose-coated flask for the whole duration of the experiment. The spheroid formation process and characteristics are presented in chapter 3.2. The spheroids were constantly kept in an atmosphere with 19% O_2 and 4% CO_2 in N_2.

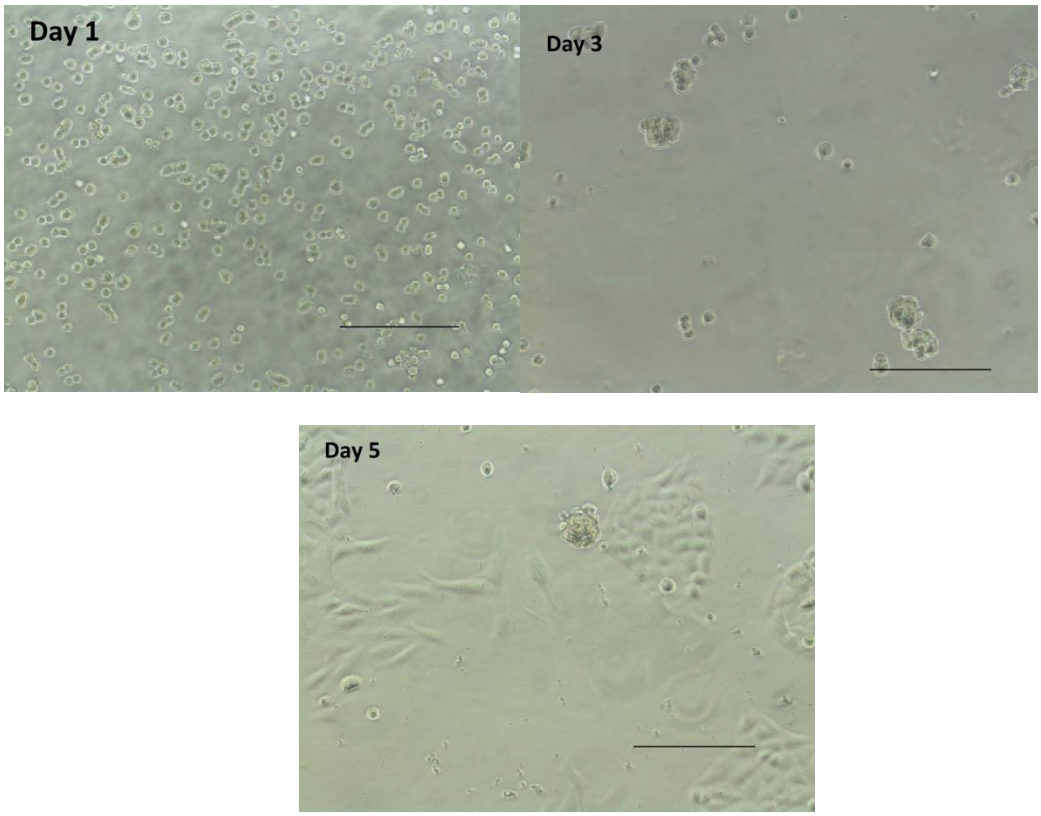

Figure D.3: Illustration of photographs acquired during the duration of the experiment in which 0.9 x 10^6 T98G cells were seeded in a pre-agarose-coated 25 cm^2 cell culture flask and maintained under orbital stirring movement at 60 rpm. The cells were kept under air environment and optimal temperature in the walk-in incubator as described in chapter 3.2. The scale bar stands for distance of 333.33 µm.

Day 1

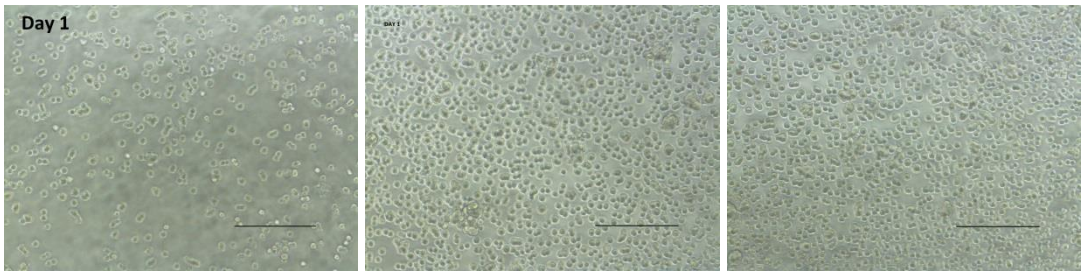

Day 3

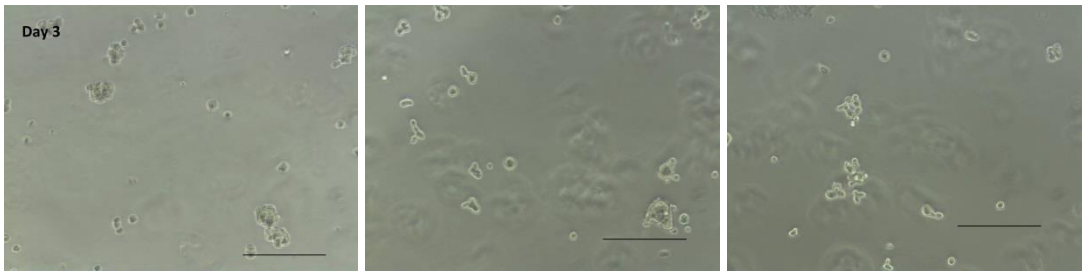

Day 5

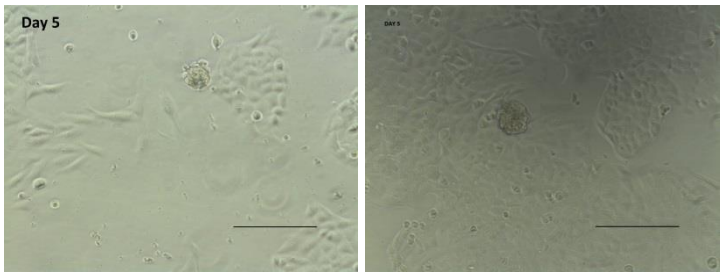

D.2.2

For the experiment reported in the present section, 0.9 x 10^6 T98G cells were seeded in a pre-agarose-coated flask and which was kept under orbital stirring at 75 rpm. The cell seeding was performed on day 0 and the end of experiment took place on day 5. Successful spheroid formation was not observed during this experiment. The density of the cellular aggregates was increased and the cellular attachment to the agarose matrix was reduced compared to the experiment reported in Appendix D.2.1 as illustrated in figure D.4. The cellular aggregates were maintained in the same agarose-coated flask for the whole duration of the experiment. The spheroid formation process and characteristics are presented in chapter 3.2. The spheroids were constantly kept in an atmosphere with 19% O_2 and 4% CO_2 in N_2.

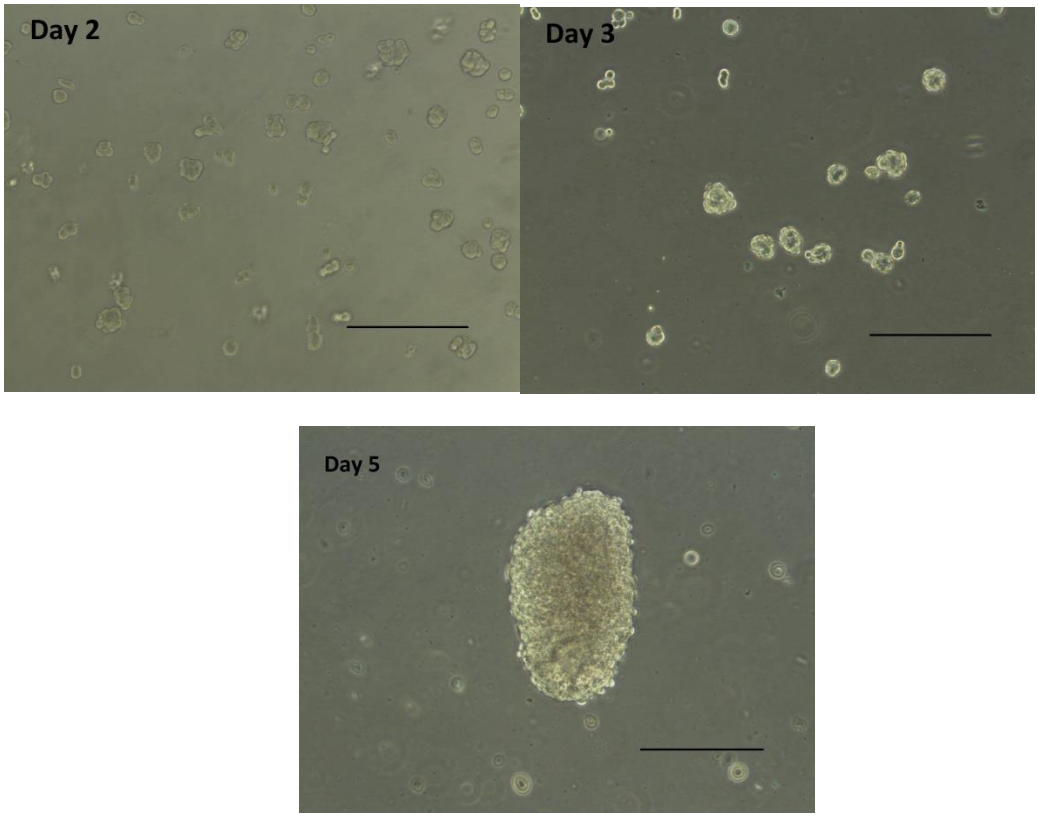

Figure D.4: Illustration of photographs acquired during the duration of the experiment in which 0.9 x 10^6 T98G cells were seeded in a pre-agarose-coated 25 cm^2 cell culture flask and maintained under orbital stirring movement at 75 rpm. The cells were kept under air environment and optimal temperature in the walk-in incubator as described in chapter 3.2. The scale bar stands for distance of 333.33 µm.

Day 2

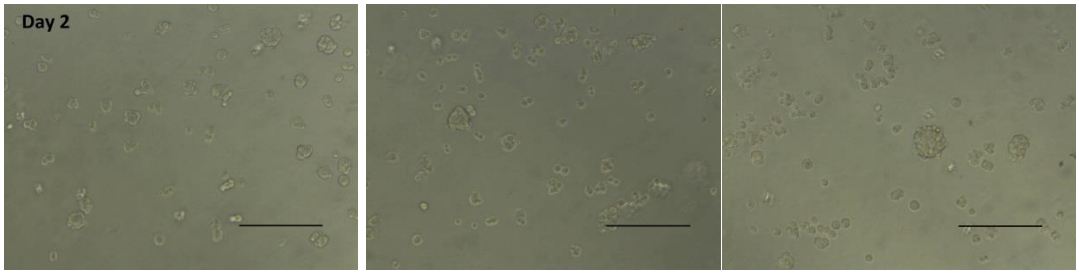

Day 3

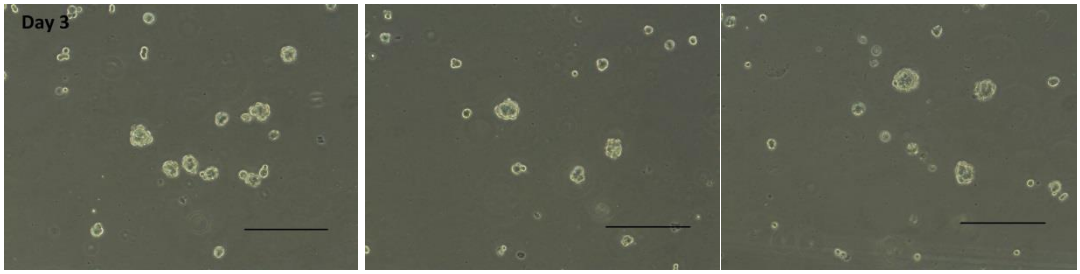

Day 5

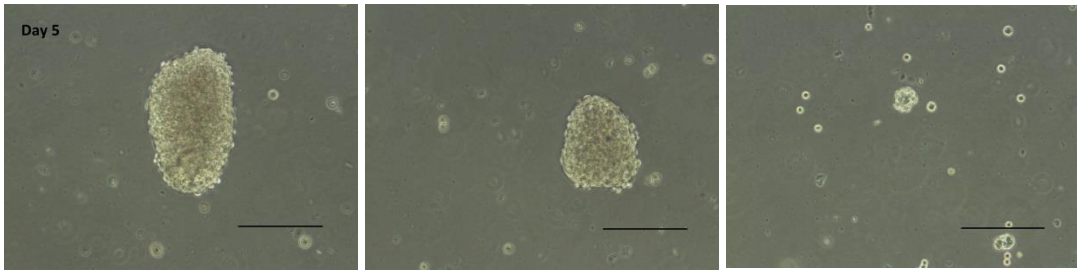

D.2.3

The description of the present experiment is reported in the chapter 4.1.4 (section 2).

Day 2

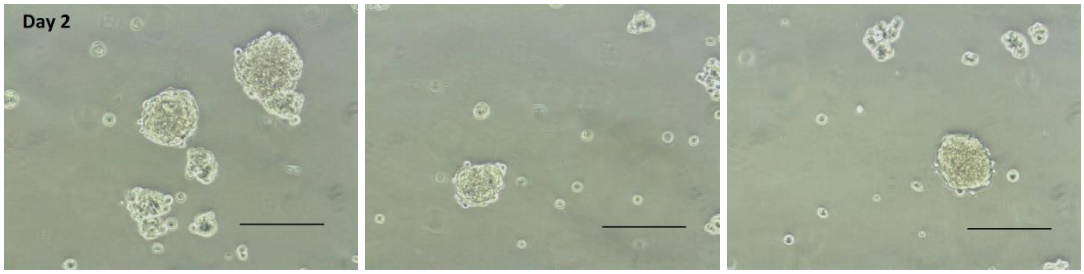

Day 3

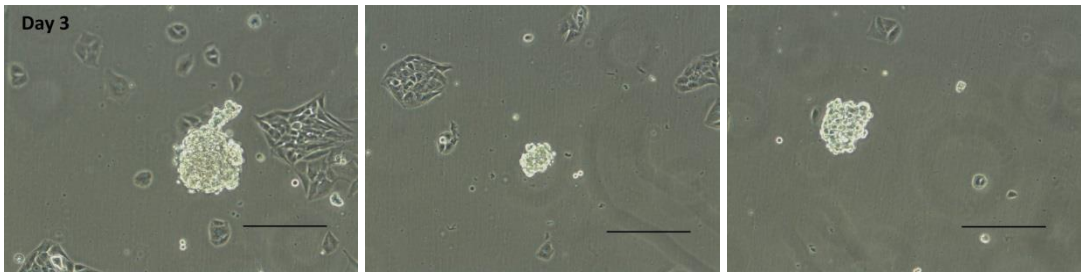

Day 5

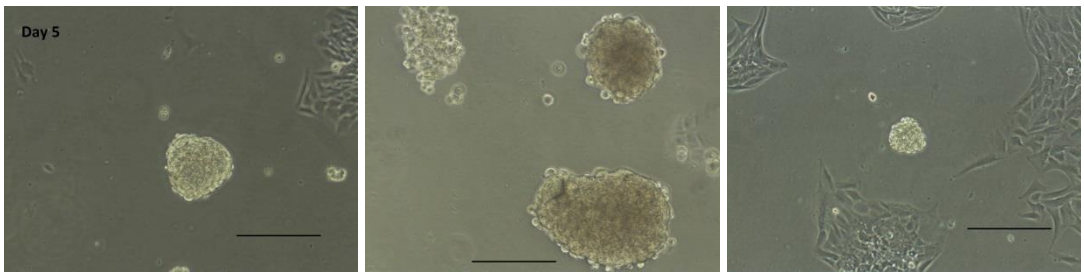

Day 9

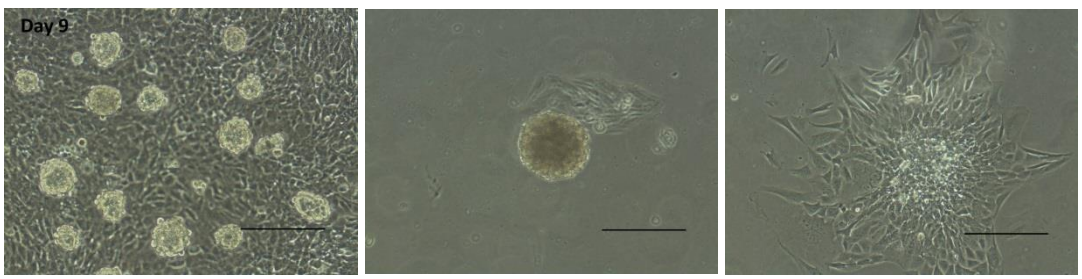

Table D.2: All the different combinations of stirring speed and initial cell number tested in agarose-coated 25 cm^2 cell culture flasks

	T98G cells seeded on day 0	
Stirring speed (rpm)	0.9 x 10^6	1.3 x 10^6
60	D.2.1	-
75	D.2.2	D.2.3

D.3

Overview of the parameters for the T98G-cell spheroids generation.

Cell type	**T98G**
Startingcellnumber	1.3 x 10^6
Stirring speed	60 rpm
Agarose-coating	Yes
Thickness of agarose layer	1 mm
Diameters of spheroid formed	150-200 µm
Day that this diameter reached by the spheroids	Day 5- Day 9
Medium volume	8 ml

Appendix E

Agarose gel recipe

80 ml Milli-Q water

1.2 gram Sigma-Aldrich agarose / 1.2 gram SeaKem agarose

Gently manual shaking

Sterilization by using an autoclave for 40 minutes in 120^0 C

For the warming up of the gel an microwave oven was used.

Appendix F

Chemical list

In this appendix, the chemicals used are listed along with manufacturer and country

Chemical	Manufacturer
Agarose Type I, Low EEO	Sigma-Aldrich, USA
EDTA	Fluka, Switzerland
Ethanol	Kemetyl Norge AS, Norway
Foetal calf serum	Euroclone, Great Britain
Glucose	Sigma, USA
Insulin	Sigma, USA
Milli-Q H_2O	Millipore, USA
PBS	Euroclone, Great Britain
Phenol red	Merck, Germany
RPMI powder with L-glutamin	JHR Biosciences, USA
SeaKem LE Agarose	Lonza, Switzerland
Sodium sulfate ≥98%	Sigma-Aldrich, USA
Trypsin	PAA Laboratories, Austria